Development of Mussel Inspired Nanocomposite Adhesives for Biomedical Applications

By

Nikhil Pandey

Presented to the Faculty of the Graduate School of
The University of Texas at Arlington in partial fulfillment
of the requirements for the degree of
DOCTOR OF PHILOSOPY

THE UNIVERSITY OF TEXAS AT ARLINGTON
August 2018

Advisors: Dr. Kytai T. Nguyen and Dr. Yi Hong

Acknowledgements

I would like to acknowledge and express my sincere gratitude to Dr. Kytai T. Nguyen for her support and guidance to me as a mentor and advisor and teaching me the importance of persistent and devout hard work towards your work and craft. Her exceptional work ethic and selfless hard-working nature has inspired me throughout my doctoral years and I hope to continue to emulate her teachings in my professional journey ahead. I also thank and acknowledge my second advisor Dr. Yi Hong for his critical assessment of my work which helped me improve my research and his guidance in my publications and during my doctoral years, enabling the completion of this doctoral research thesis. I would also like to acknowledge my collaborators, Dr. Jun Liao at University of Texas at Arlington and Dr. Phillipe Zimmern at the University of Texas Southwestern Medical Center, Dallas for their useful feedback at our UTSW meetings and the constant motivation and encouragement by Dr. Zimmern to keep working on this thesis project supplemented by his constant reminder to keep up the good work. I would also like to express my sincere gratitude and thanks to Ms. Julie Rockow and Dr. Georgios Alexandrakis for their support and advise as graduate advisor and graduate track advisor respectively and also to Dr. Liping Tang for his advice and guidance during his time as the academic advisor in my masters and as a professor in general. Special thanks to Dr. Cheng-Jen Chuong for his teachings and advices as my PhD thesis committee member and also as a faculty member during my doctoral diagnostic exam

Secondly, I want to say thank you to my lab colleagues and friends: Dat Nguyen, Aneetta Kuriakose, Serkan Yaman, Duong Leh, Amir Hossein Hakamiwala, Tyrell Pruitt, Carlos Cantu Dr. Boyd, for sharing their bright minds and beautiful friendship with me during my most tough years in graduate school. Also, thanks to: Victoria Messerschmitt, Elizabeth Lyde, Katherine Copeland McGrath Sara Rebecca McMahan for their love and friendship.

I also acknowledge my dearest friends: Tanvir Singh, Mayank Kumar, Vidhi Thakur Chauhan, Deepanshu Mittal, Yogesh Jindal, Pradeep Pandey, Khalsa brothers, Sandeep Thakur, Dr. Ashwini Kumar, Dr. Amit Pal, Amritpal Singh Shant (Amlie), Gagandeep Singh, Vaibhav Landge, Katherine Trammel, and Dianna Avyar, for their love and support.

I would also like to acknowledge my past mentors: Dr. Aniket Wadajkar, Dr. Jacque Duncan for training me to be independent and be capable of success at graduate school.

Finally, and foremost, I would like to dedicate this thesis to my parents Dr. Brahma Kishore Pandey and Ms. Vibha Pandey and my brother Dr. Nitesh Pandey, who have always believed in me despite my situations and struggles and motivated me to pursue higher education in capacity of my potential. My parents and brother trained me to have a logical outlook and each of my success is directly attributed to the values they inculcated in me and their loving upbringing Their frugality and struggles in desperate times have motivated me to keep working hard despite the odds.

-Nikhil Pandey
August 2018

Contents

List of Illustrations

List of Tables

Abstract

Popular bioadhesives, such as fibrin, cyanoacrylate and albumin–glutaraldehyde-based materials, have been applied for clinical applications in wound healing, drug delivery, and bone and soft tissue engineering; however, their performances are limited by weak adhesion strength and rapid degradation. The long-term goal of this research is to develop a strong tissue adhering nanocomposite for tissue interfacing and wound healing applications. We begin by developing a mussel-inspired, nanocomposite–based, biodegradable tissue adhesive by blending poly (lactic-co-glycolic acid) (PLGA) or N-hydroxysuccinimide modified PLGA nanoparticles (PLGA-NHS) and polydopamine nanoparticles with mussel-inspired polymers. Adhesive strength measurement of the nanocomposites on porcine skin-muscle constructs revealed that the incorporation of nanoparticles significantly enhanced the tissue adhesive strength compared to the mussel-inspired adhesive alone. To further optimize this nanocomposite system, we studied the effects of nanoparticle sizes, concentrations and types as well as types of hydrogel materials including alginate and hyaluronic acid-based materials on the tissue adhesive strengths of the nanocomposites. The nanocomposites made from alginate-based polymers were degradable and cytocompatible *in vitro and* elicited *in vivo* minimal inflammatory responses in a rat model, suggesting clinical potential of these nanocomposites as bioadhesives. The Hyaluronic acid-based polymers were found to have the best tissue adhesion at 40% w/v polymer concentration. In addition, among the tested nanoparticles (PLGA, PLGA-NHS, Silica and Polydopamine), the developed polydopamine nanoparticles at 200 nm size and 12.5 % w/v concentrations were found be the most effective in enhancing the adhesion of mussel inspired hydrogels (Alginate-dopamine and Hyaluronic acid-dopamine) with adhesive strengths increasing with further increase in nanoparticle concentrations up to 40 % w/v in the nanocomposite blends of Hyaluronic acid-dopamine polymers. Finally, we developed this optimal

nanocomposite adhesive into an antimicrobial tissue adhering degradable system and demonstrate its antimicrobial effectiveness on *E. Coli* and *S. Aureus* species of bacteria with potential applications of this nanocomposite for healing of chronic wounds.

Keywords: bioadhesives, nanoparticles, nanocomposites, tissue interfaces, tissue adhesion, antimicrobial delivery

Chapter 1
INTRODUCTION

1.1) Introduction to Tissue Adhesives

Surgical intervention plays a critical role in ensuring reconnection of injured tissues to facilitate restoration of tissue structure, function and hemostasis. The conventional methods to connect tissues during surgeries involve the use of sutures, staples, and wires which are applied to mechanically hold the tissues in close proximity to stop bleeding or fluid leakages and promote faster healing while resisting tensile loads applied to the tissue. Despite their popular use in the clinic, these methods of adhering tissues have many limitations such as causing damage to the surrounding tissues, requiring secondary surgeries for removal, and interfering with tissue healing processes [2-6]. In addition, the complete adherence of tissues using sutures, staples or wires requires a high level of experience by the operating surgeon and is not easily applicable in every clinical scenario, specially at places and locations that are hard to reach internally. Also, these mechanical methods are ineffective in adhering blood vessels and soft tissues like liver, spleen and kidney. There are approximately 114 million surgical and procedure based wounds occurring worldwide each year and the global wound closure market is predicted to reach $14 billion by 2018 [7]. In regard, to the growing healthcare costs associated with wound closure and the shortcomings of conventional methods, it becomes necessary to develop better alternatives to adhere tissues together.

One attractive option to alleviate the use of conventional methods is the use of biomaterials that can be applied over tissue surfaces and cause them to adhere together like glues. Such class of biomaterials are termed tissue adhesives or bioadhesives and they offer a simpler, quicker and suture less way of reconnecting tissues and restore tissue functionality. These tissue adhesives can simplify complex wound closure procedures while reducing surgery cost and time. A tissue

adhesive is generally defined as any substance that can polymerize *in situ* and help adhering two surfaces, one of which at least is a tissue [3]. Depending on the application, a tissue adhesive can function as an adhesive and bind different tissues together as well as allow proper healing to occur and function either as a hemostat to prevent bleeding and blood loss from tissues or function as a sealant to prevent gas or fluid leakage from tissues. Tissue adhesives can enhance tissue repair and wound healing at the same time reduce operative risks and costs. The use of tissue adhesives provides a needle free method of wound closure thus protecting the surgeon from the risk of needlestick injury while providing a better cosmetic outcome as compared to sutures. In addition, tissue adhesives also provide the potential for drug delivery in the form of slow and localized release of antibiotics to prevent wound infections and of growth factors to encourage cell growth and wound healing [5, 6]. The application of tissue adhesive with drug delivery was demonstrated as early as 1947 with the application of the gum tragacanth with a dental adhesive powder to deliver penicillin to the oral mucosa. This formulation was later known as 'Orabase' and it was made up of a mixture of polymers: gelatin, pectin, and carboxymethyl cellulose, which form a paste that sticks to the wet surfaces of the mouth for the treatment of mouth ulcers [5]. The first use of a modern synthetic tissue adhesives can be traced back to the use of cyanoacrylate adhesives developed in 1949 for use on small superficial lacerations and incisions; however, their limited physical properties and chronic inflammatory reactions made their use in the treatment of wounds ineffective. Further attempts at improving these shortcomings led to the development of n-2-butylcyanoactylates. These adhesives despite being purer and stronger could not be clinically applied due to their low tensile strength and brittleness. Following this, many different types of tissue adhesives have been developed over the past 30 years, using many different types of materials. To function as a surgical tissue adhesive an ideal material needs to demonstrate several

different properties and satisfy many clinical requirements, some of which are summarized in **Table 1.1**.

Table 1.1: Summary of desirable properties needed in an effective tissue adhesive.

Desired intrinsic property	Comments
Adhesion	Surgical adhesive must be able to hold two tissues together without external support until the wound heals, after which the adhesive should degrade into nontoxic biocompatible components.
Curing	The adhesive must have the ability to cure itself in the tissue environment, especially in a moist environment.
Flowability	The adhesive must have an ability to flow. Flowability of an adhesive relates to the movement of polymer chains and controls the amount of interpenetration between polymers and tissue surfaces.
Hydrophilicity	Hydrophilic polymers are preferred as they can form strong bonds with highly hydrophilic tissues.
Hydrogen bonding	The presence of strong hydrogen bonding groups like OH and COOH in the monomer can promote hydrogen bonding between polymer chains effecting the flowability and cohesive strength of the adhesive. A minimum cohesive strength is required of a good adhesive.
Molecular Weight	High molecular weight polymers (>100KDa) make for better adhesives as they provide higher degree of entanglement.

Surface tension (Wettability)	For any adhesive to adhere to a substrate, its surface energy must be equal to or less than the substrate. Lower surface tensions promote the polymer to spread across the substrate for better adherence.
Crosslinking	Crosslink formation in an adhesive promotes increased mechanical strength required by the adhesive to transfer shear stress across the adhered surfaces.

1.2) Adhesion Theory and Mechanisms

Adhesion involves the tendency of atoms or molecules to stick to each other. The sticking of dissimilar atoms or molecules to each other is termed adhesion whereas the sticking of similar atoms or molecules is termed cohesion. Adhesion involves molecular interactions at the interface between materials. Cohesion, on the other hand, is dictated by the intermolecular attractions between like molecules or atoms and is represented by the cohesive strength of a material or tissue

The state in which two materials, one of which is biological in nature held together for long periods of time by interfacial forces is termed as bioadhesion [5]. The term bioadhesion was first used in the 1970's to describe the ability of some synthetic and biological macromolecules and hydrocolloids to adhere to biological tissues. There are many examples of bioadhesion in nature such as, the vertical motions of gecko on upside down surfaces and the strong attachment of octopuses and mussels on underwater substrates. Generally, this type of adhesion involves the secretion of various bioadhesives made up of proteins, polysaccharides, and lipids along with manipulation of various surface physical forces like Van der Walls forces, capillary forces and suction forces induced by a pressure differential [8].

Bioadhesion differs from conventional adhesion with respect to the requirements and properties of the substrates being adhered and is governed by interfacial phenomena [5]. To achieve adhesion, an adhesive must have the ability to flow and wet the substrate to be attached and maintain a certain degree of physiochemical intermolecular forces for adherence to the substrate [5]. Depending on the adhesive and the substrate interaction, the nature of these intermolecular forces facilitating adhesion can vary, and this variance gives rise to different mechanisms of bioadhesion that are reported in literature. These mechanisms are majorly divided into: electrostatic interactions, surface wetting, adsorption, diffusion and mechanical interlocking. These mechanisms are briefly reviewed in the following sections.

1.2.1) Electrostatic interactions:

The proximity of a tissue and adhesive surface can lead to transfer of electrons between them due to differences in electron band structures, leading to the formation of an electric double layer at the interface between the tissue and the adhesive. The strength of the adhesion is due to the attractive forces present in this electric double layer, which account for the resistance to separation [5].

1.2.2) Surface wetting:

The wetting theory relies on the ability of the adhesive to spread and make molecular contact with the tissue surface. The molecular contact between the adhesive and tissue results in the development of surface forces, and these interfacial forces are the first basis of bond formation between the adhesive and tissue. Wetting is defined as the process of establishing a very close and continuous contact between the adhesive and the tissue. An adhesive can effectively wet an adherent if its surface tension is lower than the critical surface tension of the adherent. In order to have a high adhesive bond with the tissue, the adhesive has to completely wet the tissue by maximizing contact with the tissue topography by flowing into the defects and crevices of the

tissue. High quality wetting is achieved when the contact angle between the adhesive and the tissue is close to zero [9].

1.2.3) Adsorption:

The adsorption theory states that the adhesion between the adhesive and the adherent when they are pressed together is due to the surface forces acting between the chemical structures at the two surfaces [5]. The presence of polar molecules on the adhesive and the tissue surfaces cause them to interact and reorient at the interface promoting adhesion [10]. In addition, other secondary forces such as Van der Waal's forces, hydrogen bonding, and hydrophobic bonding also contribute to the adhesion between the tissue and adhesive interface.

1.2.4) Diffusion:

Semi-permanent bonds between the adhesive and tissue surface can form when polymeric chains form the adhesive interpenetrate into the tissue surface and reach sufficient depth. The interpenetration of the polymer chains is driven by concentration gradients where the polymer chains penetrate the tissue and glycoprotein chains from the tissue in turn penetrate into the adhesive until an equilibrium depth is reached. The equilibrium depth for a good bioadhesive bond to establish varies between the adhesive and tissue surfaces to be bonded but is reported to be in the range of 0.2-0.5 μm [10]. The diffusive depth of the adhesive depends on the diffusion coefficient of the tissue and the adhesive which in turn depends on the molecular weight of polymer chains and the crosslinking density of the adhesive [9, 10].

1.2.5) Mechanical Interlocking:

The interaction between adhesive and tissue can result in the adhesive penetrating into the tissue micro irregularities and interlocking with the tissue to create binding [11]. The tissues surface roughness plays an important role in mechanical interlocking as the adhesive locks on to microscopic roughness. An example of such kind of adhesion is the use of polymer based

adhesives, which penetrate the tissue and later expand once inside the microscopic crevices thus mechanically interlocking with the tissue [12]. Another example is the use of polymeric microneedles based on poly(styrene) and poly (acrylic acid), which penetrate the tissue and then later swell in the presence of water inside, leading to local tissue deformation and consequent interlocking within the tissue surface [13].

1.3) Current Surgical Adhesives:

Over the past several decades tissue adhesives have significantly contributed to the need of clinical surgeons to close tissue incisions, stop blood loss and bind tissues to promote wound healing. There have been a multitude of advances in improving the properties of tissue adhesives over the years to make them clinically more effective, leading to a number of commercially available tissue adhesives approved for use in very specific conditions. These tissue adhesives are generally classified into mainly three categories: Natural or biological, synthetic or semi-synthetic, and biomimetic adhesives. A list of FDA approved tissue adhesives and sealants along with their applications, advantages and limitations is summarized below in **Table 1.2.**

Table 1.2: Summary of FDA approved tissue adhesives and sealants in the US.

Tissue Adhesive Type	**Product name**	**Manufacturer**	**Application**	**Advantages**	**Limitations**
	Histoacryl/Histoacryl Blue (n-Butyl-2-cyanoacrylate)	B.Braun	Topical skin incisions and skin lacerations closure.	Fast curing, Strong dry adhesion.	Rapid degradation in moist conditions. Formaldehyde mediated cytotoxicity.
	Indermil (n-Butyl-2-cyanoacrylate)	Henkel	Topical skin incisions and skin lacerations closure. Barrier to microbial penetrations.		
	Dermabond	Ethicon			

Cyanoacrylates	(2-Octyl-2-cyanoacrylate)				
	Omnex (n-Octyl-2-cyanoacrylate/ butyl lactoyl-2-cyano acrylate)	Ethicon	Blocking blood loss, bodily fluids, air leaks.		
	Glubran/Glubran2 (n-Butyl-2-cyanoacrylate/ methacryloxysulpholane)	GEM Italy	surgical glue, for internal and external use, with hemostatic, adhesive, and bacteriostatic properties.		
Tissue Adhesive Type	**Product name**	**Manufacturer**	**Applications**	**Advantages**	**Limitations**
	Tisseal (Human pooled plasma fibrinogen and thrombin)	Baxter Inc.	As an adjunct to hemostasis in surgeries involving cardiopulmonary bypass and treatment of splenic injuries when control of bleeding by conventional surgical techniques, including suture, ligature, and cautery	Fast curing Biocompatibility Biodegradability	Risk of transferring bloodborne disease. Risk of allergic reaction. Risk of infection transmission.
	Evicel (Human pooled	Ethicon Inc. (Johnson & Johnson Co)			

Fibrin glue	plasma fibrinogen and thrombin)		is ineffective or impractical. As an adjunct for the closure of colostomies. Vitagel is used during surgical procedures (except neurosurgery and eye surgery) as an adjunct to clotting when control of bleeding using suture or other conventional procedures are not effective or seems impractical. The autologous Cryoseal system fibrin sealant is indicated for use as an adjunct to hemostasis on the incised liver surface in patients undergoing liver resection.		Long preparation time. Ancillary equipment required. Poor tissue adhesion. Relatively expensive.
	Vitagel (Autologous plasma fibrinogen and thrombin)	Orthovita Inc.			
	Cryoseal system (Autologous plasma fibrinogen and thrombin)	ThermoGenesis Corp.			
	Coseal (2 four-armed PEGs: one capped with glutaryl-succinimidyl ester and the other with thiols, and dilute solution of hydrogen chloride and sodium phosphate-sodium carbonate)	Baxter Inc.	Sealing suture lines and vascular graft.	Rapid gel formation. Fast hemostasis. Biocompatibility.	Risk of swelling. Possible allergic reaction.
	Duraseal (PEG ester powder and	Covidien Inc.	Sealing of cerebrospinal fluid (CSF).		

Poly (ethylene glycol) (PEG) based sealants	trilysine amine solution with FD&C blue No.1 dye)			Adhesion to tissue.	Relatively expensive.
	SprayGel	Covidien	Adhesion barrier in gynecological and colorectal procedures.		
	TissuGlu®		Prevention of seroma formation under skin flaps.		
	OcuSeal	Hyperbranch Medical Technology)	Dressing for corneal lacerations and bandage for corneal transplants.		
	Adherus		Surgical sealant for dural repair, hernia mesh fixation, spinal and cardiovascular applications.		
Tissue Adhesive Type	**Product name**	**Manufacturer**	**Application**	**Advantages**	**Limitations**
Albumin and Glutaraldehyde	BioGlue (Bovine serum albumin and 10%glutaraldehyde)	Cryolife Inc.	As adjunct to standard methods of achieving hemostasis (such as suture and staple) in open surgical repair of large vessels (such as aorta, femoral and carotid arteries).	Fast polymerization begins in 20-30 sec and reaches full strength in 2 min. Good adhesion to tissue.	Safety concerns over risk of glutaraldehyde toxicity.
	ProGel®	NeoMend	Sealing air leaks on lung tissue after surgery.		

1.4) Natural or Biological Adhesives:

Some naturally occurring materials can have intrinsic properties that make them interact with tissues and stick to them. For example, proteins rich in amine groups, polysaccharides rich in carboxyl, and hydroxyl groups can interact with tissue amine groups and adhere to them. Tissue adhesives based on natural materials are crosslinked via biochemical reactions and thus are more biocompatible compared to synthetic adhesives. Some of the biological tissue adhesives such as fibrin-based adhesives are reviewed in this section.

1.4.1) Fibrin based adhesives:

Fibrin has been applied in surgery as early as 1909 when its hemostatic properties were realized [6]. Subsequently as purified thrombin became available for use in 1938, fibrinogen and thrombin combinations were applied to enhance adhesion of skin grafts to burned soldiers during world war II [1]. The first fibrin-based glue was reportedly developed in the 1940's as an adhesive to nerves. However early formulations did not clot readily due to low concentrations of fibrin in the formulations. The success in cryopreservation of fibrinogen in the 1960's paved the way for the development of high concentration fibrin-based adhesives in the 1970's. These initial formulations of fibrin were derived from pooled blood, which significantly increased the risk of viral transmission of HIV, hepatitis B and hepatitis C. Viral elimination protocols were established after which Tisseal (Baxter Healthcare) became the first fibrin based sealant approved by FDA for clinical use in the US [1].

Fibrin is a protein found in the blood, and fibrin adhesives are based on the principle of mimicking the mechanism in which blood clots are formed during the final stages of the physiological coagulation cascade. The mechanism in which fibrin is crosslinked is depicted in **Figure 1** [1].

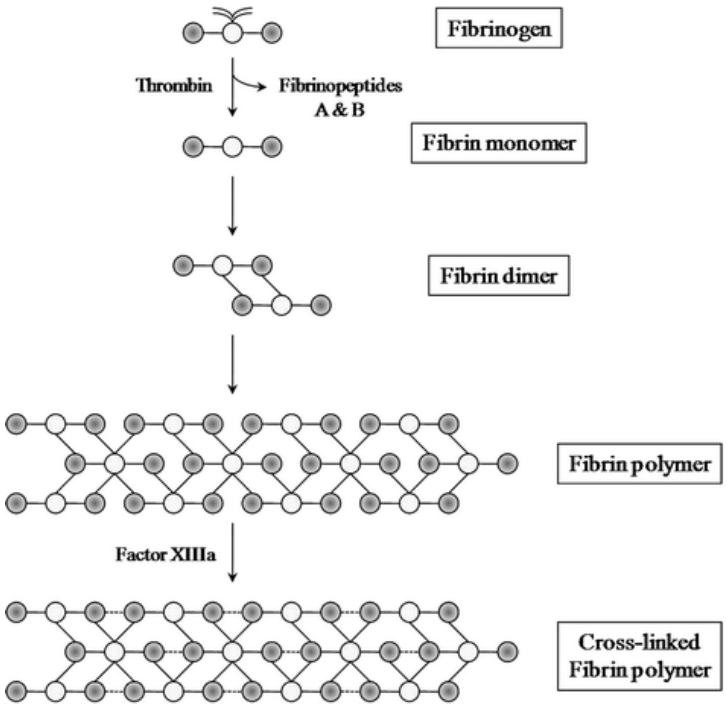

Figure 1.1: Crosslinking Mechanism of fibrin-based tissue adhesives. Thrombin mediated cleavage of fibrinopeptides A and B from fibrinogen results in fibrin monomers. The monomers then polymerize to form fibrin polymer, an unstable soft clot. Thrombin-catalyzed fibrin polymerization is followed by factor XIIIa-catalyzed fibrin crosslinking, resulting in formation of a stable fibrin clot [1].

The physiological coagulation cascade is mainly orchestrated by two key plasma proteins: thrombin and fibrinogen. Fibrinogen is first activated by thrombin cleaving the fibrinopeptides A and B to form fibrin monomer, which subsequently polymerizes via electrostatic interactions and hydrogen bonding to form a soft clot of fibrin polymer. At the same time, thrombin with the help of calcium ions also actives clotting factor XIII to XIIIa, which crosslinks the fibrin polymer via amide links between glutamine and lysine residues in proteins to form a stable clot. Furthermore fibrin also crosslinks with adhesive glycoproteins of the ECM such as collagen, fibronectin, and von Willebrand factor as well as cellular glycoproteins, which enables it to anchor the clot at the injury site [1].

Formulations of fibrin adhesives used clinically are usually a two-component system consisting of a solution of thrombin and calcium combined with a solution of fibrinogen and factor XIII to form a reaction, which is similar to the final stages of blood clotting cascade. In some cases, an anti-fibrinolytic agent aprotinin is used to prevent premature lysis of the fibrin clot [1]. The composition of a fibrin adhesive strictly dictates its adhesion profile and its degradation rate. The fibrinogen concentration directly relates to the tensile strength of the glue, while the thrombin concentration affects the curing time to achieve maximum adhesive strength [1, 14]. The optimum concentration of thrombin and fibrinogen is necessary for a fibrin glue to have the required adhesion and mechanical properties; however, the adhesion strength is also function of the substrate topography, methods of fibrinogen preparation and the presence of water, fat or collagen [2, 14, 15]. The clots produced by fibrin based adhesives are completely biodegradable and breakdown by thrombolysis within a few days to several weeks [1].

Due to the biodegradable nature and the biochemical processes by which fibrin-based adhesives can glue tissues together, they have been clinically applied in various organ systems as wound closure agents and adhesives for wound healing. In addition, they have been approved for hemostasis in surgeries involving cardiopulmonary bypass and liver resection, as well as sealing of colonic anastomoses during colostomy closure. For instance, one commercial fibrin sealant (Eviseal, J&J Ethicon) has gained approval for use in general hemostasis during surgery [1]. Fibrin based adhesives have also been used as drug delivery scaffolds and in tissue regeneration applications such as delivery of antibiotics like ciprofloxacin and ampicillin and chemotherapeutics like doxorubicin [16-18].

Despite the versatile use of fibrin adhesives, they have some important limitations to consider starting with the source of fibrinogen. Fibrinogen obtained from pooled human blood plasma

still has a risk of viral transmissions despite the antiviral protocols in place. The transmission of symptomatic parvovirus B19 has been previously reported by the use of fibrin sealant in surgery [19, 20]. Fibrin adhesives containing bovine proteins can also illicit immune responses in humans [21-23]. In addition, fibrin adhesives have a poor adhesion to tissue compared to synthetic cyanoacrylate adhesives and they are also not practical in emergency applications as a typical fibrin adhesive takes about 20 minutes to apply successfully [24, 25].

1.4.2) Collagen based adhesives:

Over the past decade, collagen-based adhesives have become popular in clinical use. The collagen based adhesives usually have collagen combined with either thrombin or fibrinogen, where collagen acts to absorb blood and coagulation products by trapping them it its matrix interstices thus allowing itself to bind to the wound where it can then deliver fibrinogen, in addition to causing the aggregation and adhesion of platelets and activation of coagulation factors [3, 6, 26-29]. There are two collagen based adhesives approved for clinical use, namely: Floseal (Sulzer Spine Tech, Anaheim, CA) for vascular surgery hemostasis and Proceed (Fusion Medical technologies, Mountain View, CA) for preventing cerebrospinal fluid leaks, both adhesives are composed of bovine thrombin and collagen [3, 6, 30, 31]. Another adhesive in development CoStasis (Cohesion Technologies, Inc) made from human plasma, bovine collagen, and thrombin has shown significant results in the control of surgical bleeding [26]. Many of the collagen-based adhesives have superior adhesion strengths to tissues compared to fibrin adhesives but lower compared to cyanoacrylate- based synthetic adhesives. In addition, collagen based hemostats can swell and cause tissue compression [32].

1.4.3) Gelatin based adhesives:

Gelatin is an irreversibly hydrolyzed form of collagen and one of the first biomaterials to be considered for use as adhesives in internal surgery due to its biocompatibility, bioresorability and ability to form strong transparent films and gels [3]. The amino groups in gelatin have been modified to cholesteryl residues to improve its adhesive properties and tissue penetration. Gelatin is often applied with a crosslinker to increase its adhesion strength and to control its degradation rate where the crosslinking can be chemical, enzymatic or photochemical. These adhesives are capable of binding to tissues and form covalent linkages with functional groups on the tissue surface. Gelatin-Ressorcinol-Formaldehyde/Glutaraldehyde (GRFG) glue is an example of chemically crosslinked gelatin-based adhesives where gelatin chains are crosslinked by aldehyde through polycondensation reactions and resorcinol molecules react with formaldehyde to form a three-dimensional network. The GRFG glue with a gelatin resorcin: formaldehyde/ glutaraldehyde ratio of 2:1 has shown a maximum adhesion strength of 48 ± 18 kPa under wet conditions [2, 3].

1.5) Polysaccharide based adhesives:

Polysaccharides and proteins are known to be natural mediators of adhesion; some microorganisms use acidic or neutral exopolysaccharides like dextran and heparan sulphate to adhere to different substrates [2]. This is possible due to the abundant presence of carboxyl, amine, and hydroxyl functional groups, which can bond to the tissue amine groups via covalent interactions through N-hydroxysuccinimide activation, Schiff base formation, Michael addition reaction, $\pi-\pi$ interactions, biaryl formation, or imine formation [2]. Dextran, Chitosan, Chondroitin sulphate are the most widely studied polymers for adhesive applications. The functional groups of these polymers often need to be derivatized to increase the adhesion property of the resulting hydrogels. These adhesives are summarized below.

1.5.1) Dextran based adhesives:

Dextran is a highly water-soluble polymer found as an exocellular bacterial polysaccharide, which has linear α-1,6-linked glucopyranose units with some degree of 1,3-branching. This polymer is nontoxic, biocompatible, and is capable of degradation inside the human body due to the action of various dextranases present in various organs like spleen, kidney, liver, and colon [33]. Dextran also contains an abundance of hydroxyl groups that can be used for chemical derivatization. In order to increase the adhesive properties of dextran-based gels, aldehyde groups are often generated into the polymer chain via periodate oxidation and the aldehyde groups react with the amine groups on tissue surfaces to promote bioadhesion. Aldehyde containing dextrans are often combined with amine containing polyethylene glycols (PEG) or gelatin to form intermolecular crosslinks to provide cohesion to the resulting adhesive. One example of a product obtained via such approach is ActaMax, which adheres to tissues and degrades hydrolytically. Various studies have shown dextran-PEG adhesives to be biocompatible and to have an adhesive strength greater than fibrin glues and similar to cyanoacrylate glues [2, 33].

1.5.2) Chitosan based adhesives:

Chitosan is a linear polysaccharide composed of randomly distributed β-(1-4)-linked D-glucosamine residues with a variable number of randomly located N-acetyl-D-glucosamine units. This polymer is biocompatible and has unique antioxidant and bacteriostatic properties [34]. It can also react with anionic biopolymers like nucleic acids, glucose amino glycans, heparin and proteoglycans which can be utilized to make soft tissue adhesives. Even though chitosan can interact with tissue functional groups, chitosan adhesives have poor cohesion which results in inadequate adhesion [33]. To counter this, the amino and hydroxyl functional groups of chitosan can be chemically modified to provide crosslinking to the polymer. For example, chitosan polymers containing photoreactive inert groups like phenyl azide have been prepared which on

exposure to UV or visible light can crosslink into a gel, and a similar photocrosslinkable hydrogel based on chitosan, 4-azidobenzoic acid (Az)-chitosan has been applied for peripheral nerve anastomosis [35]. Another example of a commercially available chitosan-based adhesive is SurgiLux which is crosslinked using a near infrared laser activation (808 nm). The laser activation strengthens the adhesion of the polymer to tissue collagen through polymer chain interactions caused due to the transient thermal expansion [36, 37].

1.6) Synthetic/Semi synthetic adhesives:

Due to certain performance limitations of biopolymers such as uncontrollable degradation, in adequate tissue adhesion, expensive and difficult purification of the polymers from natural sources, synthetic polymers have been utilized to formulate synthetic tissue adhesives. Synthetic tissue adhesives are composed of synthetic chemicals in the form of monomers, prepolymers, or non-crosslinked polymers, which undergo *in situ* polymerization or crosslinking to form an insoluble adhesive matrix when applied on a tissue. Synthetic polymeric materials provide the possibility to control the three-dimensional structure and chemical composition of the adhesive to expose functional groups that can interact with biological tissues and promote bioadhesion [33, 38]. Synthetic polymers also provide a control over the final molecular weight, which can be used to tailor the degradation and elimination rates of the adhesive from the body. Some of the synthetic tissue adhesives are reviewed below.

1.6.1) Cyanoacrylate based adhesives:

Cyanoacrylate based adhesives are a group of adhesives made form alkyl α-cyanoacrylates for tissue adhesive applications since the 1950s [2]. These adhesives can polymerize very quickly under weak basic conditions such as water or blood and are hence capable of bonding tightly to the tissue without any external initiation, which gives them a very high bonding strength. The tissue amine groups are thought to play a role in initiating the polymerization of cyanoacrylates

and forming covalent bonds with the polymer, resulting in the high adhesive strength with the adhered tissues [2, 4]. Cyanoacrylate adheres to the tissue via two independent mechanisms: (i)

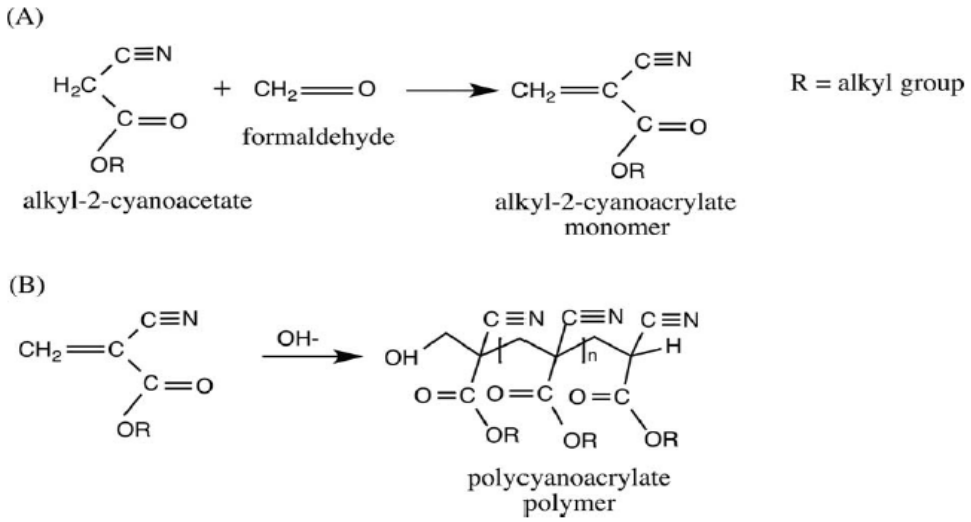

Figure 1.2: Mechanism of Cyanoacrylate polymerization.

molecular interactions via covalent bonding to proteins exposed on tissue surfaces and (ii) penetration of cyanoacrylate monomers into cracks and channels in the tissue surface (mechanical interlocking) [33]. The alkyl side chain R (**Figure 1.2**) has a significant effect on the strength and physiochemical properties of cyanoacrylate adhesives, shorter chain derivatives (-CH3, C2H5) of R form tighter and stronger bonds, resulting in brittle gels, whereas longer chain derivatives decrease the polymerization rate and give rise to more flexible gels [33]. The adhesive properties of cyanoacrylates are reported to be superior to fibrin glue and other natural adhesives in terms of tissue adhesion, rapid curing and low cost. However, the rapid polymerization of cyanoacrylates is associated with significant heat production, which can be damaging to the tissues. The degradation of cyanoacrylate based adhesives can also lead to the formation of formaldehyde, which can cause toxicity [4]. Also, depending on the alkyl group R, cyanoacrylate adhesives can illicit severe immune responses such as in the case of α-cyanoacrylates. Modifications of the alkyl

groups such as those in N-Butyl-2-cyanoacrylate-based commercial glues: Histoacryl (Germany), and Glubran (Italy) can lower the inflammatory responses making these adhesives applicable commercially for endoscopic surgeries. In addition, 2-Octyl cyanoacrylate-based glue (Dermabond (USA)) is FDA approved adhesive, but for medical use in topical applications only [2]. Despite the attractive properties and substantial strong adhesion of cyanoacrylate-based adhesives, their use is limited to topical applications owing to the toxic nature of the degradation products. Thus, cyanoacrylate adhesives have limited applications until the problem of their toxicity is resolved.

1.7) Current approaches to create tissue adhesives:

1.7.1) Mussel Inspired Adhesives:

Nature uses adhesion in a host of ways and a variety of biological species such as mussels, barnacles, and some lizards like geckos secrete substances with potential adhesiveness. These substances are usually proteins that help them stick to surfaces underwater [39]. As far as adhesiveness is concerned, mussels are the most fascinating species, which by the virtue of their adhesive secretions can stick onto rocks and ships underwater and especially well under turbulent intertidal conditions. The tissue adhesion of mussels is due to secretion of a mixture of proteins called mussel adhesive proteins (MAPs). Several researchers have studied the composition of these MAPs and have characterized the presence of at least six different mussel foot proteins (Mfp-1-

Protein	Mass (kDa)	% DOPA
Mefp-1	110	13
Mefp-2	40	3
Mefp-3	6	20
Mefp-4	80	4
Mefp-5	9	30

Figure 1.3: Different mussel adhesive proteins found in plaques of mussels and their Dopa compositions

Mfp-6) [40, 41]. These MAPs have an abundance of a particular catecholic amino acid 3,4 dihydroxyphenylalanine (DOPA), which has been implicated to be a key factor behind mussel's strong underwater adhesion [42, 43]. The amount of DOPA in each of the MAPs is summarized in the **Figure 1.3** [39].

It is postulated that each type of Mfp has its own function and contributes differently to the interfacial adhesion of mussels; however, Mfp-3, 5, and 6 are predominantly found at the mussel plaque-substrate interface and are known to contribute to the strong wet adhesion [44]. The exact mechanisms of mussel's wet adhesion are not fully understood but Dopa plays a central role in the interfacial binding and curing of the adhesive plaque proteins. Dopa molecules are capable of versatile chemistries enabling them to bind to organic and inorganic surfaces alike through the formation of reversible non covalent and irreversible covalent interactions [44].

Dopa can form strong H-bonds via its dihydroxy functionality, promoting its absorption on tissue surfaces like mucosal tissues. Catechol containing polymers have improved cohesive properties due to the benzene ring of catechol, which can interact with other aromatic rings via π-π interactions. In addition, the benzene ring can interact with positively charged ions through cation-π interactions, one of the strongest non-covalent interactions in water which enables them to bind to positively charged surfaces and to substrates rich in cationic functional groups [45, 46] . Catechol can also form strong reversible complexes with metal ions (Cu^{2+}, Zn^{2+}, Mn^{2+}, Fe^{3+}, V^{3+}, Ti^{3+}, and Ti^{4+}) and strong interfacial bonds with metal oxide surfaces. Furthermore, the oxidized form of catechol is highly reactive and can participate in intermolecular covalent cross-linking that cause curing of Dopa containing adhesives. Catechol is usually oxidized into semi-quinone or quinone by one or two electron oxidation (**Figure 1.4**) via enzymatic, chemical (periodate) or the presence of molecular oxygen and quinone is capable of reacting with serval nucleophilic

functional groups found in tissues (–NH_2, –SH, imidazole) to form interfacial covalent bonds, which can promote tissue adhesion [44]. Although Dopa is the main molecule of Mfps that contributes to their strong adhesion, there are other mechanisms between Dopa and Mfps which contribute to their adhesion and these are reviewed in the next section.

1.7.1.1) Oxidation state of Dopa:

The oxidation state of catechols strictly controls their adhesive properties [47-49]. Catechols exist in their highly adhesive reduced forms at acidic pH, when the pH approaches or exceeds the first dissociation constant of the -OH group (pK_a 9.3) on catechols, its side chain is known to autoxidize to quinone form which has a reduced adhesive strength [47, 50, 51]. To counteract this, mfp-3 and mfp-6 proteins are present at the plaque surface interface to provide an antioxidant effect, whereas mfp-3 also creates a hydrophobic environment, shielding the dopa from oxidation and subsequently enhancing adhesion.

1.7.1.2) Coacervate formation:

The fluid-fluid phase separation of ionic polymers from aqueous solutions driven by columbic forces and charge neutralization between chains of opposite charges is called coacervation. This

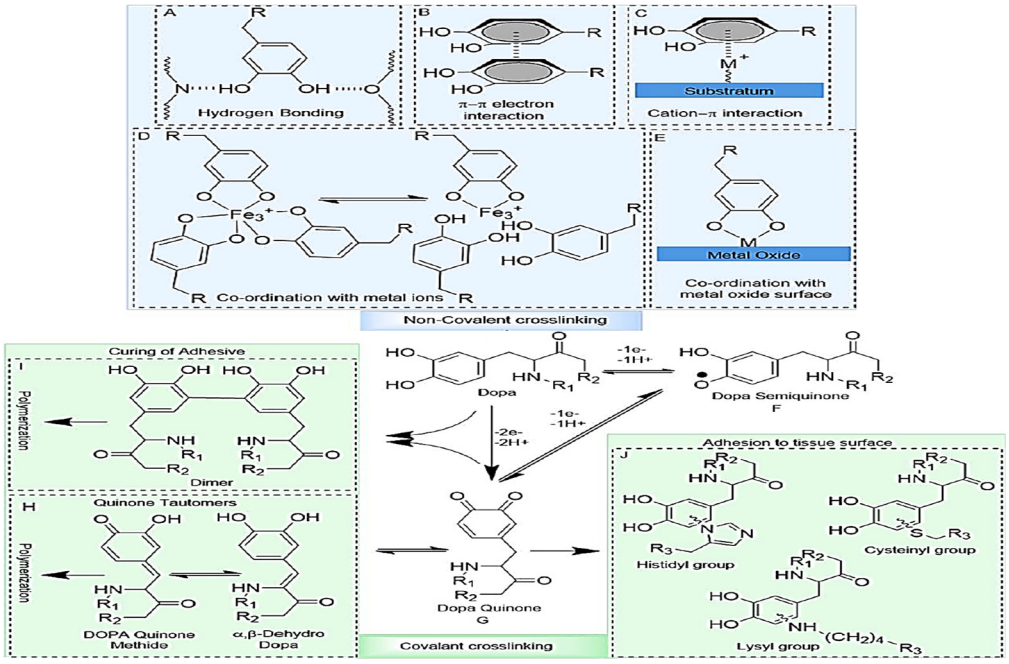

Figure 1.4: Various mechanisms catechols use to interact with different substrates.

process contributes to underwater adhesion by increasing the polymer concentration in the coacervates, improving surface wettability via decrease in interfacial energy and enhancing adhesive delivery by reducing viscosity of the phases.

1.7.1.3) Surface drying:

In underwater adhesion, interfacial molecular contact between the substrate and the adhesive is necessary. This contact can be hindered due to the presence of a layer of adsorbed water, which gives rise to strong repulsive hydration forces that compromise adhesion. Several researchers have demonstrated that Mfp-3s has hydrophobic tryptophan side chains which help in removal of the surface hydration layer. Dopa containing coacervates thus have the ability to displace interfacial water molecules and make molecular hydrogen bonds with the substrates which increases the adhesion strength [52, 53] .

1.7.1.4) Catechol modification:

Catechol modifications can significantly change their adhesive properties, for example, catechol side chain modified with an electron withdrawing nitro-groups at the para position significantly increases the reactivity and interfacial binding strength of catechols (**Figure. 1.5 (B**)) [54].

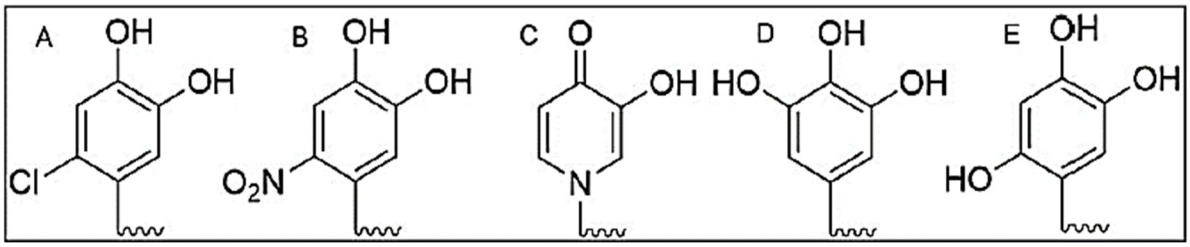

Figure 1.5: Functional group Modifications of catechol side chains and their associated configurations.

The nitro functionalization also leads to increased resistance to elevated temperature and oxidation when compared to an unsubstituted catechol [55-57]. Also, nitro-catechol exhibits increased rates of covalent crosslinking and binds to biological substrates over a wider range of pH, when compared to unmodified catechol [58]. In addition, nitro- and chloro-functionalized catechols can exhibit unique properties such as light-induced degradation and antimicrobial characteristics [59].

1.8) Strategies to synthesize catechol functionalized synthetic polymers

Due to the promising adhesion of mussel adhesive proteins and the central role of Dopa molecules in it, several researches have looked at making synthetic polymer mimics containing Dopa moieties by functionalizing synthetic polymers with Dopa and various catecholic derivatives, resulting in functional adhesive polymers which have strong adhesive properties along with the ability to cure rapidly. Dopa or catechol functionalized polymers have been prepared by the following three general strategies.

1.8.1) Direct functionalization of polymers with Dopa:

Catechol such as Dopa and dopamine can be directly coupled to polymers with functional groups such as -NH_2, -COOH, and -OH, through the formation of amide, urethane, and ester linkages [60-62] (**Figure 1.6**). This strategy has been used to successfully functionalize polymers, such as poly (ethylene glycol) (PEG), with different polymer architectures (linear, branched) by conjugating catechol as a terminal functional group. Different architectures of PEG have also been combined with polymers such as polycaprolactone (PCL) and polypropylene oxide (PPO) polymers to form

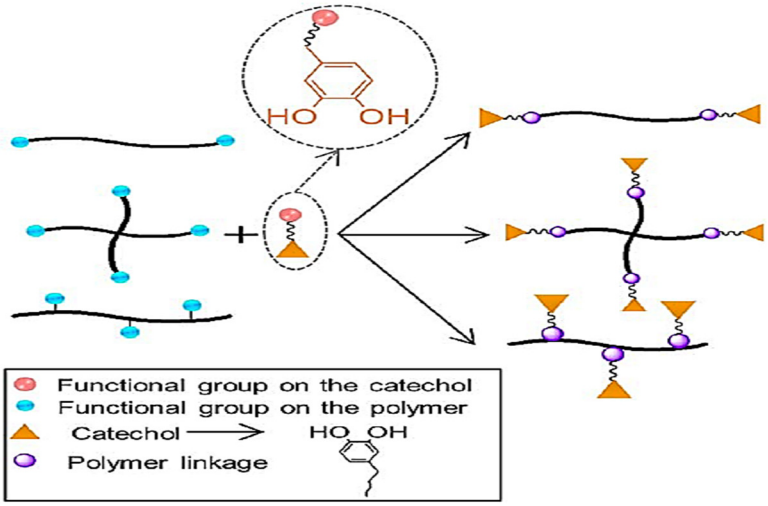

Figure 1.6: Strategies of creating dopa containing polymers of different configurations by direct functionalization of dopa into the polymers.

block copolymers, which can be further grafted with catechol onto the polymer chains [62-64]. Other polymers such as poly (methyl methacrylate) and poly(methacrylate) as well as polyurethane have also been utilized to combine with PEG polymers and catechol grafts. In addition, acid- or amine-functionalized catechol can be covalently attached to biopolymers such as dextran, chitosan, hyaluronic acid, gelatin, and alginate to form bioadhesives [65-68].

1.8.2) Polymerization of catechol-modified monomers:

Dopamine methacrylamide (DMA) is a catechol containing monomer which can undergo free radical polymerization when activated by heat or light to form acrylate-based polymers (**Figure 1.7**) [44]. DMA has been combined with other monomers such as oligomeric ethylene glycol,

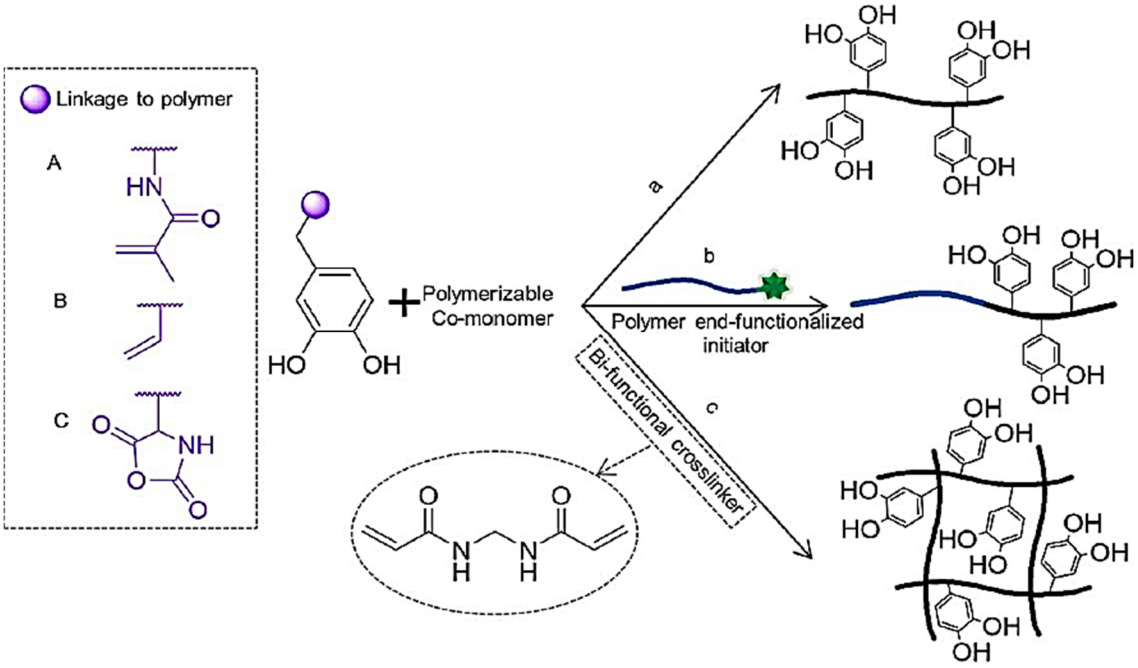

Figure 1.7: Polymerization of Catechol modified monomers. Catechol modified with polymerizable methacrylate (a), vinyl (b), and N-carboxyanhydride (c).

monoacryloxyethyl phosphate, and methoxyethyl acrylate to form dopamine grafted polymers with varying catechol contents [69-71]. Similarly, catechol containing vinyl groups like 3,4-dihyroxystyrene, 4-vinylcatechol acetonide, and 3-vinylcatechol acetonide can also be polymerized with monomeric styrene to produce polystyrene based catecholic polymers [72, 73]. A three dimensional polymer network has also been shown to be formed via copolymerization with a bi-functional crosslinker like *N*,*N*′-methylenebisacrylamide to form a network with catechol covalently tethered to its backbone [74].

1.8.3) Catechol-functionalized initiator to polymerize synthetic monomers:

Polymers with adhesive groups functional at the end can be synthesized using catechol modified initiators (**Figure 1.8**). Several groups have used this approach to create polymers such as polystyrene, poly(*N*-isopropylacrylamide), and poly (*tert*-butyl acrylate) whose ends have been

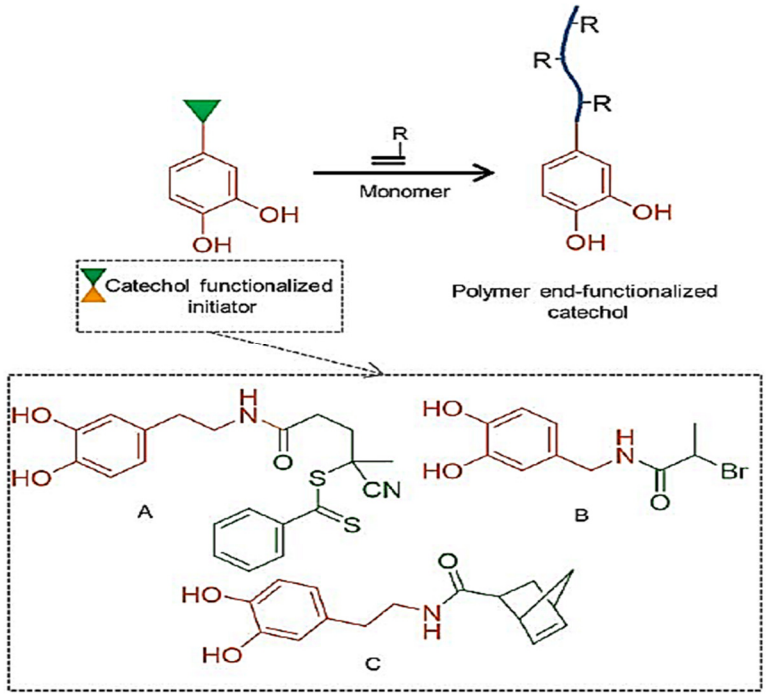

Figure 1.8: Catechol functionalized initiators to prepare catechol end terminated polymers. A) RAFT initiator, B) ATRP initiator. C) ROMP initiator

modified with a catechol moiety using dopamine functionalized with a reversible addition-fragmentation chain transfer (RAFT) agent [75, 76]. Further, alkyl bromine functionalized catechols have been used as initiators in atom transfer radical polymerizations (ATRP) to synthesize poly(mathacrylate) and poly(acrylate)-based polymers [77, 78].

Using the three synthesis strategies described above (**Figure 1.6-1.8**) many research groups have attempted to formulate mussel inspired tissue adhesives with varying dopa contents and adhesive strengths. A compilation of these mussel inspired formulations and their maximum reported adhesion strengths are summarized below in Table 3.

Table 1.3: Polymeric Mussel-Inspired Adhesives along with their Crosslinking Conditions and Maximum Reported Adhesion Strengths.

Adhesive	Adhesion Test	Test Substrate	Crosslinker	Cure time/ Condition	Reported Adhesion Strength	Reference
polytripeptide (Gly-Tyr-Lys)	shear adhesive test	porcine skin	tyrosinase	37 °C, 30 min	11.56 kPa	[79]
MAP (130 kDa)	surface tensiometer	porcine duodenal mucosa	tyrosinase	films dried under N_2	90 Pa	[80]
MAP	end-to-end	porcine skin	tyrosinase	humid, 48 h	0.95 ± 0.19 MPa	[81]
PEG-DOPA	lap shear	porcine skin	periodate	37 °C, 24 h	35.1 ± 12.5 kPa	[82]
HA/Pluronic hydrogel	tensile bonding strength	mouse skin	periodate	RT, 5 min	7.18 ± 0.93 kPa	[83]
catechol-Ala-Ala-PEG (cAAPEG)	lap shear	decellularized porcine dermis	periodate	RT, 2 h	30.4 ± 3.39 kPa	[84]
poly ((Lys.HBr)$_x$-(DOPA)$_y$)	lap-shear	porcine skin	ferric citrate	dry, 25 °C, 12 h	0.21 ± 0.10 MPa	[85]
deacetylated chitosan; oxidized and DOPA-	end-to-end	bovine cortical bone	ferric citrate	wet, 37 °C, 3 h	0.31 MPa	[86]

functionalized dextran						
PEG-dopamine-PCL	lap shear	bovine pericardium	$NaIO_4$	(1) RT, 2 h, (2) PBS, 37 °C, 1 h	107 ± 24.7 kPa	[87]
poly (AA-*co*-AANHS-*co*-MDOPA)	lap shear	porcine skin	thiol-PEG	RT, 10 min	~11.8 kPa	[88]
AbAf iCs	lap shear	porcine SIS	sodium (meta) periodate	humid chamber, 2 h	168.15 ± 17.02 kPa	[89]
iCMBA	lap shear	porcine, acellular SIS	sodium (meta) periodate (PI)	humid chamber, 2 h	123.2 ± 13.2 kPa	[61]
Click iCs	lap shear	porcine, acellular SIS	$CuSO_4$, sodium L-ascorbate; periodate	humid chamber, 2 h	223.11 ± 15.94 kPa	[90]
EGAMA-DOPA	lap shear	glass	UV-PVA	25 °C, 24 h	0.32 MPa	[91]
poly(dopamine-*co*-acrylate) (PDA)	lap shear	porcine skin	horseradish peroxide (HRP)	RT, 1 day	76 ± 13.4 kPa	[92]
*r*fp-1 (MAP)	lap shear	porcine skin	$FeCl_3$	2 h, in buffer soln (pH 8.2)	~130 kPa	[93]

LAMBA	lap shear	porcine skin	irradiation with dental curing lamp for 60 s	RT, 2 h, PBS	72.2 ± 3.7 kPa	[94]
PEU (poly (CA-Tyr-*co*-Leu))	lap shear	porcine skin	$Bu_4N(IO_4)$	RT, 24 h	9 kPa	[95]
PEU (poly (CA-Ser- *co*-Leu-*co*-PPG))	lap shear	porcine skin	$Bu_4N(IO_4)$	wet, RT, 4 h	10.6 ± 2.1 kPa	[96]
POEC-d (octanediol, PEO, citric acid, dopamine)	lap shear	porcine skin	sodium periodate	humid chamber, 2 h	33.7 kPa	[97]
DCTA (gelatin macromer, Fe^{3+}, genipin)	lap shear	porcine skin	$FeCl_3$ + genipin	37 °C, 2 h	24.7 ± 3.3 kPa	[98]
DOPA-functionalized polyester	lap shear	porcine skin	$Fe(acac)_3$	RT, 30 s	13.13 ± 1. 74 kPa	[99]
4-arm-PEG-DA and 4-arm-PEG-PBA	lap shear	porcine skin	$Fe(acac)_3$	RT, 30 min	5.2 ± 0.28 kPa	[100]
polypeptide-pluronic-polypeptide	lap shear	porcine skin	HRP	RT, 24–25 h	106 kPa	[101]

Abbreviations:

MAP, mussel adhesive protein. Tyr: tyrosine; Lys: lysine, Gly: glycine, DOPA: L-3,4-dihydroxyphenylalanine. PEG: poly (ethylene glycol).H: hyaluronic acid, Ala: alanine, PCL: polycaprolactone, AA: acrylic acid; AANHS: acrylic acid *N*-hydroxysuccinimide ester, MDOPA: *N*-methacryloyl-3,4-dihydroxy-L-phenylalanine. iCMBA: injectable citrate-based mussel-inspired bioadhesives.DAM: dopamine acrylamide; NIPAAm: *N*-isopropylacrylamide. LAMBA: light-activated mussel protein-based bioadhesive. PEU: poly (ester urea); CA: catechol. $Bu_4N(IO_4)$: tetrabutylammonium periodate. Ser: serine; PPG: poly (propylene glycol). Fe(acac): iron (III) acetylacetonate. PBA: phenyl boronic acid; DA: dopamine. HRP: horseradish peroxide.

In conclusion, mussels have figured out a way to form tenacious bonds with any substrate irrespective of the presence of water, but the synthetic mimics discussed here are far from the actual mussel adhesives in terms of adhesive performance in hydrophilic conditions. Furthermore, UV irradiation, photoinitiators, and strong oxidizing agents are used in the curing of these adhesives, which could be toxic to healthy cells around the application site and are therefore currently only suitable for topical applications. This creates an urgent need for tissue adhesives with strong adhesion, which can be used inside the body.

1.9) Overview of Research Project

This research project has been designed to develop mussel-inspired degradable nanocomposite materials for sticking tissues together. The long-term goal and specific aims of this project are described in detail below:

1.9.1) Goals/objectives

The **long-term goal** of this project is to develop **a mussel inspired tissue adhering degradable nanocomposite hydrogel for tissue interfacing and wound healing applications**.

Tissue adhesion is a challenging engineering problem and a number of research groups and published works in recent times have attempted to adopt different strategies like extraction of mussel proteins, recombinant hybrids of proteins, or DOPA/catechol functionalization of polysaccharides and synthetic polymers to develop mimics of mussel adhesives. These adhesives have demonstrated to work very well under dry conditions; however, a significant drop in adhesive strength is generally observed under wet tissue conditions where significant humidity and moisture are involved. Currently, there is not a strong tissue adhering adhesive biomaterial that is versatile enough to be used for tissue engineering applications liken tissue interfacing, prolapse treatment and wound healing. An ideal material would possess strong tissue adhesion, degradability, biocompatibility, antibacterial activity and ability to deliver growth factors for the proper healing of wounds. Thus, the final objective of this research is to develop novel mussel-inspired nanocomposite hydrogels that can stick strongly to tissue and possess antibacterial activities for tissue adhesion and wound healing applications.

1.9.2) Specific aims

As a first step towards achieving our long-term goal of developing effective mussel inspired tissue adhering nanocomposite biomaterials, the following three specific aims have been proposed:

1. **To synthesize and characterize a mussel inspired tissue adhering nanocomposite glue.**

2. **To investigate the effects of sizes, concentrations, types of nanoparticles as well as polymers on the tissue adhesiveness of the mussel-inspired nanocomposite glues.** The effects of various nanoparticles on the adhesion properties of mussel-inspired polymers developed in Aim 1 will be performed. The effects of sizes, concentrations and types of nanoparticles on the tissue adhesiveness of the mussel inspired nanocomposites will also be determined.
3. **To develop an antimicrobial tissue adhering nanocomposite glue for wound healing applications.**

1.9.3) Innovative aspects

There are several innovative aspects to this research. Firstly, this work has attempted to use biodegradable PLGA based nanoparticles to enhance the adhesion of mussel inspired hydrogels and study the adhesion profiles of such prepared nanocomposites. Up till now such an approach to use nanoparticles to enhance adhesion of mussel-inspired hydrogels hasn't been reported. The results would aid in future research in development of nanocomposite mussel-inspired glues.

1.9.4) Successful outcome

The successful completion of this research will assist in the design and development of mussel inspired nanocomposite hydrogel systems which have superior tissue adhesion compared to the current mussel inspired hydrogels. Popular bioadhesives, such as fibrin, cyanoacrylate and albumin–glutaraldehyde-based materials, have been applied for clinical applications in wound

healing, drug delivery, and bone and soft tissue engineering; however, their performances are limited by weak adhesion strength and rapid degradation. The nanocomposite glues developed in this research will be able to provide a strong adhesive, which is easily prepared, can degrade at a controlled rate and is biocompatible for *in vivo* use. Furthermore, the development of antibacterial adhesive systems will help immensely in wound healing applications.

Chapter 2

Synthesis and characterization of Tissue Adhering Nanocomposite Glues

2.1 Introduction

Tissue adhesives in biomedical research are being developed to replace surgical suturing and stapling of tissues that are more invasive in nature, sometimes require secondary surgeries for removal, cause infections in some cases, and damage to surrounding tissues during the procedure [102]. These adhesives are mainly employed as glues to hold tissues together, as hemostatic agents to control or stop bleeding, or as sealants to close tissue openings or defects [102, 103]. Many of these adhesives are made from either biologically derived or synthetic materials. Biologically derived fibrin glues mimicking the last stage of the physiological coagulation cascade, and synthetic cyanoacrylates are currently the most used tissue adhesives. However, despite having a short curing time and being biodegradable, fibrin glue is not a strong tissue adhesive and has the potential to cause immunogenic responses in the host. The cyanoacrylate-based adhesives can cause tissue toxicity although they demonstrate higher adhesive strength and slow degradation behavior over time [104, 105].

Several approaches have been developed to improve the adhesion strength of bioadhesives. One strategy was to utilize conjugating amino acids onto the backbones of carbohydrate or polyester based polymers to enhance adhesion properties [106]. Other efforts have focused on biomimetic approaches, such as gecko-inspired adhesives [107] or spider silk based adhesives [108] which mimic the nanotopography of gecko limbs or spider silk to adhere to substrates. The gecko or spider silk inspired adhesives, however, only show good adhesion under static and dry conditions [107, 108]. The adhesion strategy employed by some marine creatures such as the blue mussel Mytilus edulis [93, 106, 109, 110] is a popular biomimetic approach being currently exploited for synthesizing tissue adhesives [92, 94, 111] [109, 112-114]. The strong adhesion ability of the

mussels is attributed to a catechol containing amino acid called L-3,4-dihydroxyphenylalanine (L-Dopa) found in the structure of secreted mussel adhesive foot proteins. L-Dopa is responsible for various bonding interactions in the form of bidentate hydrogen bonding, π-π interactions and complex formation with metal and metal oxides and oxidative cross-linking via oxidation to dopa-quinone which have been pointed out as key mediators of mussel adhesion.[50] Mussel-inspired adhesives incorporating either L-Dopa or dopamine onto polymeric backbones have thus being synthesized as tissue adhesives with low to moderate adhesiveness on tissues.[98, 101, 114-121] The major limitations of such mussel-inspired adhesives are that the mechanisms underlying L-Dopa mediated adhesion remain unclear and the chemical nature of the mussels adherence to inorganic and organic substrates has not been fully characterized [50].

Additionally, it has been shown that silica nanoparticles can be used to glue non-adhering gels, with possible applications to glue tissues *in vivo*.[122] These nanoparticles increased the adhesion of tissues *in vivo* via their ability to adsorb onto polymer chains and form bridges between two connecting structures. Nanoparticles may also offer excellent potential to function as mediators of adhesion between two surfaces because of their small sizes and high aspect ratios. Thus, we hypothesized that if the nanoparticles and mussel- inspired hydrogels were combined, the nanocomposite might exhibit synergistic effects and achieve a high adhesive strength towards tissues. Furthermore, because the silica is non-degradable, we selected biodegradable polymer nanoparticles, such as poly(lactide-co-glycolide) (PLGA). Until now, this attractive material design has not been reported.

Specifically, in this work, we explored a combination of hydrogels made of dopamine functionalized alginate and PLGA based nanoparticles to improve tissue-tissue adhesion through catechol reaction with tissues and nanoparticle/tissue/hydrogel interaction (**Figure 2.1**). In addition, N-

hydroxysuccinimide (NHS) was grafted onto the PLGA nanoparticle surface, which can react with the amino groups of proteins in tissues to further enhance the adhesive. The grafted dopamine content of the polymer, and morphology and degradation rates of these nanocomposites were characterized. The adhesive strength of the material was measured using a porcine skin-muscle

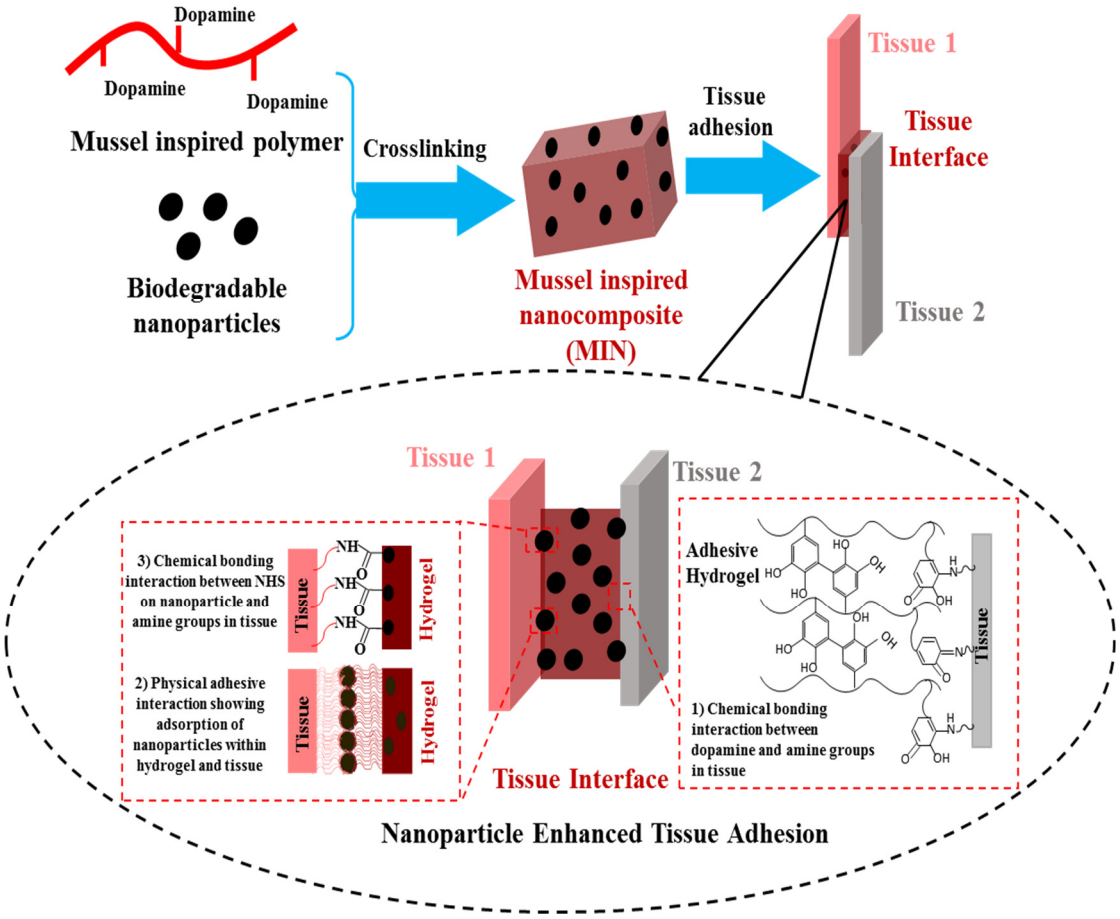

Figure 2.1: . Illustration to glue two tissues using mussel-inspired nanocomposites (MIN). The three interactions between tissues and nanocomposite adhesive might exist to enhance the adhesion. They included that 1) oxidized dopamine molecules in the hydrogel react with amine groups in tissues, 2) the tiny nanoparticles interact with both hydrogel and tissue through physical adsorption, and 3) the NHS groups on the PLGA nanoparticles can covalently react with amine groups in the tissue.

interface *ex vivo* model. The *in vitro* cytocompatibility and *in viv*o tissue compatibility of the materials were evaluated using human dermal fibroblasts and a rat model, respectively.

2.2). Experimental Section

2.2.1) Materials: Sodium alginate (molecular weight (MW)=12-40 kDa), sodium metaperiodate (PI), dopamine hydrochloride, sodium cyanoborohydride, polyvinyl alcohol (PVA, MW=31 kDa), N-hydroxysuccinimide (NHS), 1-ethyl-3-(3-dimethylaminopropyl)carbodiimide, (EDC) phosphate buffered saline (PBS), silica nanoparticle (LUDOX TM-50), and 4-morpholineethanesulphonic acid (MES) were purchased from Sigma-Aldrich, Inc, MO. Poly(lactide-co-glycolide) (PLGA, COOH terminated, lactide/glycolide molar ratio =50:50, and MW= 97 kDa) was purchased from Akina PolySciTech, Inc. All chemicals were used as received without further purification.

2.2.2) Synthesis of mussel-inspired polymers: Sodium alginate was oxidized by using periodate aqueous solution.[123] Sodium alginate (1% w/v in deionized water, 90 ml) was reacted with sodium metaperiodate (PI) (10% w/v in deionized water, 10 ml) for a period of 12 hours in the dark. The reaction was then subjected to dialysis (molecular weight cut-off (MWCO) 3.5kDa) against deionized water and subsequently lyophilized to obtain oxidized alginate. The oxidized alginate (0.2 g in deionized water, 14 ml) then reacted with dopamine hydrochloride (0.28 g in deionized water, 6 ml) in the presence of sodium cyanoborohydride ($NaBH_3CN$, 25 mM) for 24 h in a dark setting and under a nitrogen protection. The obtained mussel-inspired polymer was purified via dialysis (MWCO 3.5 kDa) against deionized water at 4°C and subsequently lyophilized.

2.2.3) Fabrication of PLGA nanoparticles and NHS modified PLGA nanoparticles: The PLGA nanoparticles were fabricated using emulsion methods. [21] A PLGA solution (2% w/v in dichloromethane, 5 ml) was added dropwise to a PVA solution (5% w/v in deionized water, 20 ml). This emulsion was sonicated (30 W, 5 minutes) and then stirred overnight at room temperature to allow solvent evaporation and particle formation. The resulting particle suspension was centrifuged

(15,000 rpm, 30 min, 10 °C) and the pellet suspension in deionized water was lyophilized to obtain PLGA nanoparticles.

To modify the PLGA particles with NHS, PLGA nanoparticle suspension (0.2 % w/v, 5 ml) in MES buffer (pH 4.75) was mixed with EDC (120 mg, 0.63 mmole) for 30 minutes at room temperature. NHS (180 mg, 1.56 mmole) was then added to the solution and allowed to mix for 2 hours at room temperature to graft NHS onto the surface of PLGA nanoparticles. The NHS modified PLGA nanoparticles (PLGA-NHS) were purified by centrifugation (15,000 rpm, 30 minutes, 10°C), then subsequently washed with deionized water and lyophilized.

2.2.4) Fabrication of mussel-inspired nanocomposites (MIN): The alginate-dopamine polymer at different concentrations was cross-linked using the cross-linker PI at equimolar concentrations with respect to the dopamine amount in the polymer. Briefly, alginate-dopamine polymer at concentration of 40 % w/v was mixed with 1X PBS (pH 7.2) to prepare a polymer precursor solution. Known amounts of the polymer precursor solution (1, 5, 20 and 40%) were then mixed with a nanoparticle suspension in 1X PBS solution. The nanoparticle concentration was fixed as 12.5% w/v in the composite. The polymer-nanoparticle mixture was then cross-linked using PI for 1 h. Equal moles of PI (0.29, 1.48, 5.95, 11.90 %w/v), with respect to the dopamine content in the alginate-dopamine polymer, were used for cross-linking and to form MINs.

2.2.5) Mussel-inspired polymer characterization: The synthesis of oxidized alginate (Alg-Ox) and mussel-inspired polymer was confirmed by Fourier transform infrared spectroscopy (FTIR). The grafting efficiency of dopamine to Alg-Ox was measured by UV-Visible spectrometry utilizing the absorbance at 280 nm of the aromatic ring in dopamine. [19] The absorbance data from a set of dopamine hydrochloride standards ranging from 0 to 1 mg/mL was used to determine the dopamine concentration in a 1 mg/mL Alg-Dopa solution (n=8). For hydrogel degradation, mussel inspired

polymer was mixed in PBS (pH 7.2) at a final concentration of 40%w/v and crosslinked using PI (11.90% w/v) for 1 hour. This cross-linked hydrogel was then immersed in a tube containing 1 ml PBS (n = 6). At predetermined time points each of the tubes were centrifuged (9,000g, 10 min) to collect the hydrogel. This collected hydrogel was lyophilized to achieve the dry hydrogel. The weight of this dry hydrogel (W_t) was recorded and compared with the initial dry weight (W_0) to calculate the % weight remaining using $W_t/W_o \times 100\%$.

2.2.6) Nanoparticle characterization: The hydrodynamic size and polydispersity of the PLGA, PLGA-NHS, and silica nanoparticles were measured via dynamic light scattering technique (DLS) (Brooke Haven, ZETA PALS). Nanoparticle solutions (0.01 % w/v in DI water) were used for this DLS analysis. The grafting of NHS onto PLGA nanoparticles was confirmed via FTIR (Thermo Electron Corporation, NICOLET 6700). The nanoparticles were also observed under high resolution transmission electron microscopy (HR-TEM, Hitachi H-9500).

2.2.7) Nanoparticle cytocompatibility: The cytocompatibility of silica, PLGA and PLGA-NHS nanoparticles was evaluated using human dermal fibroblasts (HDFs, ATCC). HDFs were seeded at a density of 10,000 cells/cm^2 into wells of a 24 well plate (n = 8) and incubated in Dulbecco's Modified Eagle Medium (DMEM, Sigma Aldrich) supplemented with 10% (v/v) fetal bovine serum (FBS, Life Technologies) and 1% (v/v) penicillium-streptomycin (Life Technologies, Inc.) at 37 ^oC and 5% CO_2 for 24 h. Nanoparticles at concentrations of 50, 100, 200, 500, 1000 µg/ml were then incubated with the cells for 24 h. An MTS assay (CellTiter 96® aqueous one solution cell proliferation Assay, Promega, Madison, WI) was performed according to manufacturer's instructions to assess cell viability. The HDFs exposed to culture media only served as a control.

2.2.8) Mussel-inspired nanocomposite characterization: The cross-sectional morphologies of nanocomposites were examined using scanning electron microscopy. A 40 % w/v solution of the

mussel-inspired polymer in PBS (pH 7.2) was combined with a 12.5% w/v solution of the nanoparticles and cross-linked using PI at a final concentration of 11.9%w/v for 1 hour. The cross-linked samples were immersed in liquid nitrogen and cut at cross-section. The frozen cross-sections were freeze-dried and imaged under a scanning electron microscope. For nanocomposite degradation, the mussel-inspired nanocomposites (MIN) containing silica, PLGA and PLGA-NHS nanoparticles were formulated using methods as described above, and the measurement protocol is the same as hydrogel degradation method.

2.2.9) Tissue adhesion strength measurement: The tissue adhesion of the mussel-inspired nanocomposites and the mussel-inspired polymer was tested on porcine skin and muscle samples (n=6) using guidelines from the American Society for Testing and Materials (ASTM) standard F2255-05. Freshly obtained porcine skin and muscle were cut into sections (30mm × 10mm × 3mm), and the mussel-inspired polymer at concentrations ranging from 1 to 40% (w/v) in PBS (pH 7.2) with or without the incorporation of nanoparticle suspensions (12.5% w/v) was allowed to cross-link on an area of 10 mm × 5 mm between the skin-muscle interface for a period of 1 hour at 37°C. To ensure the skin-muscle samples were moist and retained water, the skin-muscle interface was kept in a humid environment in a standard cell culture incubator, maintaining humidity levels greater than 90% during the incubation time. The samples were then subjected to lap shear adhesion tests on an MTS insight workstation (cross-head speed of 10 mm min^{-1}; 500 N load cell; room temperature), and then the lap shear strength was measured. The same parameters of MTS testing were also used to measure the changes in tissue adhesion of the mussel-inspired polymer over a 24-hour time period by measuring the lap shear strengths of the mussel-inspired hydrogel and the nanocomposites at predetermined time points.

2.2.10) Nanocomposite cytocompatibility: The HDFs were used to determine cytotoxic effects of the Alg-Dopa alone and the mussel-inspired nanocomposite systems (MINs). The HDFs were seeded at a density of 10,000 cells/cm^2 into the wells of a 24 well plate (n = 8) and incubated in DMEM supplemented with 10% (v/v) fetal bovine serum (FBS) and 1% (v/v) penicillium-streptomycin at 37 $^{\circ}$C and 5% CO_2 for 24 hours. These seeded cell culture plates were then used to determine the cytotoxicity of the leached products of Alg-Dopa and MINs as well as to study the effects of the incubation of these systems on the cells.

The leached products were formulated using the systems (40% w/v polymer and 12.5% w/v nanoparticles) as described above, UV sterilized and incubated them in a known amount of DMEM cell culture medium at different dilutions (1X, 5X, 10X, 100X) at 37 $^{\circ}$C and 5% CO_2 for 24 hours. Post incubation, all solutions were neutralized to pH 7.2 and added to the seeded HDFs for a period of 24 hours. MTS assays were performed on each group after the 24-hour time-point following manufacturer's instructions. The cell culture medium only and Matrigel were used as controls to compare with the viability of HDFs exposed to treated groups. The Matrigel was prepared at a concentration of 1% w/v and applied to the Transwell plates at a volume to surface area ratio of 50 $\mu L/cm^2$.

To assess the cytotoxicity of incubated hydrogels and nanocomposites, the formulated systems post UV sterilization were also placed in Transwell inserts (Pore size: 0.4 µm, growth area: 0.14 cm^2). These inserts were then placed into the cell pre-seeded 24-well plates for 24 h. MTS assays were performed in each group following manufacturer's instructions. Viability of HDFs in each group was assessed compared to the culture media alone and Matrigel.

2.2.11) Ex vivo tissue penetration depth of nanocomposites:

The different groups of MINs and the Alg-Dopa alone were cross-linked within the skin-muscle tissue interfaces for 1 hour. The adhered tissue samples were then embedded in optimal cutting temperature solutions (OCT, Tissue-tek) and frozen at -20 °C for 1 hour. The OCT embedded tissue samples were then cut into slices (10 µm thick). Image analysis was performed on the sections (n = 10) of each group of MINs and the Alg-Dopa using Image J (National Institute of Health, Bethesda, MD, USA). A baseline indicated by the white horizontal lines (**Figure 2.5A**) was chosen, and it represented the original contact between the muscle-skin and the glue. The glue penetration depth was measured based on this baseline.

2.2.12) In vivo nanocomposite biocompatibility:

All animal experiments were conducted in accordance with the animal welfare and IACUC approved protocols from the University of Texas at Arlington. Sprague-Dawley male rats (Taconic Biosciences), one year old and weighing 300-500 g, were used to test the biocompatibility of the nanocomposite adhesive. The MIN-PLGA-NHS was tested *in vivo* with suture as a control. Four incisions (1-inch-wide × 0.5-inch-deep) were made on the back of each rat (n = 4). Two of these incisions were closed by the application of the nanocomposite adhesive, while the other two were closed with silicone treated non-absorbable sutures (4-0 SILK, Davis+Geck). The rats were sacrificed at day 7 and 28, and the implants with surrounding tissues were isolated for histological analysis. The sections were embedded in OCT, and 10 µm thick cryosections were cut for analysis. Hematoxylin and eosin (H&E) staining was performed to evaluate the interaction of the nanocomposite with the host tissue at the site of implantation. Immunohistochemistry analysis using rabbit anti-integrin αM CD11b, H-61 (Santa Cruz Biotechnology, inc Santa Cruz, CA, USA) antibodies against CD11b+ cells were performed on the tissue cryosections at day 7 and 28 to

evaluate inflammatory responses in the tissue sealed by the adhesive and the suture control. The cellular infiltration into the tissue areas was quantified by calculating the number of cells per unit area using ImageJ (National Institute of Health, Bethesda, MD, USA). The tissue areas for cell counting were selected randomly around the incision site.

2.2.13) Statistical Analysis: All data analysis was executed using one-way and two-way ANOVA (Statview 5.0 software, SAS institute, Cary, NC, USA) to analyze differences between groups with one or more independent variables. $p < 0.05$ was considered as significant difference. *Post hoc* analysis was done using Tukey's honest significant difference (HSD). All data was reported as mean ± standard deviation.

2.3. Results and Discussion

2.3.1 Synthesis and characterization of mussel-inspired polymer

The mussel-inspired polymer was synthesized in an aqueous environment by conjugating dopamine with the oxidized alginate through a reductive amination between amine and aldehyde groups. Firstly, the alginate polymer was oxidized using sodium metaperiodate to generate aldehyde groups on its backbone.[124] Secondly, the dopamine was grafted onto the alginate backbone via reductive amination between the aldehyde groups and the amine groups of dopamine. The FTIR spectrum (**Figure 2.2 A**) of sodium alginate has specific peaks at 1404 cm^{-1} and 1596 cm^{-1}corresponding to symmetric and asymmetric COO stretching vibrations, respectively. Other peaks identified for alginate were located at 1023 cm^{-1} (C-O-C stretching vibration), 946 cm^{-1} (C–O stretching vibration of uronic acids), 890 cm^{-1} (C_1–H deformation mannuronic acid residues), and 820 cm^{-1} (mannuronic acid residues).[125] The chemical structure of periodate oxidized alginate was confirmed by aldehyde C=O stretching at 1720 cm^{-1} in the oxidized alginate spectrum. The alginate-dopamine polymer structure was verified by C=C aromatic stretching and C-N amine stretching at 1520 cm^{-1} and 1091 cm^{-1}, respectively**.** [126] The dopamine content in mussel foot proteins (Mfps) varies from 10-15 % in Mfp-1, 2-4% in Mfp-2, 25% in Mfp-3, 5% in Mfp-4 and 30% in Mfp-5 whereas Mfp-3 and Mfp-5 are the proteins that contact the surface and help mussels adhere to wet surfaces.[127]

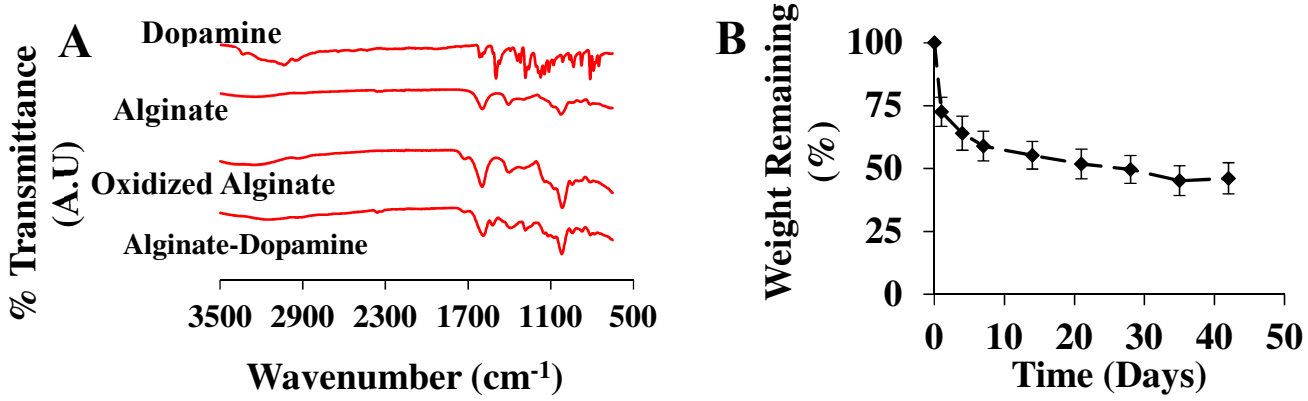

Figure 2.2: Physical characterization of Alginate-Dopamine polymer. (A) FTIR spectras of oxidized alginate and alginate dopamine polymers. **(B)** Degradation profile of alginate-dopamine hydrogel crosslinked using PI in 1x PBS solutions (pH 7.2)

Some research groups reported that the dopamine contents incorporated into alginate ranged from 10% to 42%.[66, 126, 128-130] The wide range of dopamine grafting is achieved by altering the molar ratios of alginate to dopamine. The UV-visible absorption spectroscopy at 280 nm of the alginate-dopamine polymer revealed a dopamine content of 26%, which is close to the dopamine content in Mfp-3, and also is within the range of dopamine content reported in other dopamine conjugated alginate polymers.[66, 126, 128-130]

2.3.2 Nanoparticle characterization:

The size and polydispersity of PLGA nanoparticles and N-hydroxysuccinimide (NHS) modified PLGA (PLGA-NHS) nanoparticles were characterized using dynamic light scattering and transmission electron microscopy. The PLGA nanoparticles (212 ± 45 nm) were fabricated using a single-emulsion method. The size of PLGA-NHS was 237 ± 106 nm, which is similar to the size of PLGA NPs. The silica nanoparticles (35 nm) were commercially purchased. FTIR was used to confirm the grafting of NHS onto PLGA nanoparticles. The PLGA structure was verified by specific peaks at 2910 cm^{-1} and 2940 cm^{-1} (symmetric and asymmetric C-H stretching), 1730 cm^{-1} (C=O stretching vibration), 1170 cm^{-1} (C-C-O stretching of ester group) and 1090 cm^{-1} (O-C-C stretching of ester group).[131, 132] For PLGA-NHS nanoparticles, the specific peaks to identify PLGA-NHS conjugation were located at 1778 cm^{-1} (symmetric imide C=O stretching in NHS), 1700 cm^{-1} (asymmetric imide C=O stretching in NHS and ester C=O stretching vibration in PLGA) and 1560 cm^{-1} (N-O stretching in NHS).

2.3.3 Mussel-inspired nanocomposite (MIN) formation

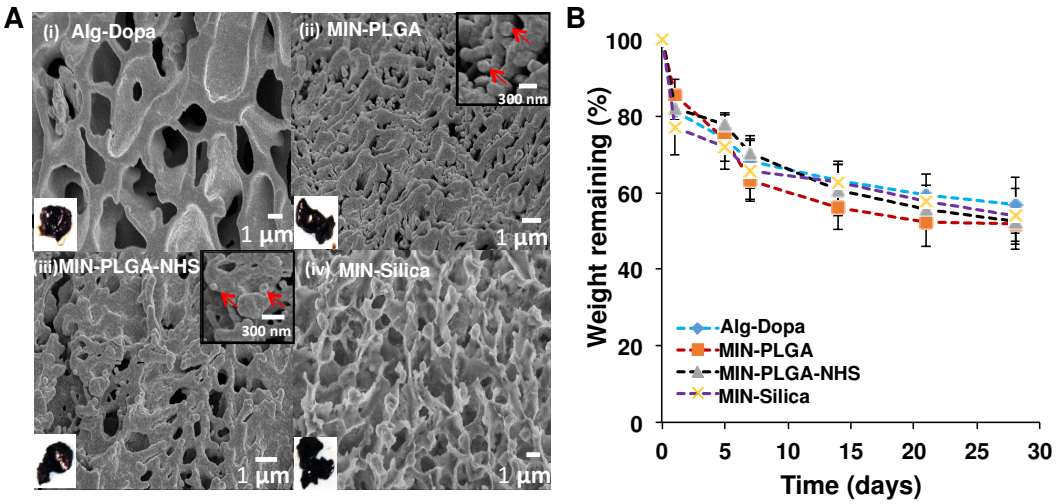

Figure 2.3: Mussel-inspired nanocomposite (MIN) morphology. (A) Including SEM images of: (i) Alg-Dopa hydrogel alone, (ii) MIN-PLGA, (iii) MIN-PLGA-NHS, and (iv) MIN-Silica. Left bottom insets showed macroscopic views of the hydrogel and nanocomposites. Right top insets in (ii) and (iii) showed magnified images of the nanocomposites and red arrows pointed to the embedded nanoparticles. **(B)** *In vitro* degradation curves of mussel-inspired nanocomposites in PBS at 37°C up to 28 days.

The mussel-inspired nanocomposites (MINs) were prepared by blending a range of concentrations from 1 to 40% (w/v) of the mussel-inspired polymer in PBS with PLGA (MIN-PLGA), PLGA-NHS (MIN-PLGA-NHS) or Silica (MIN-Silica) nanoparticles using sodium metaperiodate (PI) as a cross-linker. The nanoparticle concentration was fixed at 12.5% (w/v). The hydrogel from the mussel-inspired polymer (Alg-Dopa) was used as a control. The nanocomposites were dark brown and hydrogel-like, which was the same as the Alg-Dopa. Scanning electron microscopy images of the nanocomposites revealed embedded nanoparticles in MIN-PLGA and MIN-PLGA-NHS groups (**Figure 2.3 A**). But it is hard to observe the silica nanoparticles due to the small size (30nm). Compared to the morphology of the hydrogel alone without nanoparticles, the nanocomposites appeared more connected and less porous.

2.3.4 In vitro degradation of MIN

The periodate oxidation of the alginate leads to a change in conformation of uronate groups in alginate from closed to open chained.[133] This change in conformation makes the oxidized alginate more susceptible to hydrolysis in aqueous solutions thus conferring degradability to it.[124, 133] This degradation of the MINs was characterized by incubation in phosphate buffered saline (PBS, pH 7.2) at 37 ℃. The nanocomposites demonstrated a loss of dry weight over time indicating their degradability. The composites degraded to an extent of 53±1% over a period of 4 weeks (**Figure 2.4 B**). The degradation rate of the oxidized alginate hydrogels depends on the oxidation degree and the molecular weight of the polymer. Previous studies on the degradation of oxidized alginate hydrogels (molecular weight 270 kDa) in DMEM cell culture media showed 20% loss in dry mass over a period of 4 weeks.[134] Our results exhibited a faster degradation for the alginate-dopamine hydrogel, which may be attributed to the lower molecular weight (12-40 kDa) of alginate used in this work.[134] The incorporation of nanoparticles slightly increased the degradation rate of the nanocomposite. This could be due to the degradable nature of the PLGA nanoparticles. Furthermore, their acidic degradation products, such as lactic acid and glycolic acid, can reduce the surrounding pH and may cause the alginate hydrogel to degrade to a greater extent.[135, 136] However, the nanocomposites containing silica nanoparticles demonstrated similar degradation kinetics with the nanocomposites with PLGA NPs. It might be attributed to the diffusion of some tiny nanoparticles into the PBS when the nanocomposites were immersed in PBS during the period of degradation. High-speed centrifuge might not be able to collect all nanoparticles in the PBS. The possible diffusion, however, might not take place for tissue adhesion in tissues because the diffusion coefficient might be different in solid and/or soft tissues than that of the solution environment.

2.3.5 Ex vivo adhesion strength of mussel-inspired nanocomposites

The ability of the nanocomposites in gluing tissue interface was evaluated using a setup illustrated in **Figure 2.4 A**. The lap shear strengths of tissue adhesiveness of the cross-linked polymer at the tissue interface showed a concentration-dependent increasing trend. Previous studies have utilized the mussel-inspired approach to introduce dopamine or L-Dopa into polymers and form adhesive hydrogels, which adhere to tissues with various strengths depending on their dopamine contents.[54, 98, 121, 137] Our mussel-inspired hydrogel at a concentration of 40 %w/v adhered to the pig skin-muscle interface with a lap shear strength of 14 ± 2 kPa, which is comparable to adhesives developed in other studies using the mussel-inspired approach.[54, 98, 115, 121, 137] Furthermore, the adhesive properties of the nanocomposites demonstrated a significant increase in lap shear strengths compared to those without nanoparticles ($p<0.05$). The highest lap shear strength of 33 ± 3 kPa (**Figure 2.4 B**) was obtained in the 40% (w/v) Alginate-Dopa with PLGA-NHS nanoparticles. The role of nanoparticles in adhering tissues together was attributed to their ability to adsorb onto surfaces and dissipate energy within the interface which yields resistance to fracture propagation between the two tissue phases.[122] Recently, silica nanoparticles were investigated as a means to adhere liver tissues and gels together where silica nanoparticles could bond two non-adhering surfaces with an adhesive lap shear strength of 0.65±0.25 kPa.[122] Although the nanoparticle alone as a gluing agent provides an attractive method to glue tissues together, the adhesive strength is much lower compared to mussel adhesive hydrogels.[54, 98, 115, 121, 137] The MIN offered improved tissue adhesion performances over nanoparticles alone and mussel inspired hydrogel alone. The adhesive properties of these composites over a 24-hour period increased over time in all

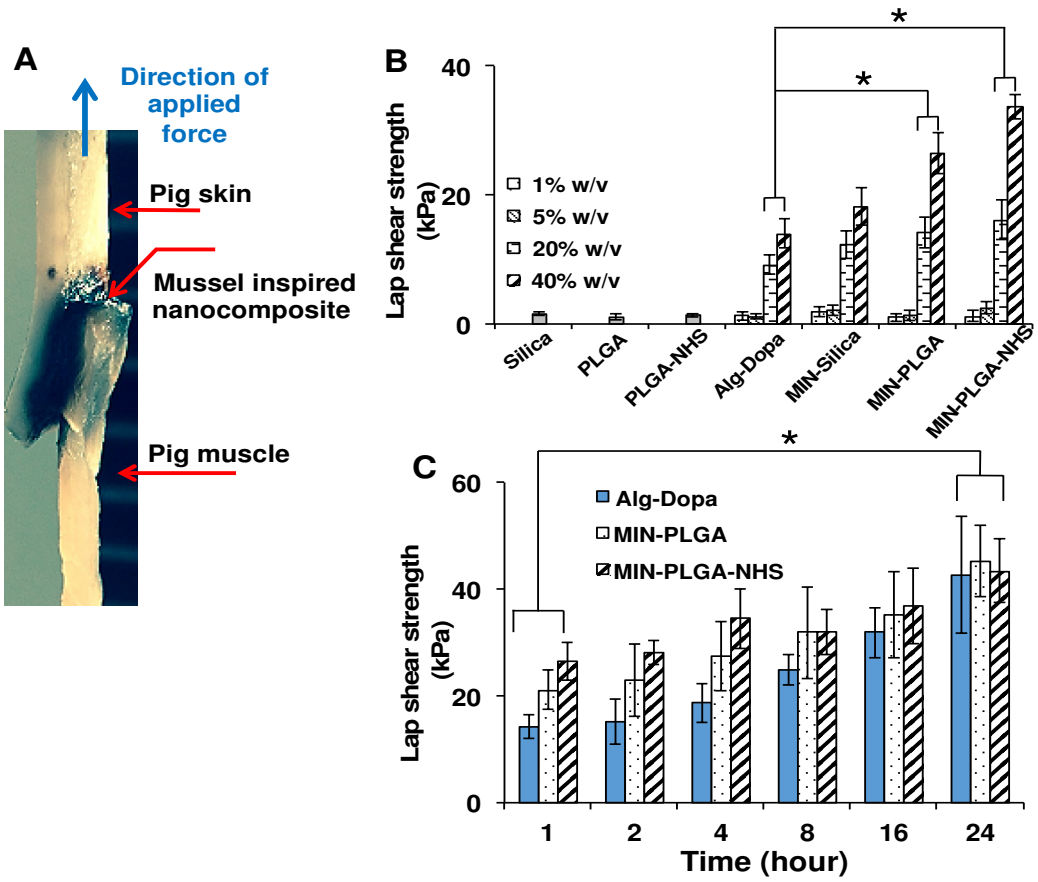

Figure 2.4: Adhesive properties of nanocomposites. (A) Digital image of an adhered skin-muscle Interface (40% w/v, MIN-PLGA-NHS). **(B)** Tissue adhesion strength of adhesives for porcine skin-muscle interface. **(C)** Time dependent adhesion strength of adhesives (Alg-Dopa concentration 40% w/v) on porcine skin-muscle interfaces.

groups. It is noted that the nanoparticle-mediated enhancement of adhesion was significant within the first 1 hour of cross-linking and tended to saturate over time. There was no significant difference in additional adhesion strength observed among the mussel-inspired hydrogels and the mussel-inspired nanocomposites at 24 hours. The penetration profile of the nanocomposites was tissue specific with more penetration into the muscle layer compared to the skin layer. It was observed that the inclusion of nanoparticles led to less penetration of the nanocomposites into the muscle tissue compared to that of the hydrogel alone. MIN-PLGA and MIN-PLGA-NHS had lower penetration into the muscle tissue compared to the adhesive alone (**Figure 2.5**). Hydrogel materials designed to be used as tissue adhesives require characteristics of both fluidity and cohesive strength to function

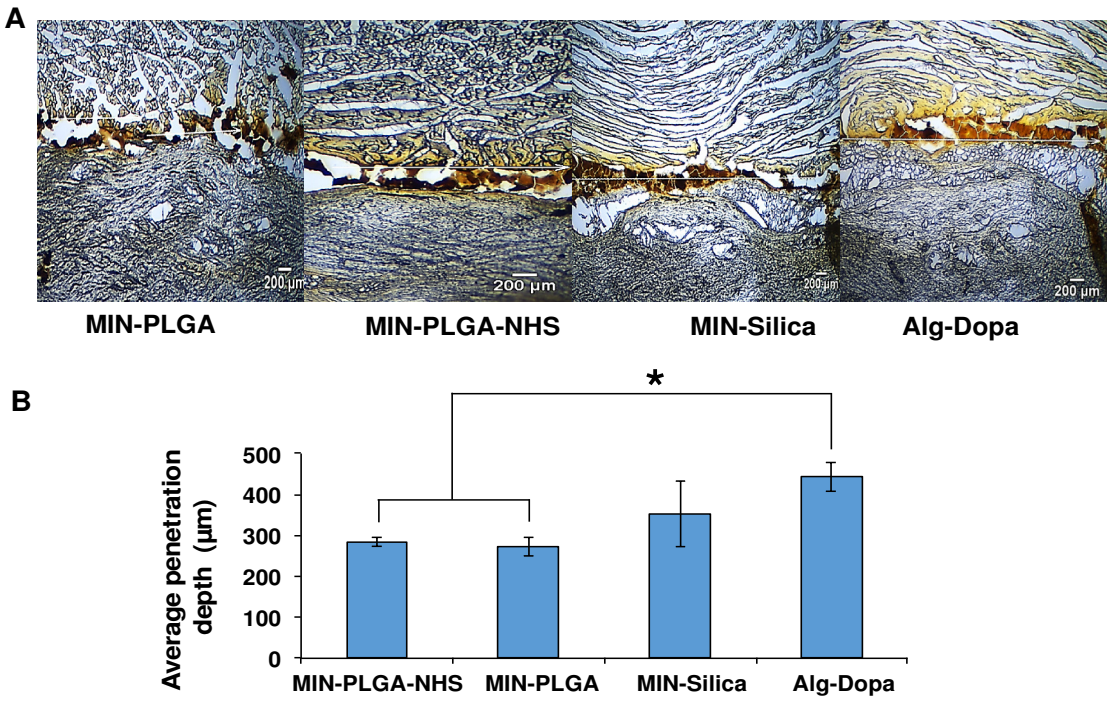

Figure 2.5: Penetration depth of nanocomposites into skin-muscle tissue. (A) Micrographs of porcine skin-muscle tissue interface showing the extent of penetration of the nanocomposites into tissues. **(B)** Quantification of the mean penetration of the nanocomposites into the skin and muscle tissue using ImageJ analysis.

as an optimal adhesive.[138, 139] The addition of PLGA and PLGA-NHS nanoparticles might increase the cohesiveness of alginate-dopamine hydrogels, which led to the hydrogel solution diffuse less into the tissues. This increase in cohesiveness may also explain the increase in adhesive strengths of PLGA and PLGA-NHS nanocomposites compared to alginate-dopamine hydrogels alone. It was reported that the inclusion of 2% laptonite into poly(acrylic acid) polymer networks resulted in increased cohesion in the hydrogels which correlated to increased adhesion to organic substrates.[140] In addition, for the PLGA-NHS group, the NHS on the nanoparticles can react with the amine groups on the tissue surface, which may limit nanoparticle and hydrogel penetration into the tissues.

2.3.6 In vitro cell compatibility of nanocomposite system

We tested several dilutions (1X, 5X, 10X, 100X) of the cell media that was incubated with the nanocomposites for 24 hours. The nanocomposites with PLGA and PLGA-NHS nanoparticles exhibited good cell compatibility to human dermal fibroblasts. Compared to the positive control Matrigel, the leached products at 1X dilution from the hydrogel alone and all composites showed less cell viability, while the 5X, 10X, 100X dilutions of the hydrogel alone, the MIN-PLGA and MIN-PLGA-NHS exhibited similar cell viability ($p>0.05$) (**Figure 2.6A**). However, the MIN-Silica showed moderate toxicity at all dilutions of the leachable contents (**Figure 2.6A).** In **Figure 2.6B**,

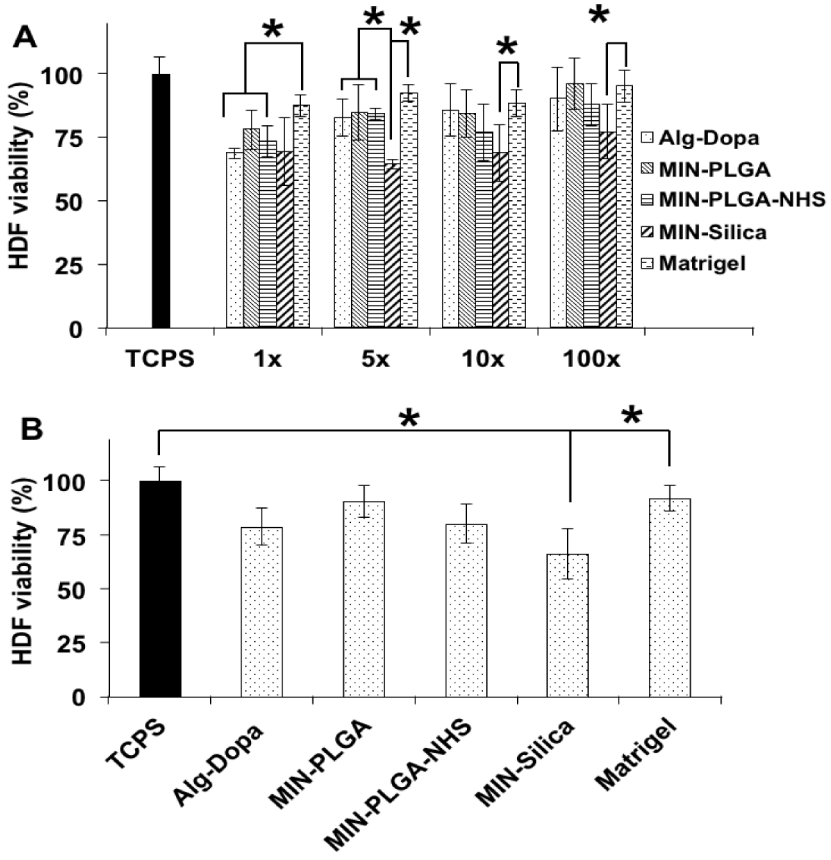

Figure 2.6: Cytocompatibility of mussel-inspired nanocomposites (MIN) with human dermal fibroblasts (HDFs). **(A)** Leachable products cytotoxicity at leachate dilutions of 1x, 5x, 10x, 100x. **(B)** Adhesive cytocompatibility with human dermal fibroblasts using a Transwell setup

only MIN-Silica exhibited less cell viability than the controls of the Matrigel and cell culture medium alone. No significant toxicity with PLGA and PLGA-NHS nanoparticles on human dermal fibroblasts was observed, whereas silica nanoparticles demonstrated a dose-dependent toxicity towards the cells. We have previously reported the PLGA nanoparticles showed good cytocompatibility with human dermal fibroblasts, human aortic endothelial cells and human aortic smooth muscle cells up to a concentration of more than 500 µg/ml, which is in agreement with the observed result in this study.[141, 142] The silica nanoparticles exhibit size-dependent cell toxicity towards various human cell lines including dermal fibroblasts.[143-146] The size of silica nanoparticles that induces toxicity usually ranges from 20-60 nm which could explain the toxicity of the 30 nm silica nanoparticles used in this study.[145]

2.3.7 In vivo biocompatibility of nanocomposite system

To further evaluate the *in vivo* biocompatibility of the nanocomposites, the MIN-PLGA-NHS was selected because of its high adhesive strength and good *in vitro* cytocompatibility. Incisions on the back of rats were successfully sealed by the nanocomposite of MIN-PLGA-NHS with the suture as a control (**Figure 2.7A**). At day 7 and day 28, the explanted tissue sections were evaluated for foreign body reactions or immune responses via Hematoxylin and Eosin (H&E) staining and immunohistochemistry analysis. The H&E staining revealed the sutured sections had healed completely both at day 7 and 28 (**Figure 2.7B**). The tissue areas filled with the MIN-PLGA-NHS showed cell infiltration and material degradation at day 7, and subsequent clearance of the composite with no residues of the composite visible at day 28. The immunohistochemical analysis revealed the presence of $CD11b^+$ inflammatory cells in the excised tissue sections around the areas sealed with the nanocomposite glue and the control suture at day 7 (**Figure 2.7C**). The area sealed with MIN-PLGA-NHS had slightly more inflammatory cells compared to the suture control. This could be

because alginate-based materials are generally known to have low immunogenic responses.[147]

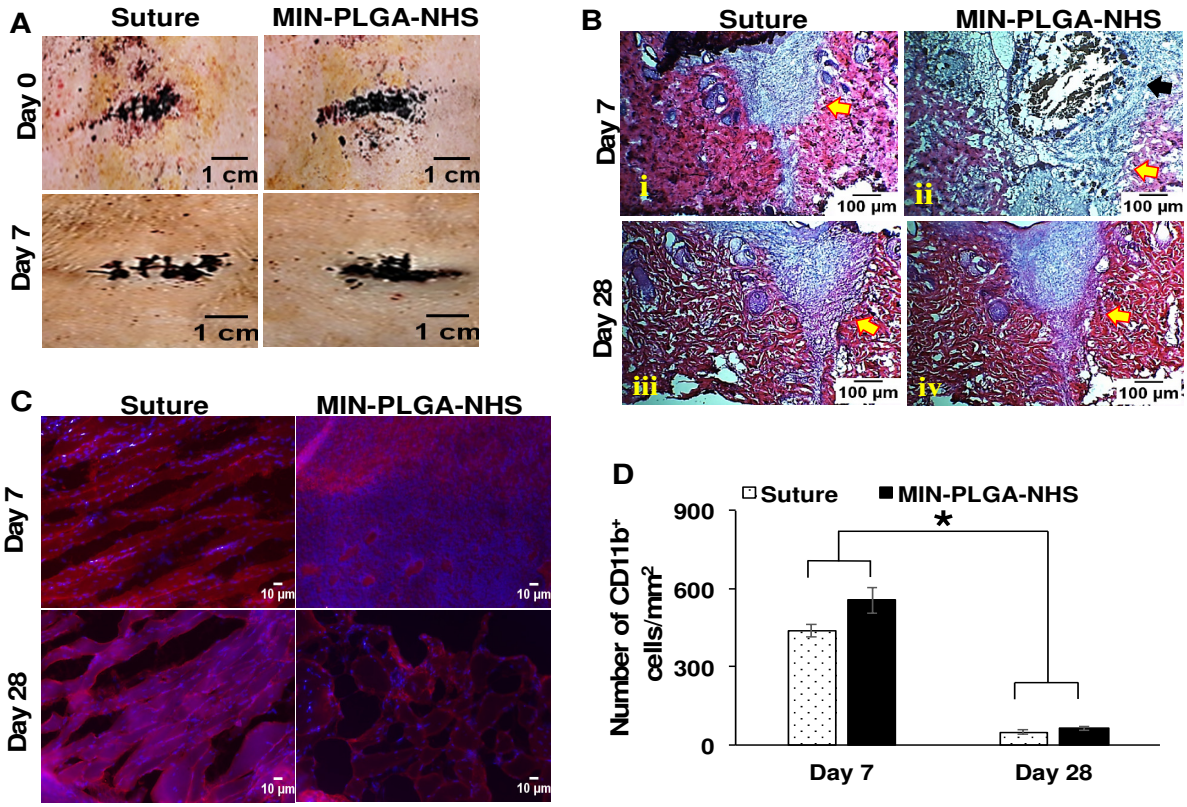

Figure 2.7: *In vivo* biocompatibility of mussel-inspired nanocomposites with PLGA-NHS nanoparticles (MIN-PLGA-NHS) **(A)** Micrographs of areas sealed by PLGA-NHS nanocomposites and the ones sutured on the back of Sprague-Dawley rats at Day 0 and Day 7 **(B)** H&E staining of wound areas that were sutured and adhered with MIN-PLGA-NHS at day 7 and day 28. **(C)** Immunohistochemistry staining of macrophages in tissue sections. **(D)** Quantification of number of cd11b$^+$ cells per millimeter square area near the tissues adhered with MIN-PLGA-NHS and the suture.

Alginate has been shown to activate macrophages in a murine model via activation through the NF-κB pathway, leading to the production of interleukins including IL-1β, IL-6, IL-12 and TNF-α, and the promotion of a pro-inflammatory environment.[148] Some studies have shown that the foreign body reaction towards alginate-based materials varied depending on the content of glucuronic acid, and the higher content (>60%) induced greater foreign body responses.[149-151] The alginate used in this study had less than 50% glucuronate residues, which could achieve the low foreign body response. The H&E stained tissue sections of the area sealed by the MIN nanocomposite showed

some evidence of gel fragments at day 7 (**Figure 2.7B**). These gel fragments in the micrometer size can possibly activate phagocytes leading to further inflammatory conditions in the tissue.[152] In such cases MΦ macrophages are mainly responsible for sustaining this pro-inflammatory environment.[152] However the presence of inflammatory cells markedly subsided over the course of 28 days in both the suture and the nanocomposite groups, indicating a normal wound healing process. There was no significant difference in the number of $CD11b^+$ cells between the tissue sutured and the one sealed with the MIN-PLGA-NHS (**Figure 2.7C-D**), indicating that the nanocomposite did not generate any lasting inflammatory reaction, Furthermore, the inclusion of PLGA-NHS nanoparticles into the alginate hydrogel did not alter the immunogenicity of alginate hydrogels.

4. Summary

In summary we successfully synthesized mussel inspired nanocomposite glues (MINs) by incorporating biodegradable nanoparticles into cross-linked alginate-based mussel-inspired hydrogels. The tissue adhesive properties of the hydrogels were enhanced by blending nanoparticles. The PLGA-NHS nanoparticles performed best to enhance hydrogel adhesion between skin-muscle tissues compared to the silica and PLGA nanoparticles. The adhesive properties of the nanocomposites increased over time within the tissue interface. The degradable adhesive nanocomposites were cytocompatible and exhibited a lower penetration into the pig muscle than that of the hydrogel alone. The in vivo implantation of MIN-PLGA-NHS did not generate significant inflammatory responses. This biodegradable and biocompatible nanocomposite with high adhesive ability may be a suitable candidate for adhering tissue interfaces as a bio-glue in wound closure.

Chapter 3

Enhanced tissue adhesive strength of hyaluronic acid-based nanocomposites and polydopamine nanoparticles

3.1) Introduction

There have been many different approaches to improve the tissue adhesion of synthetic bioadhesives as summarized in chapter 1 relating to the development of mussel inspired polymers. The blending of nanoparticles with hydrogels can create composite materials with unique and potentially useful properties caused by synergistic enhancement of each component caused by their union that are not found in the individual components, giving rise to new materials with diverse applications in varying fields of electronics, catalysis, biosensing, drug delivery as well as biomedical applications [153]. Properties imparted to the composites depend on the types of nanoparticles incorporated and their interactions with the hydrogel materials. In chapter 2, we explored this combination of PLGA nanoparticles with mussel inspired alginate-dopamine hydrogel and found a synergistic increase in adhesive strengths of hydrogels upon blending of the nanoparticles.

The medical adhesive field over the recent years has been innovating to produce different alternatives to current synthetic tissue adhesives to replace their unfavorable cytocompatibility and adhesion profiles. For example, the development of poly (glycerol sebacate acrylate) based laser crosslinked tissue adhesive for blood vessel surgeries is an approach in improving the cytocompatibility profiles of synthetic adhesives like cyanoacrylates and polyurethanes [154]. Subsequent research in nature inspired adhesion strategies like mussel inspired polymeric hydrogels containing catechol groups like Dopa has gained widespread attention, and has yielded improved tissue adhesives with higher adhesion strengths to tissue and favorable cytocompatibility compared to the synthetic analogs [44, 92, 97, 112, 155, 156] [61, 157]. Furthermore, biomimetic nanostructured polymeric materials inspired by gecko's foot adhesion are also gaining attention

for development of tissue adhesives [102]. However, with respect to these recent approaches, research in nanoparticle incorporated surgical glues has been demonstrated as being the most promising approach [102]. This interest in nanoparticles as tissue glues has been spurred mainly by the findings relating the ability of silica and iron oxide nanoparticles to form strong bonding with tissues [158].

The blending of such nanoparticles with hydrogels to create nanocomposites could be an attractive approach to create superior adhesives. Properties imparted to the composites would depend on the type of nanoparticles incorporated and their interaction with the hydrogel material. We have previously explored the combination of PLGA nanoparticles with mussel inspired alginate-dopamine hydrogels and found a synergistic increase in adhesive strengths of hydrogels upon blending of the nanoparticles.

The ability of dopamine to self-polymerize under aqueous conditions to form thin polydopamine films has been extensively studied [159, 160]. Polydopamine films have intrinsic adhesive properties due to its ability to bond to surfaces via non-covalent interactions such as hydrogen bonding, aromatic π- π interactions and metal chelations. This intrinsic adhesive ability of polydopamine can be utilized in improving the tissue adhesion of mussel inspired polymers. Thus, in this chapter, we explore the combination of polydopamine nanoparticles with mussel inspired hydrogels and investigate the effect of these nanoparticles on the tissue adhesion strengths of these hydrogels. We specifically investigate the sizes, concentrations, and types of nanoparticles on the adhesive strengths of mussel inspired nanocomposites

3.2) Experimental Section

Materials: Ssodium metaperiodate (PI), dopamine hydrochloride, sodium cyanoborohydride, polyvinyl alcohol (PVA, MW=31 kDa), N-hydroxysuccinimide (NHS), 1-ethyl-3-(3-dimethylaminopropyl)carbodiimide, (EDC) phosphate buffered saline (PBS), silica nanoparticle (LUDOX TM-50), and 4-morpholineethanesulphonic acid (MES) were purchased from Sigma-Aldrich, Inc, MO. Poly(lactide-co-glycolide) (PLGA, COOH terminated, lactide/glycolide molar ratio =50:50, and MW= 97 kDa) was purchased from Akina PolySciTech, Inc. Sodium hyaluronate (HA) (MW: 151-300KDa) was purchased from Life Core Biomedical, MN. All chemicals were used as received without further purification

3.2.1) Synthesis of polydopamine nanoparticles:

Nanoparticle synthesis was carried out in water-alcohol mixed solvent using a mixed solvent oxidation protocol [160]. Briefly a 40 ml water: ethanol mixed solvent was prepared at ethanol: water percentages of 10% (v/v) or 50% (v/v). Aqueous ammonium hydroxide was added into this mixed solvent system at final percentages 0.25 or 2 %. The pH of the solution was then set either to 7 or 9, followed by the addition of dopamine hydrochloride (0.5 mg/ml or 2 mg/ml). The final reaction was then allowed to proceed for 30 hrs at a stir rate of 1200 rpm. After the reaction was complete, the nanoparticles were centrifuged at 15000 rpm for 30 minutes using a Hitachi ultracentrifuge and washed with DI-water. The purified particles were then suspended in DI water solutions and freeze dried. Subsequently the dried particles in a 0.1 % w/v in DI water were used for sizing via Dynamic Light Scattering (DLS).

3.2.2) Tissue adhesion strength measurement of polydopamine nanoparticles: The tissue adhesion of the polydopamine nanoparticle was tested on porcine skin and muscle samples (n=6) using guidelines from the American Society for Testing and Materials (ASTM) standard F2255-05. Freshly obtained porcine skin and muscle were cut into sections (30mm × 10mm × 3mm), and

various sizes of polydopamine nanoparticles (100-1000 nm) suspensions at concentrations of 12.5 % (w/v) in PBS (pH 7.2) were allowed to cross-link using sodium meta periodate (PI) at a final concentration of 11.9%w/v, on an area of 10 mm × 5 mm between the skin-muscle interface for a period of 1 hour at 37°C. To ensure the skin-muscle samples were moist and retained water, the skin-muscle interface was kept in a humid environment in a standard cell culture incubator, maintaining humidity levels greater than 90% during the incubation time. The samples were then subjected to lap shear adhesion tests on an MTS insight workstation (cross-head speed of 10 mm min^{-1}; 500 N load cell; room temperature), and then the lap shear strength was measured. The testing of 200 nm polydopamine nanoparticles in the concentration ranging from 5 to 50% (w/v) in PBS (pH 7.2) were also carried out using the same PI concentration and the conditions as described above.

3.2.3) Synthesis of mussel inspired hyaluronic acid dopamine polymer:

A mussel-inspired hyaluronate-based polymer (HA-Dopa) was synthesized by grafting dopamine onto a sodium hyaluronate backbone (HA) (MW: 151-300KDa, LifeCore Biomedical, MN) under aqueous conditions using EDC-NHS carbodiimide chemistry [68]. Briefly 300 mg of HA was dissolved in 30 ml MES (pH 6.2), and the solution was later nitrogen purged for 30 mins, subsequently 493 mg EDC and 291 mg NHS were added to the solution, that was nitrogen purged for 30 min, and 0.5 g Dopa was dissolved in 2ml MES (pH 6.2) and added to this HA solution. The solution was nitrogen purged again for 30 min and covered with a foil and stirred for 12-16 hrs. The post reaction solution was dialyzed (MWCO 3500 Da) against DI water for 24 hours. The dialyzed solution was lyophilized to obtain the HA-Dopa polymer.

3.2.4) Mussel-inspired hyaluronic acid dopamine polymer characterization:

The synthesis of hyaluronic acid-dopamine (HA-Dopa) polymer was confirmed by Fourier transform infrared spectroscopy (FTIR). The grafting efficiency of dopamine to the polymer was measured by UV-Visible spectrometry utilizing the absorbance at 280 nm of the aromatic ring in

dopamine [19]. The absorbance data from a set of dopamine hydrochloride standards ranging from 0 to 1 mg/mL was used to determine the dopamine concentration in a 1 mg/mL HA-Dopa solution (n=8).

3.2.5) Tissue adhesion strength measurement of mussel inspired hyaluronic acid dopamine polymer and nanocomposites*:* mussel-inspired HA-Dopa polymer at concentrations ranging from 1 to 40% (w/v) in PBS (pH 7.2) with or without the incorporation of PLGA, PLGA-NHS and polydopamine nanoparticle suspensions (12.5% w/v) was allowed to cross-link using PI (11.9 %w/v) on an area of 10 mm × 5 mm between the skin-muscle interface for a period of 1 hour at 37°C. The same conditions of incubation and lap shear testing as described in section 3.2.2 were applied. To test the effects of varying nanoparticle concentrations on the adhesive strengths of HA-Dopa nanocomposites, the PLGA, PLGA-NHS and polydopamine nanoparticle suspensions in PBS (pH 7.2) were combined with HA-Dopa polymer in PBS (pH 7.2) so that the final concentration of polymer was 40% w/v and the final concentrations of nanoparticles ranged from 0-20%w/v.

To test the effects of various sizes (100-1000 nm) of polydopamine nanoparticles, NP suspensions at concentrations of 12.5 % (w/v) in PBS (pH 7.2) were allowed to cross-link using sodium meta periodate (PI) at a final concentration of 11.9%w/v, on an area of 10 mm × 5 mm between the skin-muscle interface for a period of 1 hour at 37°C. The testing of 200 nm polydopamine nanoparticles in the concentrations ranging from 10-50% (w/v) in PBS (pH 7.2) were also carried out using the same PI concentration and the conditions as described above. The same parameters of MTS testing were also used to measure the changes in tissue adhesion of the HA-Dopa polymer over a 24-hour time period by measuring the lap shear strengths of the mussel-inspired hydrogel and the HA-Dopa-polydopamine nanocomposites at predetermined time points.

3.2.6) HA-Dopa Nanocomposite cytocompatibility: The HDFs were used to determine cytotoxic effects of the HA-Dopa alone and the mussel-inspired nanocomposite gels (formulated using 40% w/v polymer concentration and 12.5% w/v nanoparticle concentration). The HDFs were seeded at a density of 10,000 cells/cm^2 into the wells of a 24 well plate (n = 8) and incubated in DMEM supplemented with 10% (v/v) fetal bovine serum (FBS) and 1% (v/v) penicillium-streptomycin at 37 $^{\circ}$C and 5% CO_2 for 24 hours. These seeded cell culture plates were then used to study the effects of the incubation of these systems on the cells. To assess the cytotoxicity of incubated hydrogels and nanocomposites, the formulated systems post UV sterilization were also placed in Transwell inserts (Pore size: 0.4 µm, growth area: 0.14 cm^2). These inserts were then placed into the cell pre-seeded 24-well plates for 24 h. The cell culture medium only and Matrigel were used as controls to compare with the viability of HDFs exposed to treated groups. The Matrigel was prepared at a concentration of 1% w/v and applied to the Transwell plates at a volume to surface area ratio of 50 µL/cm^2. MTS assays were performed in each group following manufacturer's instructions (Promega, Inc). Viability of HDFs in each group was assessed compared to the culture media alone and Matrigel.

3.2.7) Statistical Analysis: All data analysis was executed using one-way and two-way ANOVA (Statview 5.0 software, SAS institute, Cary, NC, USA) to analyze differences between groups with one or more independent variables. $p < 0.05$ was considered as significant difference. *Post hoc* analysis was done using Tukey's honest significant difference (HSD). All data was reported as mean ± standard deviation.

3.3 Results and Discussion

3.3.1) Size optimization of polydopamine nanoparticles using factorial design:

We used the Design Expert software (Stat Ease) to design a 2 level 4 factor factorial experiment (n =3) and synthesized polydopamine nanoparticles particles according to the designed experimental parameters. We chose a mixed solvent (Ethanol: Water) system for the synthesis of PDA NPs as this solvent system has been shown previously to yield relatively monodisperse nanoparticles and has a greater degree of dopamine conversion to its polymeric form [160].

The analysis of the hydrodynamic sizes of each of the synthesized particles obtained using the designed experimental runs revealed that pH of the reaction, ethanol: water ratio and ammonia: water ratio were significant ($p < 0.01$) factors, with pH and ethanol: water ratio being the most significant of factors strongly effecting the size of polydopamine nanoparticles (PDA NPs) .Interestingly, dopamine concentration and the pH of the reaction had an interaction effect in the way they influenced PDA NP size . The difference in PDA NP size at increasing dopamine concentrations was significantly ($p < 0.01$) greater at pH 7 than at pH 9, indicating that it is easier to fine tune PDA NP size at pH 9 whereas it is possible to drastically change the PDA NP size at pH 7 by varying the dopamine concentration. In addition, the PDA NP size difference between the two pH conditions increased to a greater extent at higher dopamine concentrations than at lower dopamine concentrations. Overall, a basic pH ($pH > 8.0$) of the reaction favored smaller particles, with the smallest particles being formed at higher dopamine concentrations (**Figure 3.1 A**). The increase in ammonia: water ratio (0.25 % -2% v/v) overall lowers the PDA NP size in agreement with previous research on PDA nanoparticle synthesis in mixed solvent systems [160-162]. Moreover, in addition to these previous reports, we also demonstrated that the nanoparticle size lowering trend with increasing ammonia: water ratio is only significant ($p < 0.01$) at lower dopamine concentrations (0.5 mg/ml), in contrast to these observations it has been shown

previously that PDA nanoparticles with sizes ranging from 800-120 nm have been synthesized in similar mixed solvent systems at dopamine concentrations of 3.5 mg/ml by varying ammonia: water ratio from 0.28-1.4 %v/v; however, the pH of these systems is not widely reported which can vary between 9-11 depending on the amount of ammonia added to the reactions [161, 163]. In our results this may be explained by the relation between pH and dopamine concentrations where a higher dopamine concentration and higher pH of 9 leads to smaller nanoparticle size (**Figure 3.1A**). In our analysis using the design expert software, we could also generate a predictive equation (**Equation 3.1**) that relates the size of polydopamine nanoparticles (PDA NPs) to the various significant factors thus providing simulations for reaction conditions that can enable synthesizing a particular size of PDA NPs.This predictive equation was validated by synthesizing PDA NPs using the simulated experimental parameters suggested by the software and measuring the size of nanoparticles using dynamic light scattering (DLS) techniques and electron microscopy analysis (**Figure 3.1B-C**).

$$\left[\textbf{[Sqrt(Particle Size)]}^{-1} = \{ (-0.028567) - [(0.071845) *(\textbf{Dopamine Concentration})] + [(4.53835E003)*(\textbf{Ammonia: Water})] + [(6.88872E-003)* (\textbf{pH})] + [(6.37498E-004)* (\textbf{Alcohol: Water})] + [(9.45342E-003)*(\textbf{Dopamine Concentration})] *(\textbf{pH}) - [(1.54010E-004)* (\textbf{Dopamine Concentration}) *(\textbf{Alcohol: Water})] \}\right] \quad (\textit{Equation 3.1})$$

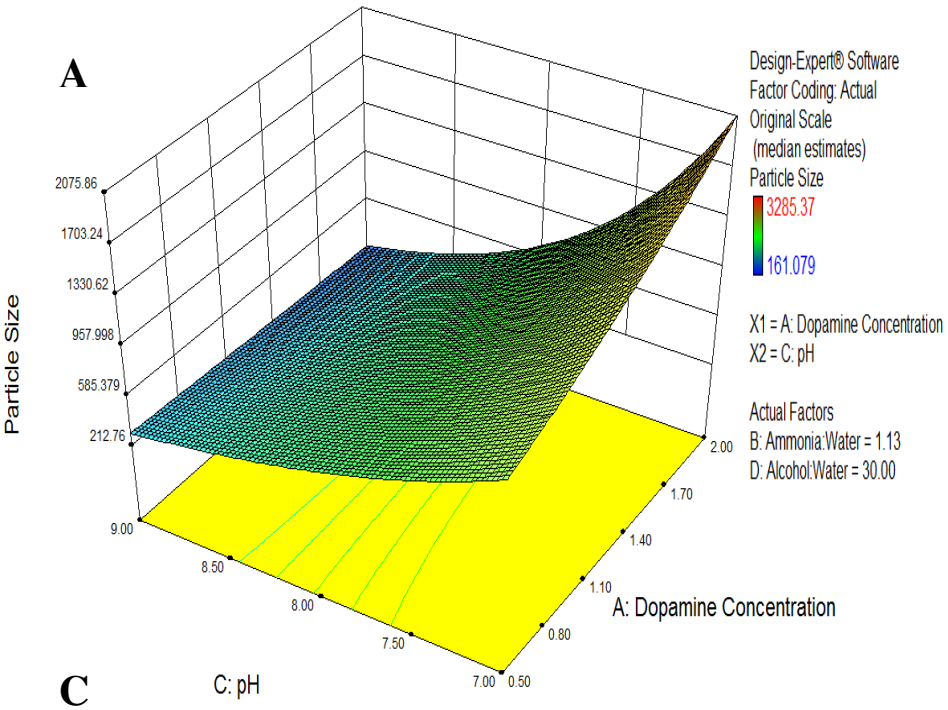

B

Predicted Nanoparticle Size (nm)	Experimental Nanoparticle Size (nm) by DLS
100 nm	150 ± 72
200 nm	223 ± 300
500 nm	501 ± 170
1000 nm	1029 ± 240

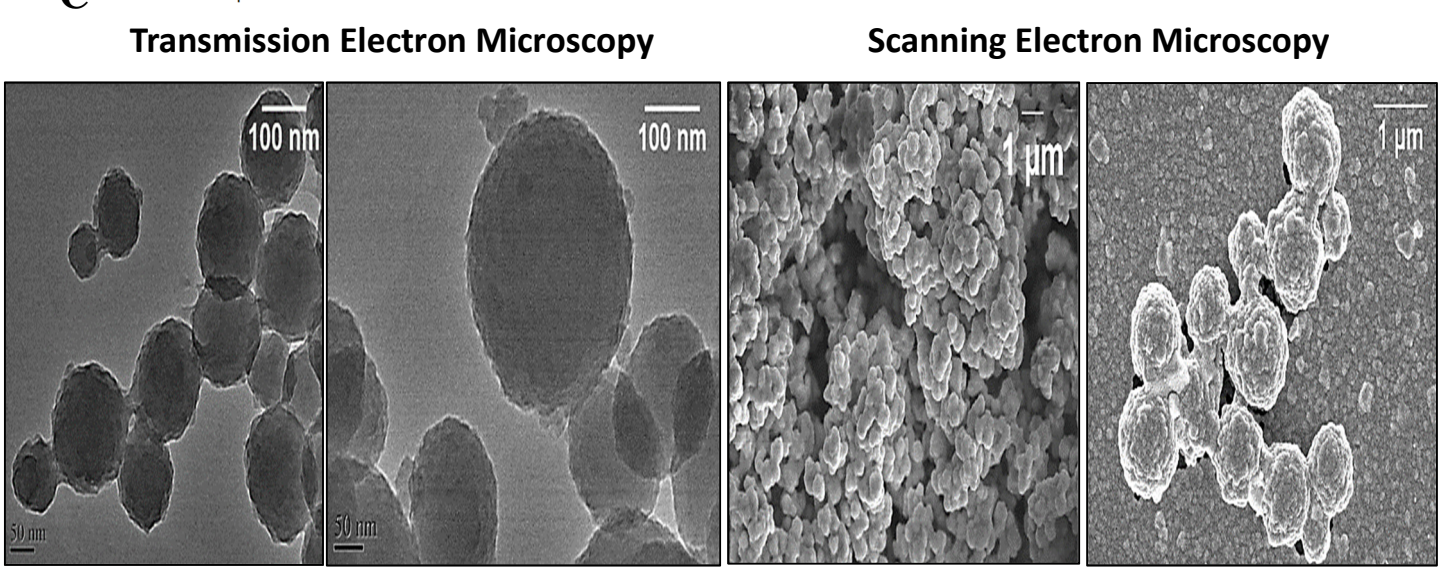

Figure 3.1: Optimization of polydopamine nanoparticles size. **(A)** 3D Plots depicting the effect of pH and dopamine concentration on the polydopamine nanoparticle size. **(B)** Dynamic light scatter measurements of optimized nanoparticle formulations compared to the predicted size. **(C)** Transmission and scanning electron microscopy images of optimized 100 nm, 200 nm, 500 nm and 1000 nm sized particles.

3.3.2) Effects of polydopamine nanoparticle sizes on adhesive strengths:

The lap shear strengths of tissue adhesiveness of polydopamine nanoparticles at the tissue interface showed a size-dependent adhesion trend (**Figure 3.2**). The adhesion of PDA NPs was significantly higher ($p<0.05$), compared to silica and PLGA-NHS nanoparticles a shown in **Figure 3.2**, although the silica and PLGA-NHS nanoparticles were 30 nm and 250 nm in size. Tissue adhesive profiles of polydopamine nanoparticles favored greater adhesion to smaller particles sizes with adhesivity

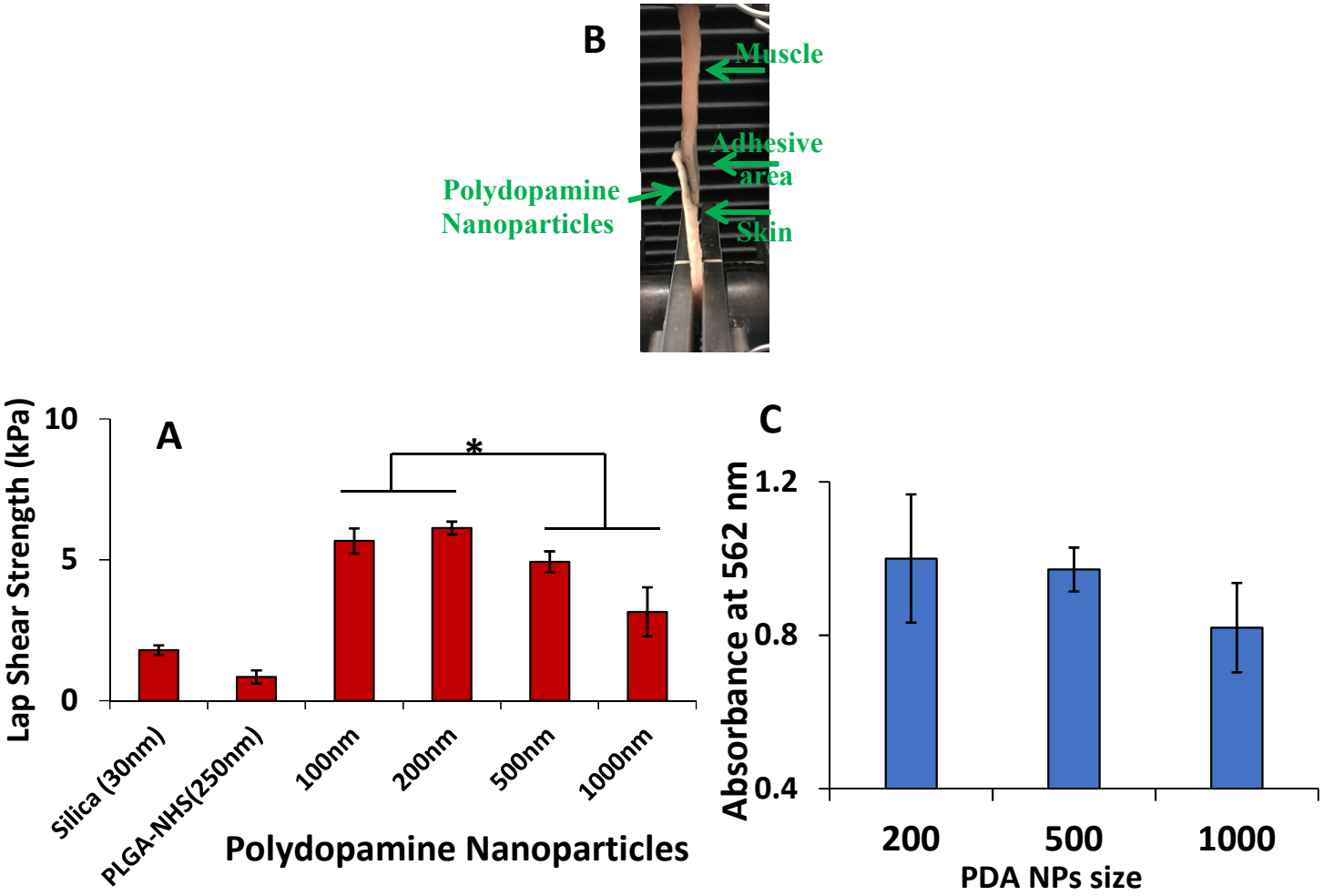

Figure 3.2 Adhesive properties of polydopamine nanoparticles **(A)** Tissue adhesion strength of nanoparticle suspensions (100-1000 nm) (12.5% (w/v)) on porcine skin-muscle interface **(B)** Digital image of an adhered skin-muscle interface (12.5% w/v, 200 nm polydopamine nanoparticle suspension). **(C)** Relative reactive phenol hydroxyl groups on 1% PDA NPs suspensions reprinted as absorbances based on micro BCA assays at 562 nm.

decreasing as size of the particle increased. Several studies detailing the dynamics of single nanoparticle interaction and adhesion on substrates of varying stiffness have reported the work of adhesion to be inversely proportional to the radius of nanoparticles [164-167]. In addition, other repots studying the effects of nanoparticle sizes on cell adhesion also show that smaller sized nanoparticles adhere to cell surfaces to a greater extent than larger sized nanoparticles [168, 169]. Smaller nanoparticles have greater surface area to volume ratios which may contribute to greater adhesivity of 200 nm sized polydopamine nanoparticles relative to 1000 nm sized polydopamine nanoparticles. In contrast, adhesion studies on various particle-substrate interactions including elastic polymeric spherical particles, report the adhesion force to increase in proportion to particle radius [170-172]. However, it is important to note that the particles analyzed in these studies are micron sized particles with sizes greater than 10 μm, which may have different contact profiles with substrates and thus influence adhesion forces. In similar studies of polymeric microparticles adhesion, on substrates it has been reported that particles with sizes less than 5 μm adhered so strongly to substrates that it becomes difficult to un-adhere them using the same kind of applied forces that were used for larger particles (>10 μm), indicating changes in adhesive behaviors when the particle size reaches submicron and nanoscale domains [173, 174].

Adhesion of particle to substrates is a complex process and is highly influenced by many factors such as surface roughness, electrostatic charge of the particle, and vander walls forces to name a few. Given the increase in dominance of these interfacial forces with decrease in particle size [175], the observed increased adhesiveness of smaller sized polydopamine nanoparticles on the porcine skin-muscle interface may be due to the increased interactions of these surface forces with the tissue interface. Our experimental results show that 200 nm polydopamine nanoparticles had the highest tissue adhesion (6.1 ± 1.6 kPa) which did not significantly differ from 100 nm sized

particles, because 100-200 nm polydopamine nanoparticles achieved the highest adhesion, for further studies we selected 200 nm sized particles. The 200 nm polydopamine nanoparticles also showed a concentration dependent increase in adhesion on the pig skin-muscle interface with the adhesion strength increasing significantly up to a polydopamine nanoparticle suspension concentration of 40 % (w/v) (**Figure 3.3**), thereafter there was no significant increase in adhesion with increase in polydopamine nanoparticle concentration. In recent reports, tantalum oxide-silica core shell nanoparticles were shown to be adhesive towards liver tissues and showed a similar concentration dependent increase in adhesion from 0.1-1 kPa with a nanoparticle concentration increase from 10-40 % w/v [176]. Adhesive interactions between polymeric nanoparticles and substrates and their adhesion strengths have been reported to increase in proportion to the number of nanoparticles per unit surface area in contact with the substrate surface [177]. In addition, the number of nanoparticles per unit surface area is directly proportional to the volume fraction or

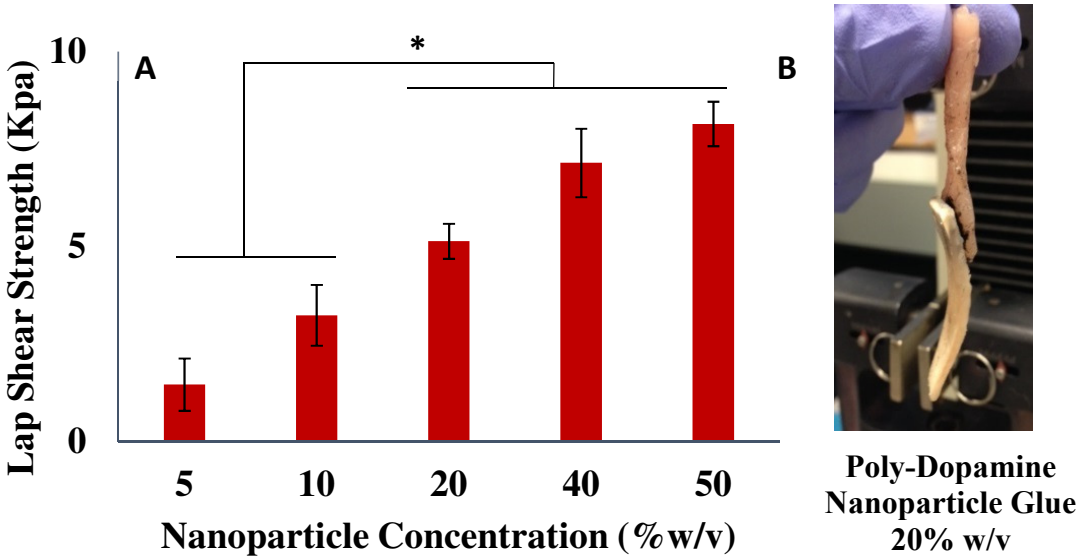

Figure 3.3: Adhesive properties of 200 nm polydopamine nanoparticles **(A)** Tissue adhesion strength of nanoparticle suspensions (size: 223 ± 31 nm) 5-50% (w/v)) on porcine skin-muscle interface **(B)** Digital image of a 200 nm polydopamine glue adhered skin-muscle interface ((20%w/v) nanoparticle suspension)

concentrations of the nanoparticles thus supporting the increase in adhesion along with the concentrations of polydopamine nanoparticles [178]. In our adhesion studies the maximum adhesion at 50 %w/v of nanoparticle concentration was calculated to be (8.1 ± 1.3 kPa).

3.3.3) Synthesis and characterization of hyaluronic acid-dopamine polymer*:*

We modified hyaluronic acid polymer by grafting dopamine onto the polymer backbone using EDC-NHS aqueous chemistry (**Figure 3.4 A**), using a method previously described [179]. The successful grafting of dopamine onto hyaluronic acid backbone was confirmed by the FTIR analysis of purified HA-Dopa polymer. The FTIR spectras of HA polymer had the characteristic peaks (**Figure 3.4 B**) at 3260 cm^{-1} (-OH, -CNH, =CNH stretch), 2875 cm^{-1} (C-H stretch), 1600-1610 cm^{-1} (amide I, C=O stretch), 1550-1560 cm^{-1} (Amide II, C-N stretch), and 1030 cm^{-1} (C-O-C stretch), which were in agreement with previous reports on FTIR analysis of HA polymers [180]. These peaks were also present in the HA-Dopa polymer in addition a unique peak at 1700 cm^{-1} (aromatic C=C bending) confirmed the presence of the aromatic ring of dopamine, confirming the grafting of dopamine onto the polymeric backbone of HA. The UV visible spectrophotometric determination of dopamine content in the polymeric backbone revealed a dopamine grafting amount of around 33% (**Figure 3.4 C**). The grafting of dopamine onto hyaluronic acid polymer backbone using EDC/NHS aqueous chemistry has been attempted by various research groups with

dopamine grafting amounts ranging from 1%- 42% depending on the molecular weight of the polymer used [154, 181-183].

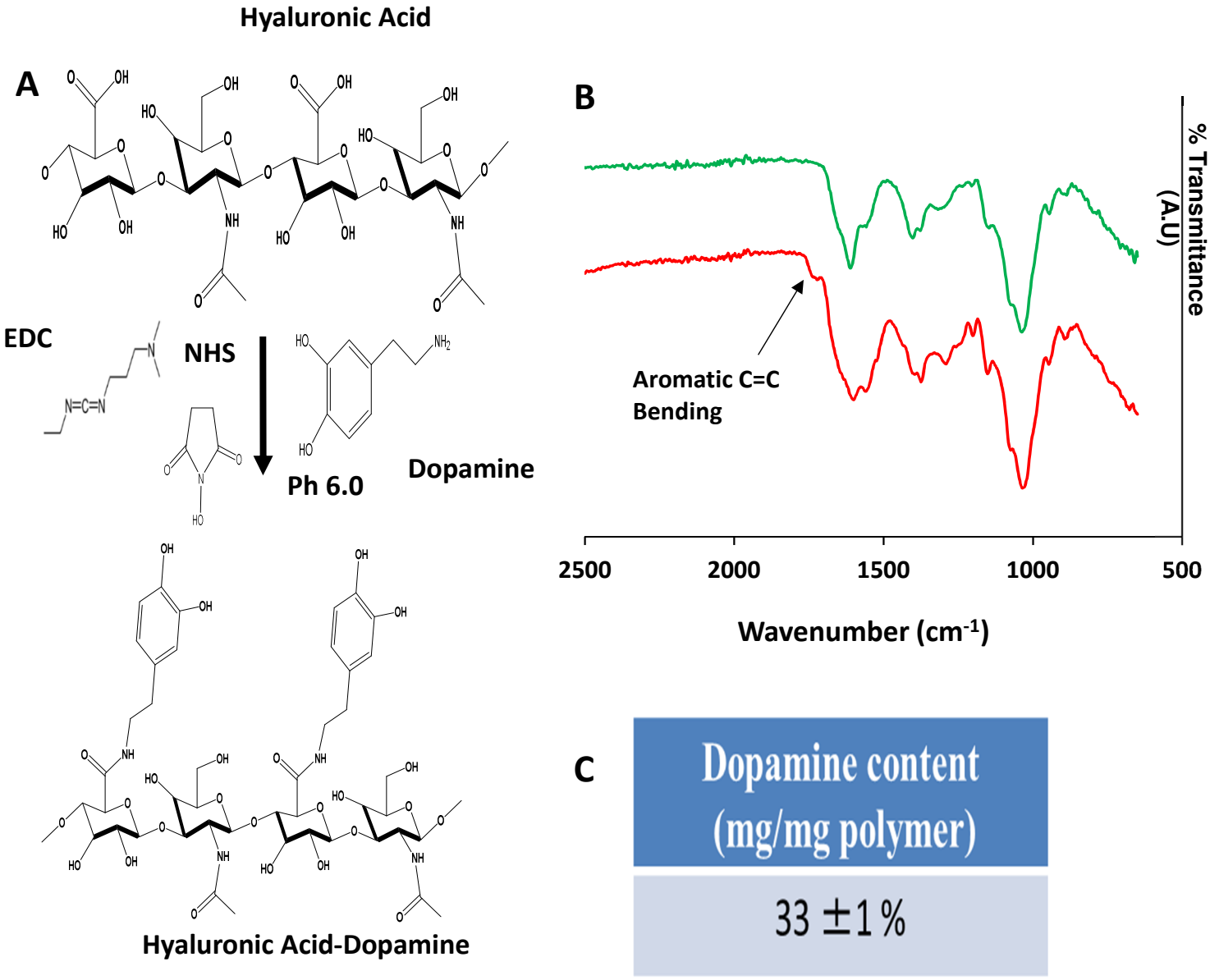

Figure 3.4: Hyaluronic Acid-Dopamine polymer synthesis and characterization. (A) Synthetic scheme of grafting of dopamine onto hyaluronic acid using carbodimide chemistry to achieve hyaluronic acid-dopamine polymer (HA-Dopa). **(B)** FTIR spectra of hyaluronic acid the dopamine grafted hyaluronic acid (HA-Dopa) to verify the grafting of dopamine onto the polymer. **(C)** Dopamine grafting amount determined by UV vis sepctrophotometry.

3.3.4) *Ex vivo* adhesion strength of mussel-inspired HA-Dopa nanocomposites

After the synthesis of HA-Dopa polymer, the effects of inclusion of nanoparticle types: PLGA, PLGA-NHS and polydopamine nanoparticles on the adhesion strengths of HA-Dopa hydrogels was investigated. As the polymer concentrations were increased from 1 %-40 % (w/v), there was a corresponding increase in tissue adhesion across the HA-Dopa group as well as all groups of nanocomposites at 12.5 % w/v nanoparticle concentration (**Figure 3.5A**).

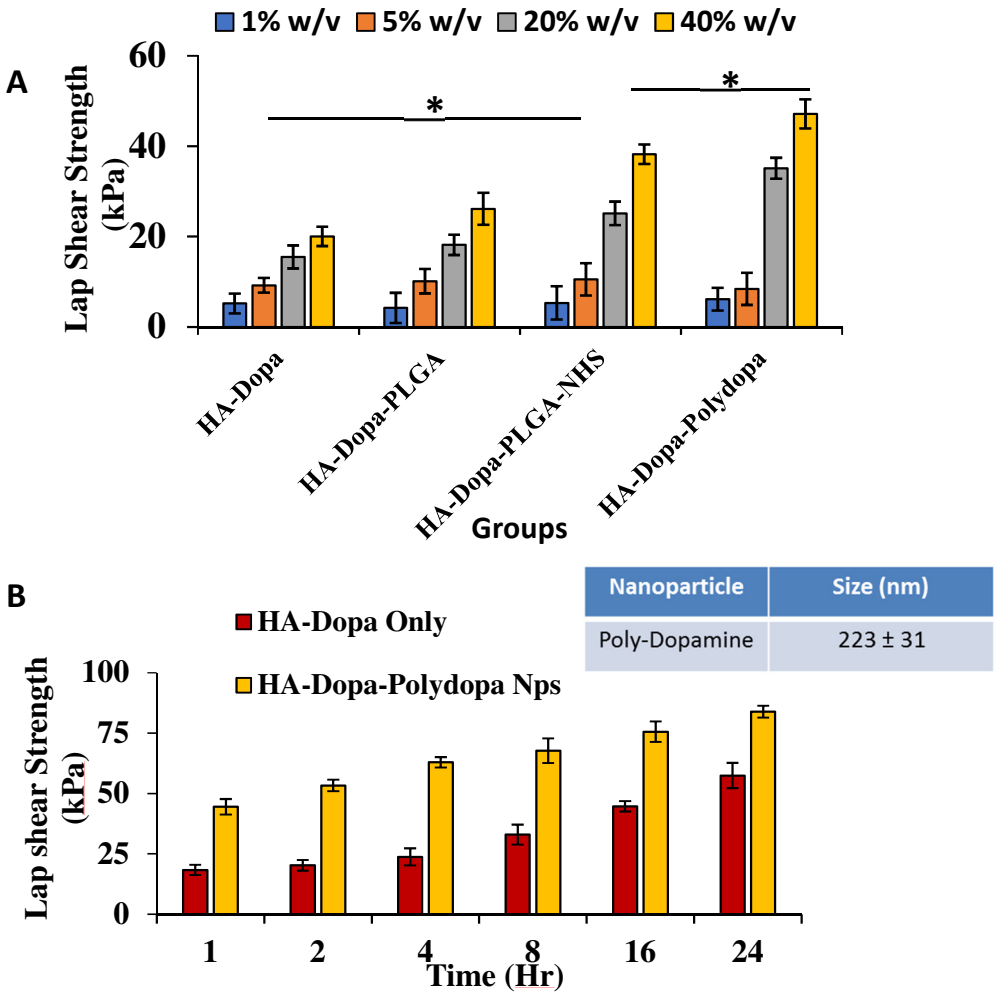

Figure 3.5: Adhesive properties of HA-Dopa nanocomposites. (A) Tissue adhesion strength of adhesives for porcine skin-muscle interface (12.5% w/v, nanoparticle suspension) **(B)** Time dependent adhesion strength of adhesives (HA-Dopa concentration 40% w/v, 12.5 % w/v polydopamine nanoparticle suspension) on porcine skin-muscle interfaces

This increase in adhesion can be attributed to the increase in available dopamine groups which has a high affinity to nucleophiles like amines and thiols present on the tissue surface [60, 183-185].

We have previously studied the effects of inclusion of PLGA based nanoparticles on the adhesion strengths of alginate-dopamine hydrogels and had found that these nanoparticles to enhance the adhesion of these hydrogels on porcine skin-muscle interfaces [186]. The bare HA-Dopa hydrogels at 40% w/v in the present study showed greater adhesion (20 ± 2 kPa) compared to our previous alginate-dopamine hydrogels (14 ± 2 kPa) which may be a direct consequence of the improved grafting of dopamine onto HA polymer (33%) compared to that of alginate (26%), this is also indicated by adhesive strengths starting to significantly improve at 5% w/v HA-Dopa concentrations as opposed to 20% w/v in the case of alginate-dopa hydrogels [186].

The inclusion of nanoparticles at 12.5 %w/v had a significant effect in improving tissue adhesion only when the polymer concentrations increased to 20% w/v and greater. We have previously attributed this nanoparticle mediated increase in adhesion to nanoparticles ability to provide cohesive stability to the hydrogel. In addition, the nanoparticles can also dissipate energy at the tissue interface via surface interactions [186]. Further, the addition of nanoparticles to polymer matrix has been reported to improve material properties of the polymeric gels and due to the nanoscale of the particles they are able to interact with the polymeric chains with high surface energy that leads to stronger interactions with the polymer chains, also adhesive forces are influenced by interfacial forces such as van der wall forces, hydrogen bonding and electrostatic interactions which are more pronounced as the size approaches the nanoscale which may explain the superior adhesion of HA-Dopa nanocomposites [187]. In addition, the nanoparticles can improve the stiffness and elastic modulus of the nanocomposites without effecting the toughness. This can prevent adhesive

failure resulting in higher adhesivity which may explain the significant increase in adhesion due to inclusion of nanoparticles [188-190].

In our studies the inclusion of PLGA-NHS nanoparticles significantly increased tissue adhesion of bare HA-Dopa hydrogels (37. ± 3 kPa compared to 20 ± 2 kPa); however, polydopamine nanoparticles had the most improved effect on adhesive strengths of the hydrogels (47. ± 5 kPa compared to 37. ± 3 kPa). This difference in adhesion strengths can be attributed to polydopamines ability to react with tissue amines relatively strongly compared to the NHS ester group. It has been shown previously that polydopamine can react and bind strongly to amines via Schiff base formation and result in improved adhesion of cells to polydopamine coatings [184, 191]

We further tested the time dependent adhesion profiles of HA-Dopa nanocomposites blended with polydopamine nanoparticles which revealed an increase in adhesion of the HA-Dopa hydrogel as well as the nanocomposites over a 24-hour period (**Figure 3.5 B**). The polydopamine nanoparticle-mediated enhancement of adhesion was significant at each time point and there was a significant difference ($P < 0.05$) in additional adhesion strength observed among the mussel-inspired hydrogels and the mussel-inspired nanocomposites at the end of 24 hours.

3.3.5) Effect of variation of the type and concentration of nanoparticles on the adhesion strength of mussel-inspired HA-Dopa nanocomposites:

The effects of varying PLGA, PLGA-NHS and polydopamine nanoparticle concentrations from 0-20 % (w/v) on the tissue adhesion strengths of 40 % w/v HA-Dopa hydrogels were investigated. It was observed that the PLGA-NHS and polydopamine nanoparticles start to significantly improve tissue adhesion of bare HA-Dopa hydrogels at nanoparticle concentration of 5 % w/v and greater (**Figure 3.6**).

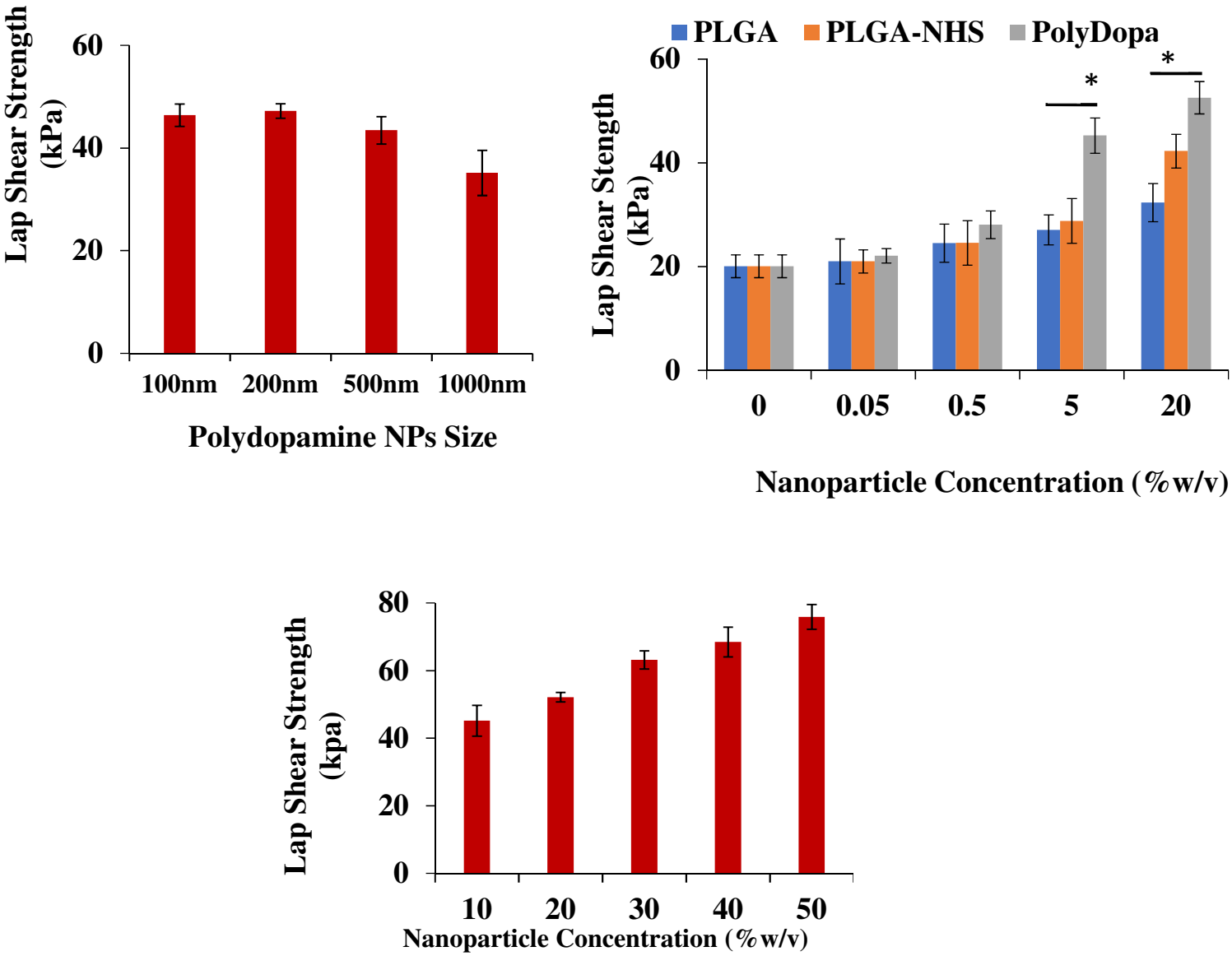

Figure 3.6: Adhesive properties of different nanoparticle concentrations on HA-Dopa hydrogels **(A)** Tissue adhesion strength of HA-Dopa hydrogels (40% (w/v)) blended with (100-1000 nm) polydopamine nanoparticles (12.5% (w/v)) on porcine skin-muscle interface. **(B)** Adhesive profiles of HA-dopamine hydrogels blended with PLGA, PLGA-NHS and polydopamine nanoparticle suspensions 0-20% (w/v)) on porcine skin-muscle interface. **(C)** Tissue adhesion strength of HA-dopa hydrogels (40% (w/v)) blended with varying concentrations of 200 nm sized polydopamine nanoparticles.

The polydopamine nanoparticles result in significantly superior adhesion profiles at nanoparticle concentrations of 5% w/v and greater compared to PLGA-NHS nanoparticles with maximum lap shear values reaching 52 ± 8 kPa at 20% w/v nanoparticle concentration. The tissue adhesive strengths of polydopamine blended HA-Dopa nanocomposites showed a size dependent adhesion

trend (**Figure 3.6A**). The results indicated no significant differences in tissue adhesive strengths of nanocomposites blended with 100 nm, 200 nm and 500 nm polydopamine nanoparticles with the maximum lap shear strength of 47 ± 3 kPa displayed by the nanocomposites blended with 200 nm polydopamine nanoparticles. 1000 nm polydopamine nanoparticle blended nanocomposites had significantly lower adhesion strengths (35 ± 6 kPa) compared to the 200 nm group. Since the 200 nm polydopamine nanoparticles were the most adhesive, for further studies we selected 200 nm sized particles. In further studies when the concentration of 200 nm polydopamine nanoparticles was varied from 10-50 % (w/v) there was a concentration dependent increase in tissue adhesive strength up to 30 %w/v nanoparticle concentration after which there were no significant increase in lap shear values. The increase in polydopamine nanoparticle concentration could increase the tissue adhesive strength up to 76 ± 5 kPa in the 50% w/v nanoparticle concentration group.

3.3.6) *In vitro* cell compatibility of HA-Dopa nanocomposite system

The *In vitro* exposure of HA-Dopa hydrogels and HA-Dopa nanocomposites with human dermal fibroblasts for 24 hours did not show signs of cell toxicity in all groups of hydrogels

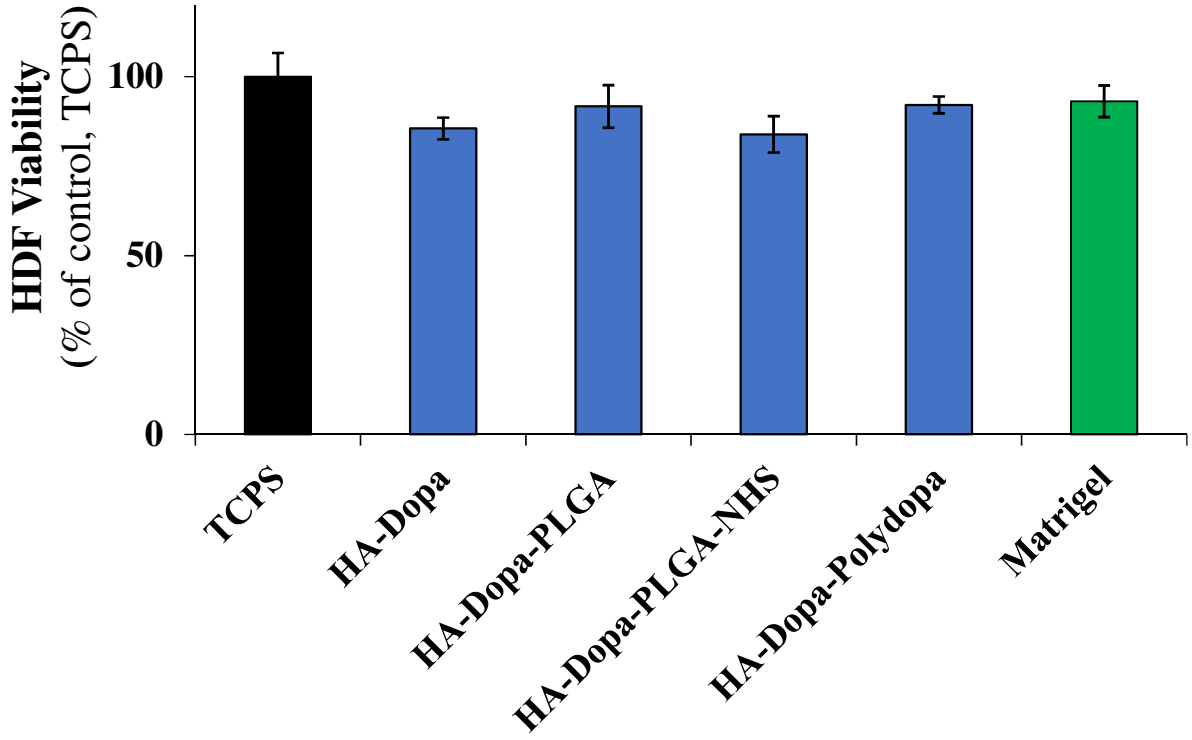

Figure 3.7: Cytocompatibility of HA-Dopa mussel-inspired nanocomposites (MIN) with human dermal fibroblasts (HDFs). Adhesive cytocompatibility with human dermal fibroblasts using a Transwell setup.

and nanocomposites tested. All HA-Dopa nanocomposites tested had similar cell viability profiles as the positive control Matrigel. The HA-Dopa-PLGA, HA-Dopa-PLGA-NHS and HA-Dopa-Polydopa all exhibited similar cell viability ($p>0.05$) (**Figure 3.7**).

3.4. Conclusion

We successfully synthesized polydopamine nanoparticles and optimized the synthesis process to formulate 100 nm -1000 nm size ranged nanoparticles. We investigated the adhesive properties of these polydopamine nanoparticles and found them to have size dependent and concentration dependent tissue adhesion with 100-200 nm sized nanoparticles being the most adhesive. We further synthesized a new mussel inspired polymer based on hyaluronic acid (HA-Dopa). The inclusion of polydopamine nanoparticles into HA-Dopa hydrogels resulted in nanocomposites with superior adhesive profiles compared to our previously developed alginate-dopamine nanocomposites. These HA-Dopa-polydopamine nanocomposites were cytocompatible with normal human skin cells and showed an increase in tissue adhesion over time for 24 hours. In future studies we will study the *in vivo* biocompatibility of the HA-dopamine-polydopamine nanocomposites in a rat subcutaneous model. We will also evaluate the tissue penetration profiles of polydopamine blended nanocomposites using tissue sections and image analyses.

Chapter 4

Aim 3: To develop an antimicrobial tissue adhering nanocomposite glue for wound healing applications

4.1) Introduction

Bacterial and fungal infections are major concerns for the treatment of chronic wounds and can be a hindrance in the use of surgical devices or implants for wound closure and wound repair. Microbial incidences can result in prolonged wound healing, wound dehiscence, abscess formation and sepsis formation and this becomes especially complicated in cases of large area wound repair such as in the case of burn wound repairs [192-195]. In addition, wound closure for patients suffering from diabetes or other immune compromising diseases, and in infection prone areas such as diabetic foot ulcers becomes especially complicated [196]. Bioadhesives have been applied towards wound healing applications to close the wound and provide delivery of growth factors. However, traditional bioadhesives typically lack anti-bacterial and anti-fungal properties, which necessitates additional anti-bacterial and anti-fungal drug delivery to treat infections with repeated doses of antifungal or antibacterial compounds [90]. The inconvenience of these repeated doses and the resulting increase in cost as well as the toxicity concerns of repeated drug doses continue to limit the application of current bioadhesives towards healing chronic wounds. In addition, antimicrobial drugs are incorporated into the adhesives for delivery but in some cases sustained release of the drug is difficult to achieve and the burst release of drugs often results in undesired systemic toxicity [197].

Tissue engineering approaches to address the wound closure and healing challenges revolve around the combination of growth factors, antimicrobial peptides and in some cases even stem cells, with scaffold materials that provide a support matrix and help cover the area of the wound [198]. These scaffold materials are usually referred to grafts or wound dressings or as skin

substitutes in some cases, depending on the layer of the skin being replaced or grafted on and the severity of the wound [198]. Several types of commercially available autologous and allogenic skin grafts use combination of differentiated cells such as fibroblasts and keratinocytes. Some examples of such graft materials include the popular Dermagraft (Organogenesis, Inc), Apligraft (Organogenesis, Novartis, Inc). These grafts provide a support matrix along with matrix proteins and enable the secretion of growth factors from the encapsulated fibroblasts and keratinocytes enabling host cell infiltration and re-epithelialization of the wound [199, 200]. However, such allogenic grafts are prone to disease transmission and graft rejection [201]. In addition, it has been found that allogenic differentiated cells in allogenic grafts fail to persist at the wound site over a period of 6 weeks [202, 203]. Autologous split thickness skin grafts address some of the limitations of allogenic grafts but are limited in applications towards chronic wounds while also having complications of donor site morbidity and poor healing rates [204]. Epidermal skin grafts offer improved outcomes in chronic wound healing compared to split thickness skin grafts but are limited by cumbersome and time consuming harvesting techniques, in addition these grafts do not often possess antimicrobial properties to defend against wound infections [205]. This creates an urgent need for the development of biocompatible bioadhesives with intrinsic antimicrobial properties for applications in tissue/wound closure, wound dressing, and chronic wound healing. Hydrogel materials are an ideal starting point to engineer materials with antimicrobial properties due to their ability to be functionalized and derivatized in addition to their advantage of providing moisture to the wound environment, which is essential to the cellular immunological activity facilitating the wound healing processes [206]. Several hydrogel based antimicrobial wound dressings have been looked at, mostly based on natural polysaccharides like alginate, dextran and more popularly chitosan due to its inherent antimicrobial property [34, 206]. In addition, synthetic

polymers like poly(vinyl alcohol), polyethylene oxide, poly(acrylic acid) and protein based biomaterials such as fibrin and gelatin have also been explored as wound dressings; however, these materials do not possess sufficient adhesive properties to facilitate optimal wound area coverage [207].

In this chapter, we describe the development of a mussel-inspired tissue adhering nanocomposite glue with an inherent antimicrobial property for the treatment of chronic wounds. We previously demonstrated the synthesis and characterization of alginate-dopamine based mussel inspired nanocomposites containing PLGA based nanoparticles and showed that the inclusion of nanoparticles leads to an increase in adhesion strength of the mussel inspired hydrogels in chapter 2. In chapter 3, we further optimized the tissue adhesion of hyaluronic acid-based hydrogels by using polydopamine nanoparticles. In Aim 3, we will explore novel antibacterial nanocomposite systems which can used as antimicrobial adhesives for wound healing applications.

In this chapter, further building on hyaluronic acid grafted dopamine polymers blended with polydopamine nanoparticles, we explored new polydopamine coated PLGA nanoparticles and their combination with HA-Dopa polymers to formulate new adhesive nanocomposites. In addition, a broad-spectrum antibiotic gentamycin, active against both gram positive and negative bacteria was loaded onto the polydopamine and polydopamine coated PLGA nanoparticles, which were then blended with HA-Dopa polymers to formulate gentamycin releasing antimicrobial nanocomposite adhesives. The adhesive profiles of these antimicrobial nanocomposites and the gentamycin loading and release profiles of nanoparticles and the nanocomposite hydrogels at different pH conditions simulating the wound environment were characterized. Further, antimicrobial testing of the nanoparticles and the nanocomposite hydrogels on gram positive (*S. Aureus*) and gram-negative bacteria (*E. Coli*), characterizing their inhibitory and bactericidal

activities in the form of zone of inhibition tests and time kill analysis over a period of 24 h on these bacterial species were also performed. Finally, the interactions of these antimicrobial nanocomposites on *E. Coli* and *S. Aureus* biofilms grown under controlled conditions to simulate an *in vitro* wound environment were investigated.

This chapter describes in detail the afore mentioned testing, characterization and development of these degradable antimicrobial nanocomposite adhesives.

4.2) Experimental Section

4.2.1) Materials:

Sodium Hyaluronate (MW:151-300 kDa) sodium metaperiodate (PI), dopamine hydrochloride, polyvinyl alcohol (PVA, MW=31 kDa), N-hydroxysuccinimide (NHS), 1-ethyl-3-(3-dimethylaminopropyl)carbodiimide, (EDC) phosphate buffered saline (PBS) and 4-morpholineethanesulphonic acid (MES) were purchased from Sigma-Aldrich, Inc, MO. Poly(lactide-co-glycolide) (PLGA, COOH terminated, lactide/glycolide molar ratio =50:50, and MW= 97 kDa) was purchased from Akina PolySciTech, Inc. Barium Chloride Dihydrate (Bacl2.2H2O, MW = 244.26 Da) was purchased form Fisher Scientific. Sulfuric Acid (H2SO4 Fulka, Inc), Sterile bacterial disks (Biogram). All chemicals were used as received without further purification.

4.2.2) Synthesis of polydopamine nanoparticles and polydopamine coated PLGA nanoparticles:

The PLGA nanoparticles were fabricated using standard emulsion methods [21]. PLGA solution (2% w/v in dichloromethane, 5 ml) was added dropwise to a PVA solution (5% w/v in deionized water, 20 ml). This emulsion was sonicated (30 W, 5 minutes) and then stirred overnight at room temperature to allow solvent evaporation and particle formation. The resulting particle suspension was centrifuged (15,000 rpm, 30 min, 10 °C) and the pellet suspension in deionized water was lyophilized to obtain PLGA nanoparticles. The lyophilized PLGA nanoparticles were then mixed in

0.1 M Tris buffer (Ph 9.0) at 0.2 % w/v nanoparticle concentration and were dispersed for 30 mins followed by the addition of dopamine hydrochloride (2 mg/ml). The reaction was allowed to proceed under dispersion for a period of 12 hours. The polydopamine coated PLGA nanoparticles were purified via centrifugation at 80,000g and were washed thrice with DI water followed by lyophilization. The polydopamine nanoparticles were synthesized following the same protocols developed in chapter 3, section 3.2.1.

4.2.3) Physical characterization of Nanoparticles:

The hydrodynamic size, zeta potential and polydispersity of the polydopamine and polydopamine coated PLGA nanoparticles were measured via dynamic light scattering technique (DLS) (Brooke Haven, ZETA PALS). Nanoparticle suspensions (0.01 % w/v in DI water) were used for this DLS analysis. Zeta potential measurement was performed in PBS solutions at various pH conditions. The coating of polydopamine on PLGA nanoparticles and the loading of gentamycin onto polydopamine nanoparticles and polydopamine coated PLGA nanoparticles was confirmed using FTIR analysis of freeze-dried nanoparticles. The nanoparticles were also visualized using high resolution transmission electron microscopy (HR-TEM, Hitachi H-9500) by casting an aqueous dispersion of nanoparticles (10 µL, 0.1~0.05 % w/v in DI water) onto a carbon-coated copper grid (FF200-Cu-50, Electron Microscopy Sciences, Hatfield, PA, USA) followed by staining with uranyl acetate (10 µL, 1 % w/v in DI water) (SPI-ChemTM, SPI, West Chester, PA, USA) solution. The nanoparticles were also visualized and analyzed using Cytoviva imaging and hyperspectral analysis (Cytoviva Inc) by preparing microscopy slide (Corning micro slides 2947-75x25) with samples of aqueous dispersion of nanoparticles (10 µL 0.1-0.05 %w/v in DI water) and drying the samples under vacuum followed by sealing them with embedding adhesives.

4.2.4) Nanoparticle cytocompatibility:

The cytocompatibility of PLGA and polydopa coated-PLGA nanoparticles was evaluated using human dermal fibroblasts (HDFs, ATCC). HDFs were seeded at a density of 10,000 cells/cm^2 into wells of a 24 well plate (n = 8) and incubated in Dulbecco's Modified Eagle Medium (DMEM, Sigma Aldrich) supplemented with 10% (v/v) fetal bovine serum (FBS, Life Technologies) and 1% (v/v) penicillium-streptomycin (Life Technologies, Inc.) at 37 ºC and 5% CO_2 for 24 hours (hrs). Nanoparticles at concentrations of 50, 100, 200, 500, 1000 µg/ml were then incubated with the cells for 24 hrs. An MTS assay (CellTiter 96® aqueous one solution cell proliferation Assay, Promega, Madison, WI) was performed according to manufacturer's instructions to assess cell viability after exposure of these NPs. The HDFs exposed to culture media only served as a control.

4.2.5) Drug loading and drug release from nanoparticles:

Gentamycin sulphate was loaded onto polydopamine NPs and polydopamine coated PLGA nanoparticles by incubating the nanoparticles (10 mg) and drug in a 1:0.05 and 1:0.1 weight ratio in Tris.Hcl buffer (0.1 M, 8 ml, pH 9) at room temperature in a rocking shaker for a period of 6 h to study optimal loading conditions. At the end of each time point the nanoparticles were purified by ultracentrifugation (100,000 g, 45 mins), and the supernatant was used for drug loading analysis. Further, once the optimal ratio of gentamycin to polydopamine nanoparticles was determined, the optimal ratio was incubated as above for a period of 12h, 16h, 1, 2, 3 and 4 days to determine the optimal incubation time for maximal loading of gentamycin.

For drug loading analysis, a spectrophotometric determination of gentamycin complexation with o-pthaldialdehyde was used [208]. Briefly, a gentamycin stock solution (200 µg/ml) was prepared and varying volumes of the stock solution were added to 1 ml of o-pthaldialdehyde solution which was mixed previously in 1.5 ml of isopropanol. The final volumes were made up to 5 ml with DI water

so as to prepare gentamycin standards in the concentration range:10µg/ml – 100 µg/ml. Volumes of 0.5 ml of the unknown gentamycin supernatant from the nanoparticle centrifugation was taken and mixed with 2.5 ml of the o-pthaldialdehyde- isopropanol mixture as before and the final volume was made up to 5 ml with DI water. The sample and the standards were incubated for 1 hour at room temperature on a rocking shaker and the absorbances of each tube was read in a UV transparent 96 well plate (100 µL per sample, n =6, per tube) at a wavelength of 333 nm. The absorbances of the standards were used to construct a linear standard curve which was then used to correlate the absorbance of the supernatant to determine the amount of drug loading onto the surface of the nanoparticles using the equation below.

$$\textbf{Gentamycin loading efficiency } \% = \boldsymbol{D_L} = \frac{C_i - C_s}{C_i} \times \mathbf{100} \text{ ----- } (\textit{Equation 4.1})$$

Where C_i = Initial amount of gentamycin used during loading. C_s = Amount of gentamycin detected in supernatant. For drug release studies, 10 mg of gentamycin loaded nanoparticles (n= 3) were suspended in 1x PBS solutions (5 ml) either at pH 7.2 or pH 5.5 or pH 9.0 and incubated at 37 °C in a rotary shaker. At predetermined time points (30 mins, 1 h, 2 h, 4 h, 8 h, 16 h, 24 h, 2, 4, 7 and 14 days) the tubes were centrifuged (100,000 g, 45 mins) to collect the supernatant while fresh 5 ml PBS was added as replacement and the nanoparticles were allowed to continue their incubation at 37 °C as before. The supernatant was used to detect gentamycin using the same spectrophotometric methods as described in drug loading analysis. The amount of gentamycin detected at each time point was added in a cumulative fashion to determine the cumulative release of gentamycin over time.

4.2.6) Antimicrobial testing using *S. Aureus* and *E. coli* bacteria:

The *S. Aureus* (ATCC, Wichita strain, Catalog #: 29213,) and *E. coli* (Carolina Biosciences, K12 strain, Cat # 155065) bacterial cultures were grown from frozen stocks. Briefly, 2% LB agar media was prepared and autoclaved before use. In a biosafety clean air hood, standard bacteriological petri dishes (BD Falcon, 100 mm x 15 mm) were used to prepare agar plates (30 ml LB agar each) for bacteria cultures later. An inoculating loop was used to pick some of the frozen culture from the respective bacteria vials and streaked on to the prepared agar plates using standard bacterial streaking techniques. The plates were sealed using parafilm and incubated at 37 °C for 12-14 hours to allow bacterial colonies to develop.

To optimize bacterial growth conditions and corelate the overnight grown bacterial cultures, $O.D_{600}$ values with viable bacteria counts, colony forming assays were performed at various dilutions following standard protocols [209] . Briefly, a single colony for each bacterium was picked using a sterile inoculation loop and inoculated into 3 ml of 2% w/v LB broth (Sigma Aldrich, Cat: L3022). This procedure was repeated in triplicates, and the inoculated bacteria was grown for 12-14 hours along with a sterility control containing only LB broth. The O. D_{600} of these overnight grown bacterial cultures were later recorded, and the cultures were diluted 1:30 for remeasurement of O. D_{600} in case the values exceeded unity.

Subsequently, for colony forming unit analysis, each of the respective overnight bacteria cultures and their three replicates were serially diluted from 10^{-2} to 10^{-7} in 2% w/v LB broth. For each bacterium and their replicates, 100 µl of each dilution from 10^{-4} to 10^{-7} was spread onto agar plates previously prepared using a sterile L shaped spreader. The spread agar plates were incubated at 37 °C overnight (12-14 hours) and the resulting number of colonies at each dilution which was able

to be counted were recorded for both *S. Aureus* and *E. coli*. The equation 4.2 was used to calculate the number of colony forming units/ml in the overnight grown bacterial cultures.

$$\mathbb{N} = \frac{C \times 10}{10^{-D}} \quad -----(\textit{Equation } 4.2)$$

Where, N= number of colony forming units/ml. C = Number of estimated colonies per plate at a particular dilution. D = The exponent of the particular dilution that resulted in C colonies.

To determine gentamycin minimal inhibitory concentrations on *S. Aureus* and *E. coli* bacterial cultures, gentamycin dilutions in autoclaved 2% LB broth in the range 0.06 µg/ml -256 µg/ml were prepared by serially diluting a gentamycin stock solution (512 µg/ml). Overnight grown bacterial cultures of *S. Aureus* and *E. Coli* were diluted in 2% LB broth making use of the correlation between overnight OD_{600} and CFU/ml to obtain a culture dilution containing 1 x 10^8 CFU/ml for each bacteria, this was further diluted to 1: 100 using LB broth, and 50 µl of this diluted bacteria was added to the wells of a sterile 96 well plate (n = 6, for each gentamycin concentration being tested) followed by addition of 50 µl of each of the antibiotic dilutions into the respective wells giving rise to gentamycin final concentration in the range (0.03 µg/ml-128 µg/ml) and a final bacterial inoculum of 5 x 10^5 CFU/ml. A sterility control containing 100 µl of LB broth only and a growth control containing 100 µl of the 5x10^5 CFU/ml bacterial culture were also included. The 96 well plates for each bacterium were sealed with parafilm and incubated at 37 °C in a humid environment for 16-20 h. Subsequently, 100 µl of the bacteria suspension from each of the wells was spread onto agar plates, and CFU analysis was performed on each plate as described earlier to estimate the MIC values of gentamycin.

4.2.7) Antimicrobial activity characterization of nanoparticles:

Zone of Inhibition studies: *E. Coli* and *S. Aureus* bacteria were grown into overnight cultures using the colony picking and broth inoculation methods as described earlier in section 4.2.6. A so called MacFarland 0.5 standard was prepared by mixing 1% $Bacl_2$ (100 µl) solution in DI water with 1% sulfuric acid (19.9 ml) solution in DI water. The overnight grown bacterial culture was diluted to match the OD_{600} value of the MacFarland 0.5 standard prepared above. Subsequently, 200 µl of the diluted culture of each bacterial strain was plated onto 2% agar plates and spread using a L spreader. Sterile discs were inoculated with 50 µl of either 5x MIC values of gentamycin for the respective bacteria to serve as a positive control or LB broth to serve as negative control. Also, 50 µl of Gentamycin loaded nanoparticles as well as unloaded nanoparticles at concentrations 5% and 12.5 % were inoculated onto the sterile discs to serve as samples. The discs and the plates were dried inside a sterile culture hood for 10 mins following which the discs including the samples, positive and negative controls were applied onto the bacteria containing agar plates. The plates were then sealed with parafilm and incubated at 37 °C for 20 h. Finally, the plates were imaged using a standard camera and the diameter of the resulting zones of inhibition were analyzed using Image J software.

Time kill kinetic studies: *E. Coli* and *S. Aureus* were grown from colonies using the same methods as described in section 4.2.6. Further, these overnight grown cultures were diluted to adjust their OD_{600} values to the MacFarland 0.5 standard as before. Gentamycin loaded nanoparticles and unloaded nanoparticles in concentrations groups of 0.05, 0.1 and 1 % w/v were prepared at 3X these concentrations in sterile 2% LB broth (5 ml). Gentamycin concentrations at 1X, 2X and 5X MIC concentrations were also prepared to 3X of these concentrations in sterile 2% LB broth.

The diluted bacterial inoculums above and each of the gentamycin loaded nanoparticles, the bare nanoparticle samples as well as the gentamycin MIC (1X, 2X, 5X) groups were mixed together in 1: 2 volume ratios into sterile tubes (n=3 for each group) which were then incubated at 37 °C. At predetermined time points of 4 h, 8 h, 12 h, 16 h, 20h and 24 h, bacterial samples were collected form each tube and diluted to 10^{-4} -10^{-6}, and each dilution plated in 2% agar plates which were further incubated at 37 °C to perform colony forming unit analysis using the same methods as described in section 4.2.6. The estimated colony forming units were converted to a log scale and plotted against time to construct time kill curves of the two bacterial species with respect to the gentamycin controls as various MIC's and the gentamycin loaded and unloaded nanoparticles.

4.2.8) Fabrication of Antimicrobial nanocomposites

The HA-dopamine polymer was cross-linked using the cross-linker PI at equimolar concentrations with respect to the dopamine amount in the polymer. Briefly, HA-dopamine polymer at concentration of 40 % w/v was mixed with 1X PBS (pH 7.2) to prepare a polymer precursor solution. The polymer precursor solution (40%) was then mixed with a nanoparticle suspension (5% or 12.5 5) in 1X PBS solution. The polymer-nanoparticle mixture was then cross-linked using PI for 1 h.

4.2.9) Characterization of Hyaluronic acid-gentamycin loaded nanocomposites:

The cross-sectional morphologies of nanocomposites were examined using scanning electron microscopy. A 40 % w/v solution of the HA-Dopamine polymer in PBS (pH 7.2) was combined with a 12.5% w/v solution of the nanoparticles and cross-linked using PI at a final concentration of 12 %w/v for 1 hour. The cross-linked samples were immersed in liquid nitrogen and cut at cross-section. The frozen cross-sections were freeze-dried and imaged under a scanning electron microscope. For hydrogel degradation, mussel-inspired polymer was mixed in PBS (pH 7.2) at a final concentration of 40%w/v and crosslinked using PI (12 % w/v) for 1 hour. This cross-linked

hydrogel was then immersed in a tube containing 1 ml PBS (n = 6) concentrated with 100 u/ml of hyaluronidase. At predetermined time points each of the tubes were centrifuged (9,000g, 10 min) to collect the hydrogel. This collected hydrogel was lyophilized to achieve the dry hydrogel. The weight of this dry hydrogel (W_t) was recorded and compared with the initial dry weight (W_0) to calculate the % weight remaining using $W_t/W_o \times 100\%$.

4.2.10) Adhesive testing of antimicrobial nanocomposites

The tissue adhesion of the mussel-inspired nanocomposites and mussel-inspired polymer hydrogels was tested on porcine skin and muscle samples (n=6) using guidelines from the American Society for Testing and Materials (ASTM) standard F2255-05. Freshly obtained porcine skin and muscle were cut into sections (30mm × 10mm × 3mm), and the mussel-inspired polymer at concentration of 40% (w/v) in PBS (pH 7.2) with or without the incorporation of nanoparticle suspensions (0-50 % w/v) was allowed to cross-link on an area of 10 mm × 5 mm between the skin-muscle interface for a period of 1 hour at 37°C. To ensure the skin-muscle samples were moist and retained water, the skin-muscle interface was kept in a humid environment in a standard cell culture incubator, maintaining humidity levels greater than 90% during the incubation time. The samples were then subjected to lap shear adhesion tests on an MTS insight workstation (cross-head speed of 10 mm min^{-1}; 500 N load cell; room temperature), and then the lap shear strength was measured.

4.2.11) *Ex vivo* tissue penetration depth of nanocomposites: Different groups of nanocomposites and the HA-Dopa hydrogel alone were cross-linked within the skin-muscle tissue interfaces for 1 hour. The adhered tissue samples were then embedded in optimal cutting temperature solutions (OCT, Tissue-tek) and frozen at -20 °C for 1 hour. The OCT embedded tissue samples were then cut into slices (10 µm thick). Image analysis was performed on the sections (n = 10) of each group of nanocomposites and the HA-Dopa hydrogel using Image J (National Institute of Health, Bethesda, MD, USA). A baseline indicated by the white horizontal lines was chosen, and it represented the

original contact between the muscle-skin and the glue. The glue penetration depth into the tissue was measured based on this baseline.

4.2.12) Nanocomposite cytocompatibility:

The HDFs were used to determine cytotoxic effects of the HA-Dopa alone and nanocomposite gels. The HDFs were seeded at a density of 10,000 cells/cm^2 into the wells of a 24 well plate (n = 8) and incubated in DMEM supplemented with 10% (v/v) fetal bovine serum (FBS) and 1% (v/v) penicillium-streptomycin at 37 $^{\circ}C$ and 5% CO_2 for 24 hours. These seeded cell culture plates were then used to determine the cytotoxicity of the leached products of Ha-Dopa and nanocomposite gels. The leached products were formulated using the systems (40% w/v polymer and 12.5% w/v nanoparticles) as described above, UV sterilized and incubated them in a known amount of DMEM cell culture medium at different dilutions (1X, 5X, 10X, 100X) at 37 $^{\circ}C$ and 5% CO_2 for 24 hours. Post incubation, all solutions were neutralized to pH 7.2 and added to the seeded HDFs for a period of 24 hours. MTS assays were performed after the 24-hour time-point following manufacturer's instructions. The cell culture medium only and Matrigel were used as controls to compare with the viability of HDFs exposed to treated groups. The Matrigel was prepared at a concentration of 1% w/v and applied to the Transwell plates at a volume to surface area ratio of 50 $\mu L/cm^2$. To assess the cytotoxicity of incubated hydrogels and nanocomposites, the formulated systems post UV sterilization were also placed in Transwell inserts (Pore size: 0.4 µm, growth area: 0.14 cm^2). These inserts were then placed into the cell pre-seeded 24-well plates for 24 h. MTS assays were performed in each group following manufacturer's instructions. Viability of HDFs in each group was assessed compared to the culture media alone and Matrigel.

4.2.13) Characterization of antimicrobial properties of nanocomposites:

Zone of inhibition*:* The bacterial inoculum for both *E. Coli* and *S. Aureus* and the bacteria containing plates were prepared using the same methods as in section 4.2.7. The gentamycin loaded polydopamine (G-PDA NPs) and polydopamine coated PLGA nanoparticles (G-PDA-PLGA NPs) containing nanocomposites as well as the nanocomposites containing bare nanoparticles were prepared in the same way as in section 4.2.8. A 5% nanoparticle concentration group and a 12.5% nanoparticle group were used for the antimicrobial testing. The nanocomposites were allowed to gel within metallic rings (diameter: 10 mm) to form disc shaped nanocomposites to be used for the study. The positive controls containing 50 µl of the 5X MIC concentration of gentamycin for each bacterial specie as well as the negative controls containing 2% sterile LB broths were inoculated onto sterile testing discs using the same methods as described in section 4.2.7. The nanocomposites or HA-Dopa hydrogels alone once cross linked for 1 hour were placed onto the bacteria containing agar plates and the plates were incubated at 37 °C for 20 h. Subsequently, the plates were imaged using a standard camera and the diameters of the resulting zones of inhibition were analyzed using Image J.

Bacterial time kill kinetic studies**:** *E. Coli* and *S. Aureus* were grown from colonies using the same methods as described in section 4.2.6. The OD_{600} value of the bacterial cultures were adjusted to MacFarland standard 0.5, preparation of gentamycin concentrations, the growth and sterility controls, mixing of the bacteria inoculum and the samples in a 2:1 ratio were preformed using the same methods as described in section 4.2.7. HA-Dopa hydrogel and HA-Dopa nanocomposites were introduced into the final diluted bacteria inoculum and all tubes for each group: gentamycin (1X, 2X, 5X), growth control, HA-Dopa hydrogel, nanocomposites containing gentamycin loaded nanoparticles, and nanocomposites containing bare nanoparticles. (n = 3) were incubated in an orbital shaker at 225 rpm and 37 °C for 24 h. At predetermined time points of 4 h, 8 h, 12 h, 16 h,

20h and 24 h, bacterial samples were collected from each tube and diluted to 10^{-4} -10^{-6}, and each dilution plated in 2% agar plates which were further incubated at 37 °C to perform colony forming unit analysis using the same methods as described in section 4.2.6. The estimated colony forming units were converted to a log scale and plotted against time to construct time kill curves of the two bacterial species with respect to the gentamycin controls at the various MIC's, HA-Dopa hydrogels, gentamycin loaded nanocomposites as well as the nanocomposites containing bare polydopamine and polydopamine coated PLGA nanoparticles.

Biofilm eradication Study*:* Biofilms of *E. Coli* and S. Aureus were grown using slight modifications of protocols optimized for *in vitro* biofilm growth on a 8 chamber slide [210]. Briefly, bacterial colonies for both bacterial for both species were grown in an overnight culture using the same methods of inoculation as described in section 4.2.6. The overnight culture was growth continuously until an OD_{600} of 0.5 was reached for both species. Subsequently the bacterial culture was diluted 1:6 in sterile 2% LB broth and further incubated at 37 °C in an orbital shaker at 225 rpm for 4 hours to precondition the bacterial inoculum to reach mid-log phase. Further, each of the two mid log bacterial suspensions were diluted to 1:2500 in prewarmed 2% sterile LB broth and 200 µl of the dilution was pipetted into each well of 8 well chamber slides corresponding to each of two bacterial species. The chamber slides were then incubated for 16 h at 37 °C, after which the chamber media was replaced with fresh prewarmed 2% sterile LB broth and subsequently for every 12 h to maintain bacterial viability.

At the 24 h time point, HA-Dopa hydrogels, nanocomposites containing gentamycin loaded nanoparticles at nanoparticle concentration of 12.5 % as well as nanocomposites containing bare nanoparticles at 12.5% as prepared in section 4.2.8 were introduced into respective wells of the

chamber slide for each bacterial specie. These treatment groups were incubated with the chamber slide at 37 °C for 24 hours with media change (2% sterile LB broth) every 12 h.

Visualization of Biofilm: At the end of 24 h, the bacterial biofilm was visualized by aspirating the LB media from each chamber well and washing each well twice with 0.9 % sterile saline solution. To stain the bacterial biofilm, 200 µl of Baclight Live/Dead stain was added to each well and incubated at room temperature for 15 mins under light protection thereafter. The wells were washed twice with 0.9 % sterile saline solution and fixed by incubating at room temperature with 200 µl of neutral buffered formalin in each well, followed by washing twice with 0.9 % sterile saline solution. The wells were removed, and a cover slip was added with a sealant to examine the biofilm slides under a confocal microscope.

4.4.14) Statistical Analysis: All data analysis was executed using one-way and two-way ANOVA (Statview 5.0 software, SAS institute, Cary, NC, USA) to analyze differences between groups with one or more independent variables. $p < 0.05$ was considered as significant difference. *Post hoc* analysis was done using Tukey's honest significant difference (HSD). All data was reported as mean ± standard deviation.

4.3) Results and Discussion:

4.3.1) Characterization of polydopamine nanoparticles and polydopamine coated PLGA nanoparticles:

The polydopamine nanoparticles were synthesized using the same mixed solvent protocols as described in chapter 3 section 3.4.1. The polydopamine NP solutions at 0.1% w/v concentration in 1x PBS buffers exhibited pH dependent change in surface charge with zeta potential values changing form -40 mV to +30 mV between pH 9.0 and 2.0 (**Figure 4.1 A**). The most rapid surface charge change was observed with pH ranges 6-3, with a 35 mv change in this transition. This pH dependent surface charge can be useful in capturing and releasing of charged molecules such as gentamycin sulphate (pKa 12.0) using polydopamine nanoparticles.

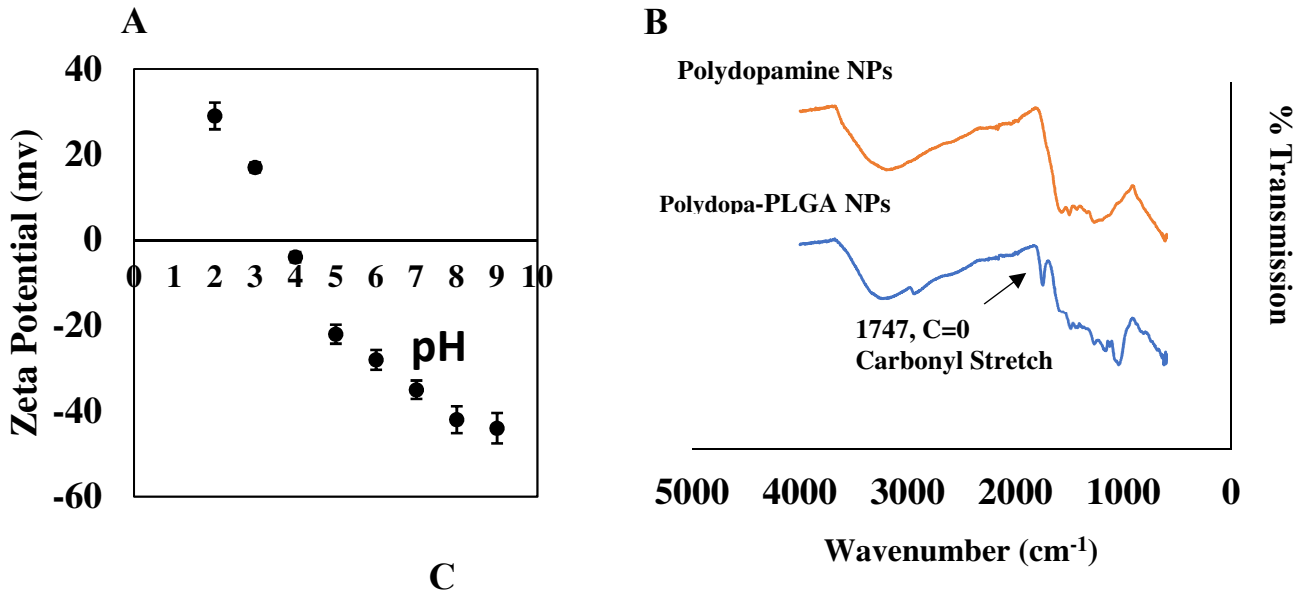

C

Nanoparticles	Size (nm)
PDA	212 ± 45.6
PDA-PLGA	350 ± 51

Figure 4.1: Physical characterization of polydopamine and polydopamine coated PLGA NPs. (A) Zeta potential trend of 0.1 % w/v polydopamine nanoparticles in 1x PBS buffers at varying pH values. **(B)** FTIR spectras of polydopamine nanoparticles and polydopamine-coated PLGA nanoparticles (Polydopa-PLGA NPs).

The coating of polydopamine onto PLGA nanoparticles was confirmed by the FTIR spectras of the nanoparticles (**Figure 4.1 B**). The polydopa-PLGA nanoparticle spectrum had the carbonyl C=O stretching peak at 1747 cm^{-1} from the PLGA polymer, whereas the peaks at 3158 cm^{-1} in the polydopa-PLGA NP spectrum were attributed to the OH- and N-H stretch from the polydopamine coating confirming successful coating of PDA onto the PLGA nanoparticles. The polydopamine coating increased the size of the PLGA nanoparticles from 200 nm to 350 nm.

4.3.2) Drug loading and drug release from nanoparticles

The pH-dependent surface charge of polydopamine nanoparticles (**Figure 4.1 A**) was utilized to physically adsorb the positively charged gentamycin (pKa 12.0) at a pH of 9.0 in Tris buffer. The loading conditions for the antibiotic gentamycin onto polydopamine nanoparticles were found to be optimal at 40 hours incubation with the particles at room temperature (**Figure 4.2 A**) at gentamycin: polydopamine NP weight ratio of 0.05:1. Further, varying of the weight ratio of gentamycin ratio from 0.05 up till 0.5 resulted in improved loading of the drug only up to 0.1 weight ratio with although higher loading amount of gentamycin was achieved at the 0.5 ratio, the loading efficiency did not show any significant difference compared to the 0.1 ratio (**Figure 4.2 B**). Subsequently, gentamycin to polydopamine nanoparticle weight ratio of 0.1:1 and a 3-day incubation period was chosen as optimal for maximal loading and applied to successive loading experiments. The gentamycin loading efficiency at this ratio onto polydopamine nanoparticles was calculated to be 72 ± 4 %. The gentamycin release profiles from polydopamine and poldopamine coted PLGA nanoparticles at pH values of 5.5, 7.2, 9.0 revealed significantly enhanced release ($p < 0.01$) of gentamycin at acidic pH of 5.5 compared to release at pH 7.2 and pH 9.0 for both group of particles.

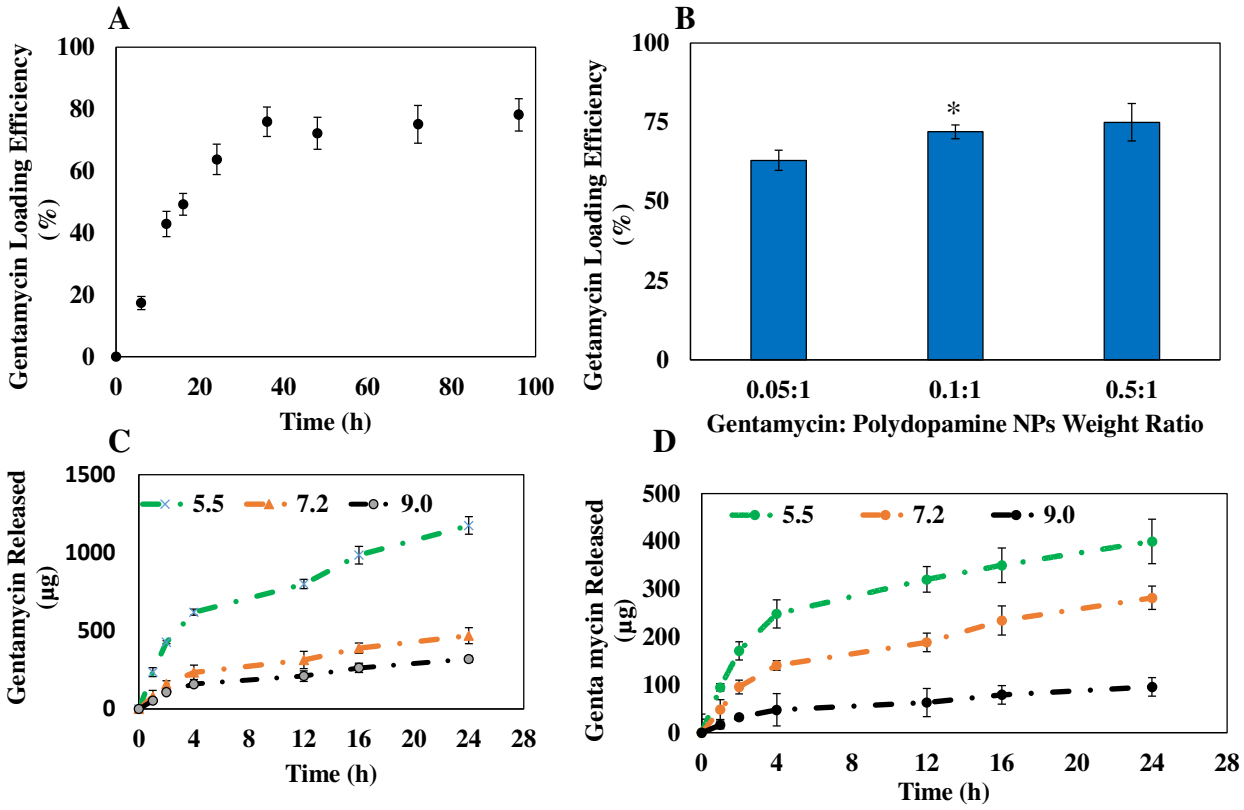

Figure 4.2: Gentamycin loading and release profiles from polydopamine and polydopamine coated PLGA nanoparticles. (A) Loading optimization of gentamycin (0.05:1 weight ratio of gentamycin: polydopamine) onto polydopamine nanoparticles with respect to incubation time. **(B)** Gentamycin loading efficiency at different weight ratios of drug to nanoparticles over a 3-day incubation period. **(C)** Gentamycin release profile from polydopamine nanoparticles at pH values 5.5, 7.2 and 9.0. **(D)** Gentamycin release profile from polydopamine coated PLGA nanoparticles.

4.3.3) Antimicrobial testing using *S. Aureus* and *E. coli* bacteria and gentamycin MIC determination

The colony forming unit analysis on overnight grown (12-14 h) *E. Coli* and *S. Aureus* cultures was important because of the dependence of optical density of bacterial cultures on the optical configurations of a particular spectrophotometer which is well known to change between different optical configurations [211-213]. Among the various dilutions 10^{-6} and 10^{-7} were most useful in

analyzing colony count. Our analysis revealed the relationship between OD_{600} values of 14 h cultures and the viable bacterial count in terms of colony forming units/ml as summarized in

Table 4.1. The average CFU/ml of *E. Coli* and *S. Aureus* in our analysis at t = 14 h of growth was in agreement with currently reported growth rates and CFU values of *E. Coli* and *S. Aureus* cultures grown under similar conditions [214].

Table 4.1: OD 600 corelation between bacterial cultures and viable bacterial counts in terms of colony forming units/ml

Bacterial Specie	OD_{600}*	(Colony Forming Units/ml) *10^8
E. Coli	0.37	210 ± 10
S. Aureus	0.28	120 ± 25

*Optical density at 600 nm of bacterial cultures grown in 2% sterile LB media for 14 hours.

The minimal inhibitory concentration (MIC) testing of gentamycin on *S. Aureus* and *E. Coli* cultures in logarithmic phase revealed the minimal inhibitory concentrations to be 4 µg/ml and 8 µg/ml respectively (**Figure 4.3**)

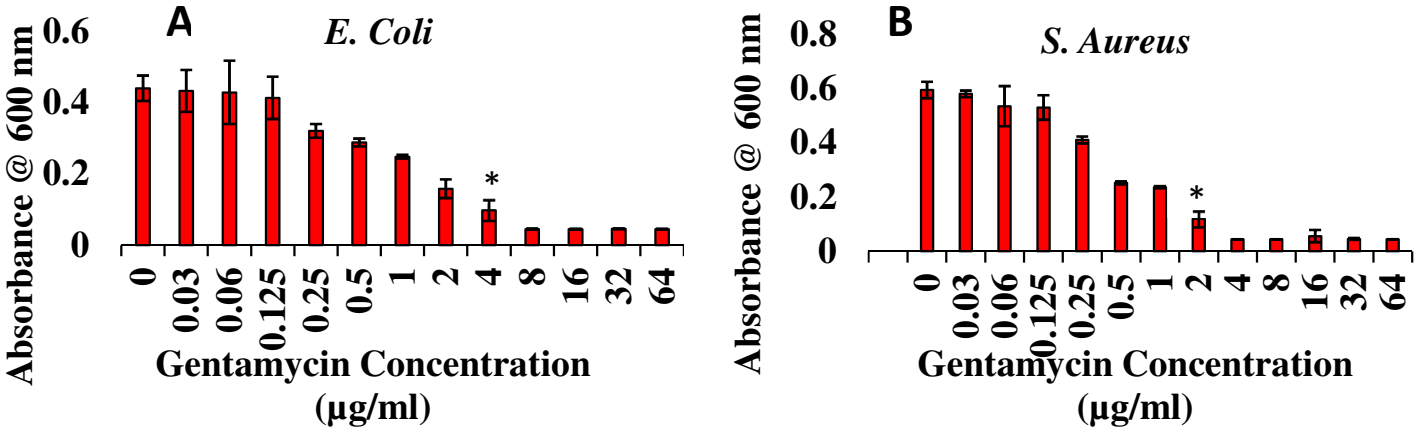

Figure 4.3: Minimal Inhibitory concentration testing of gentamycin at various concentrations on bacterial cultures. (A) Optical density profiles of E. Coli treated with decreasing concentrations of gentamycin in 2% LB broth, revealing a significance increase in OD_{600} corelating bacterial growth at 4 µg/ml ($p < 0.01$). **(B)** Optical density profile of S. Aureus treated with different concentrations of gentamycin in 2% LB broth, revealing significant increase in OD_{600} corelating to bacteria growth at 2 µg/ml ($p < 0.01$).

4.3.4) *In vitro* antimicrobial activity characterization of nanoparticles:

The testing of gentamycin-loaded polydopamine nanoparticles (G-PDA NPs), polydopamine coated PLGA nanoparticles (G-PDA-PLGA NPs) at 12.5 % w/v concentrations on bacterial species *E. Coli* and S. Aureus grown on agar plates revealed distinct zones of inhibitions for both the nanoparticles (**Figure 4.4**). The polydopamine nanoparticles were included to investigate potential inherent antimicrobial activity of these nanoparticles; however, the lack of development of the zone of inhibitions suggest that polydopamine nanoparticles had no inherent antimicrobial activity towards both bacterial species.

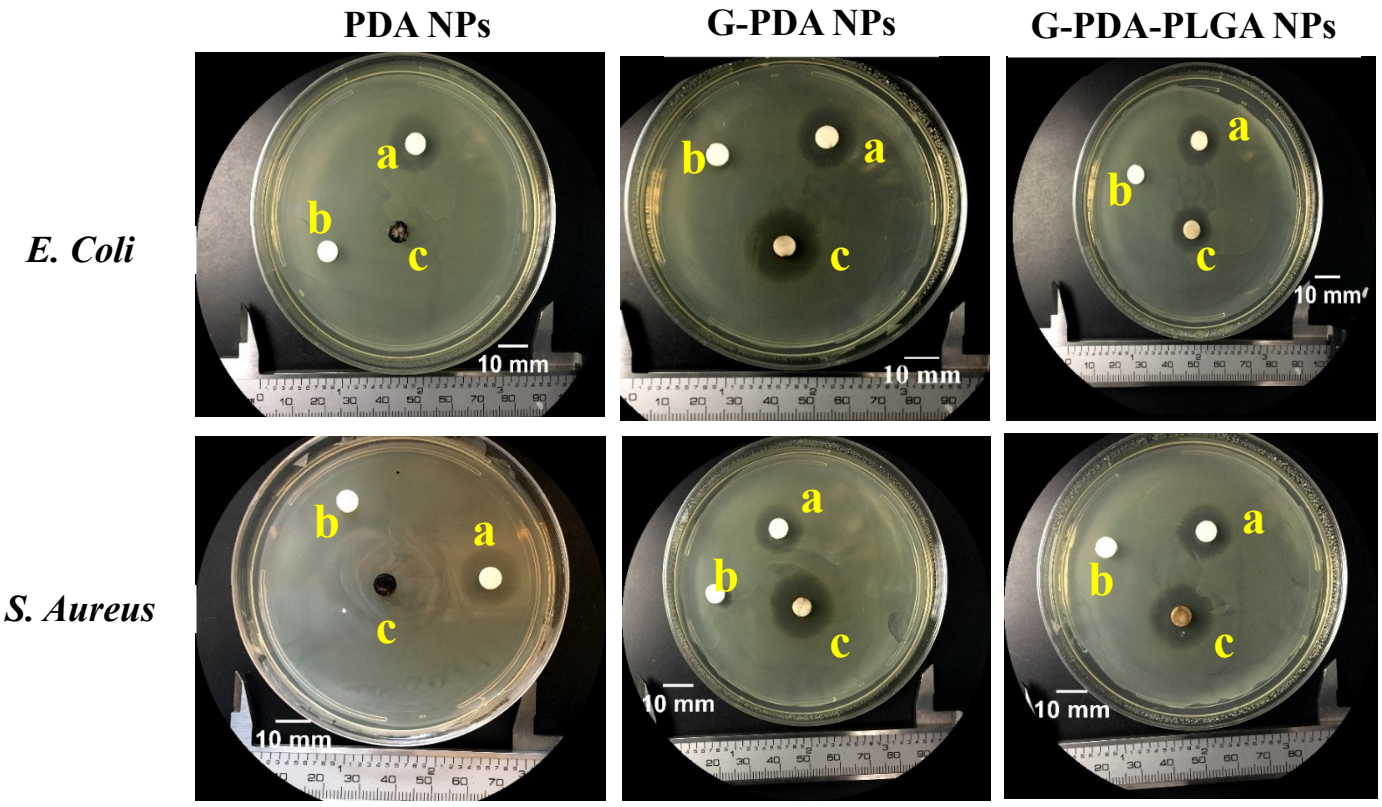

***a: Gentamycin at 5X MIC; b: 2% LB Broth; c: Nanoparticles**
***G-PDA: Gentamycin loaded polydopamine NPs at 12.5 % w/v;**
PDA-PLGA: Gentamycin loaded polydopamine coated PLGA NPs at 12.5 % w/v.

Figure 4. 4: *In vitro* antimicrobial testing of gentamycin loaded nanoparticles on *E. Coli* and *S. Aureus*. Zone of inhibition images of 2% agar plates inoculated with bacteria and incubated with test samples (c) and antibiotic controls (a) and 2% LB broth negative controls (b) over a period of 20 hours.

The zone of inhibition analysis revealed that both type of gentamycin loaded nanoparticles (G-PDA and G-PDA-PLGA NPs) could successfully release gentamycin in LB agar plates to inhibit the growth of both bacterial species. Given these observations it was important to look at the bactericidal effects of these drug loaded using time kill kinetic analysis of nanoparticles incubations in active bacterial broth cultures over a period of 24 hours.

The time kill analysis revealed that gentamycin loaded nanoparticles were effective in killing bacterial species over time starting at 4h from start of exposure to cultures with significant differences in bacterial viability ($p < 0.01$) between untreated control culture and the drug loaded nanoparticle groups (**Figure 4.5**). Interestingly, the polydopamine nanoparticle group (PDA-1.0) showed a significant difference in bacterial viability from the *E. Coli* growth control at the 4 h time point which was absent from the *S. Aureus* growth curve.

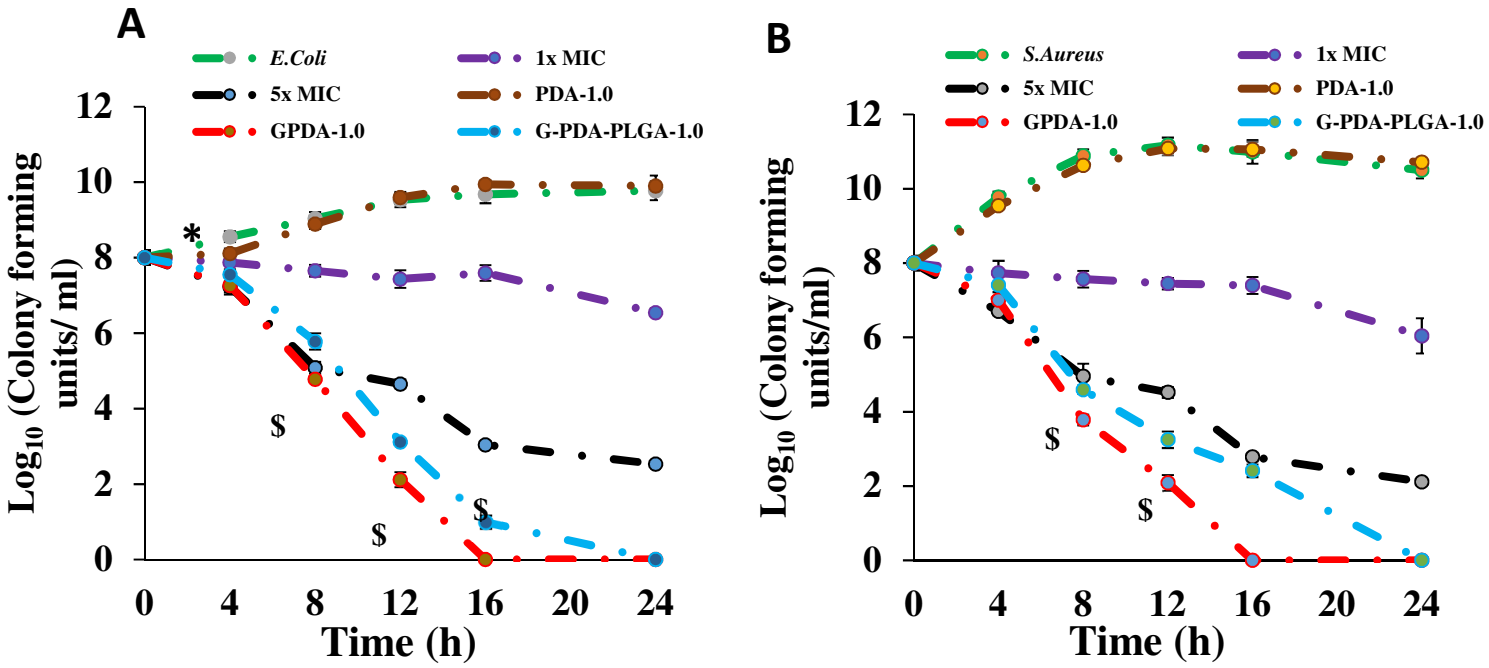

Figure 4.5: I*n vitro* bacterial growth kinetics and time kill analysis of gentamycin loaded nanoparticles. **(A)** Growth kinetics of *E. Coli* cultures treated with gentamycin loaded nanoparticles in terms of Log_{10} (Colony forming units/ml) over a time period of 24 h. **(B)** Growth kinetics of *S. Aureus* cultures treated with gentamycin loaded nanoparticles in terms of Log_{10} (Colony forming units/ml) over a time period of 24 h

The *E. Coli* bacterial inoculum showed approximately a 3-fold log reduction in viable bacteria counts compared to an approximately 4-fold log reduction in *S. Aureus* cultures for the groups treated with both type of gentamycin loaded nanoparticles in the first 8 hours of bacterial growth. Among the drug containing nanoparticle groups, there was observed to be a significant difference in bactericidal activity at 8 h time point with gentamycin loaded polydopamine nanoparticles (G-PDA-1.0) having a significant ($p < 0.05$) 1-fold log reduction on bacterial viability compared to gentamycin loaded PLGA nanoparticles (G-PDA-PLGA-1.0). In addition, the G-PDA-1.0 group was able to achieve absolute bactericidal effect at 16 h time point as compared to the same being achieved by G-PDA-PLGA-1.0 later at the 24 h time point.

4.3.5) Characterization of Hyaluronic acid-gentamycin loaded nanocomposites

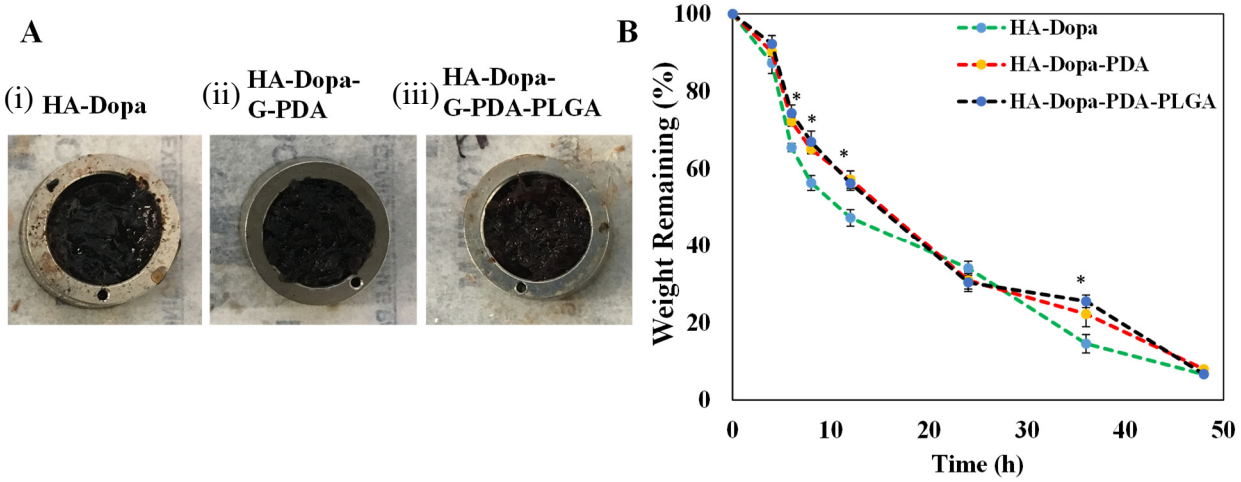

Figure 4.6: Physical characterization of antimicrobial nanocomposites. (A) Digital image of (i) Hyaluronic acid dopamine hydrogels at 40 % w/v (HA-Dopa). (ii) HA-Dopa hydrogels blended with 12.5 % w/v concentration of gentamycin loaded polydopamine nanoparticles (HA-Dopa-G-PDA) (iii) HA-Dopa hydrogels blended with 12.5 % w/v concentration of gentamycin loaded polydopamine coated PLGA nanoparticles (HA-Dopa-G-PDA-PLGA). **(B)** Degradation profiles of non-drug containing nanocomposites in 1x PBS in the presence of hyaluronidase (100 u/ml)

The antimicrobial nanocomposites physically did not appear any different from the HA-Dopa control hydrogels. The degradation rates of non-drug containing nanocomposites in the presence of hyaluronidase (100 u/ml) however differed significantly from the HA-Dopa control at time points of 6 h, 8 h, 12 h and 36 h respectively. All samples degraded up to 95 % weight loss in 48 hours of incubation with hyaluronidase.

4.3.6) Adhesive testing of antimicrobial nanocomposites

The adhesive testing of HA-Dopa nanocomposites blended with gentamycin loaded polydopamine and polydopamine coated PLGA nanoparticles at various concentrations revealed that gentamycin surface loading onto the nanoparticles did not significantly alter their adhesive profile. The improvement of adhesion strengths was observed with increase in nanoparticle concentrations with significant increase in adhesion occurring at 5% nanoparticle concentrations with lap shear values approaching 45 ± 5 kPa (HA-Dopa-Polydopa) and 40 ± 4 kPa (HA-Dopa-Polydopa-PLGA) compared to 20 kPa ± 3 kPa in the HA-Dopa control (**Figure 4.7**).

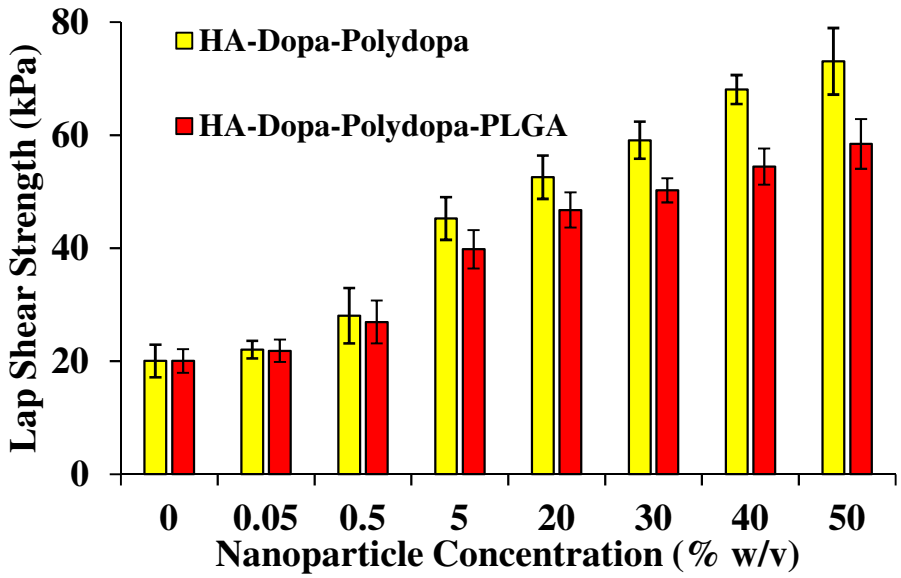

Figure 4.7: Adhesive profiles of antimicrobial nanocomposites blended with gentamycin containing polydopamine and polydopamine coated PLGA nanoparticles at 12.5 % w/v.

Nanocomposites containing polydopamine nanoparticles had superior adhesive profiles compared to those of polydopamine coated PLGA nanoparticles, with nanoparticle concentrations of 30% and higher showing significant differences in adhesive strengths (**Figure 4.7**).

4.3.7) Nanocomposite cytocompatibility

Cells incubated with the leached-out effluents of nanocomposites incubated in cell media showed a degree of cytotoxic response compared to the untreated control at 1x and 5x dilutions with cell media (**Figure 4.8**). The HA-Dopa group had a significant difference in cell viability ($p < 0.05$) at these dilutions when compared with both the untreated control: Tissue culture on poly(styrene) (TCPS) as well as the Matrigel control. The same effect was also observed in the polydopamine coated PLGA nanoparticle containing composite (HA-Dopa-PDA-PLGA). The polydopamine nanoparticle containing nanocomposites, on the other hand only differed in cell viability with respect to the untreated control (TCPS) at 1x and 5 x dilutions and had similar cytotoxicity response as the Matrigel effluents.

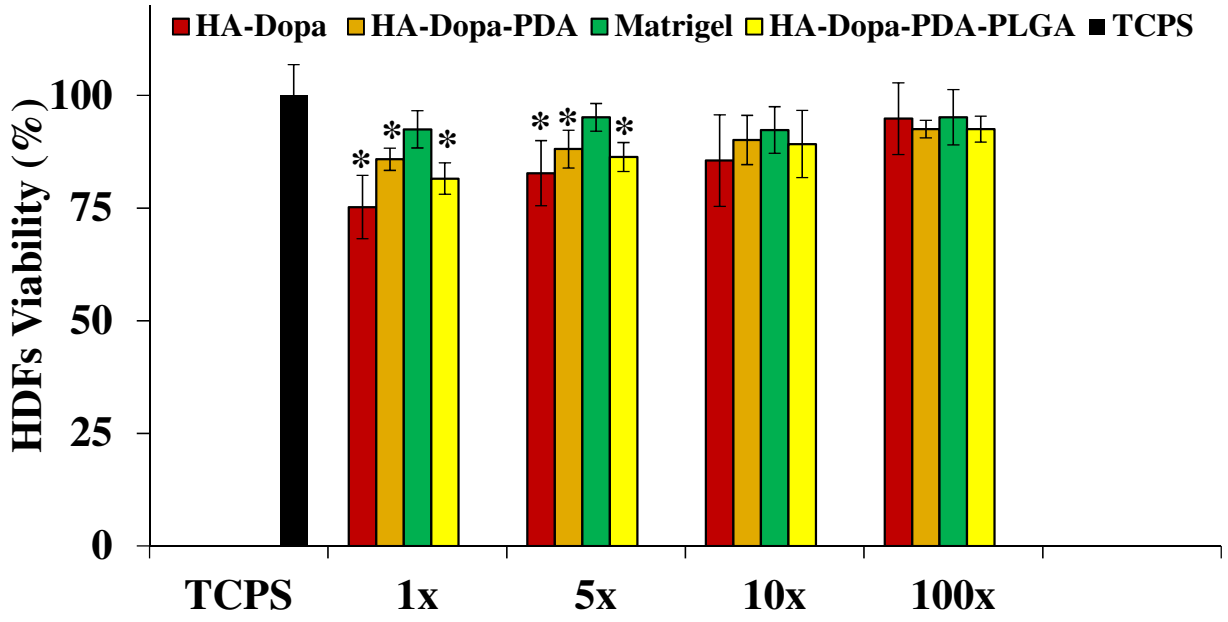

Figure 4.8: *In vitro* cytocompatibility profile of leached products of nanocomposite incubations in cell media.

4.3.8) Antimicrobial activity characterization of nanocomposites:

The testing of antimicrobial nanocomposites containing gentamycin loaded polydopamine nanoparticles (HA-Dopa-G-PDA) and polydopamine coated PLGA nanoparticles (Ha-Dopa-G-PDA-PLGA) at 12.5 % w/v concentrations on bacterial species *E. Coli* and S. Aureus grown on agar plates revealed their bacteria inhibition ability in the form of clear zones of inhibitions for both types of nanocomposites (**Figure 4.9**).

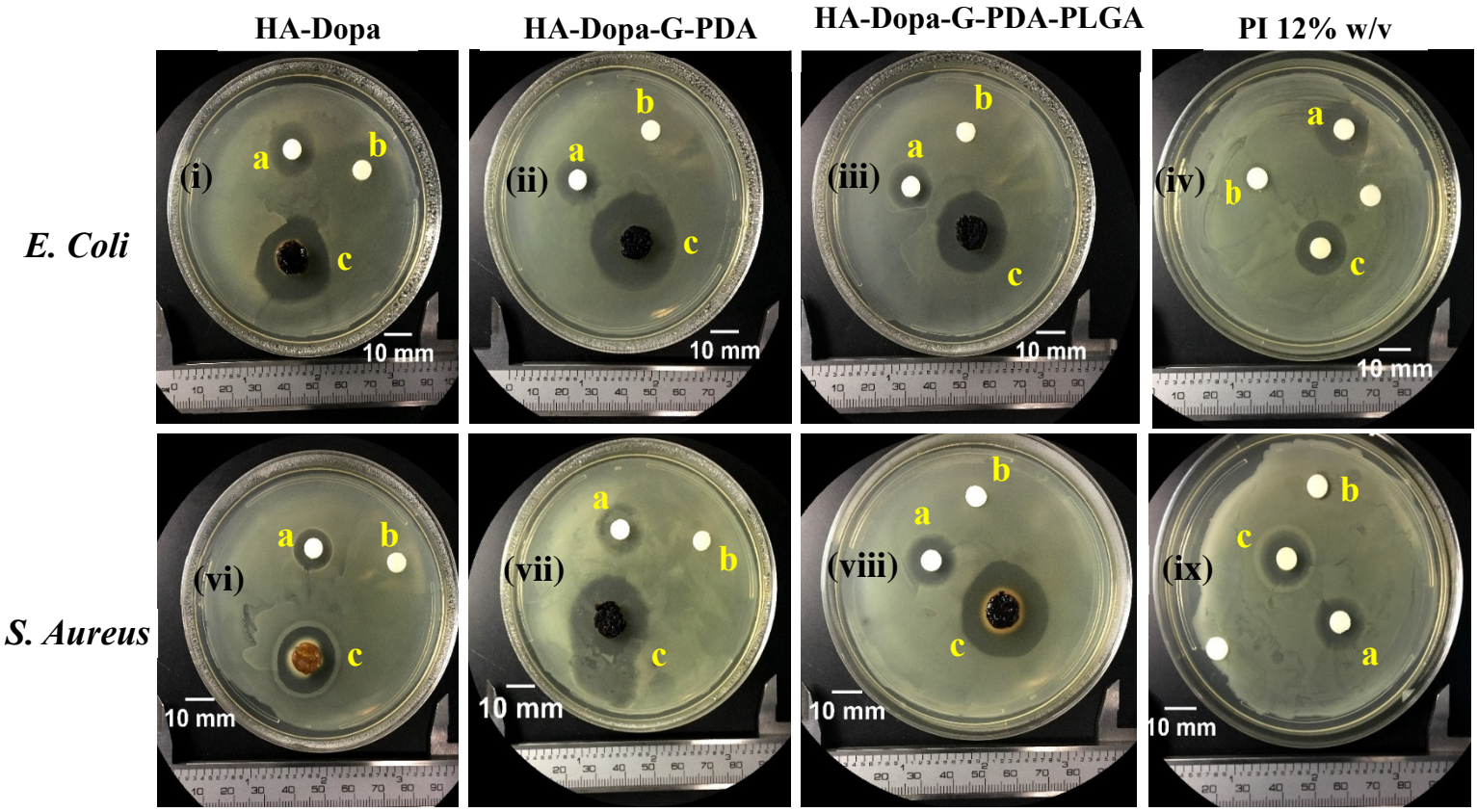

***a: Gentamycin at 5X MIC; b: 2% LB Broth; c: Nanocomposite or hydrogel**
***HA-Dopa-G-PDA: Hyaluronic acid hydrogel blended with gentamycin loaded polydopamine NPs at 12.5 % w/v; HA-Dopa-G-PDA-PLGA: Hyaluronic acid hydrogel blended with gentamycin loaded polydopamine coated PLGA NPs at 12.5 % w/v; HA-Dopa: Hyaluronic acid dopamine hydrogel at 40% w/v.**

Figure 4.9: *In vitro* antimicrobial testing of gentamycin loaded nanoparticles on *E. Coli* and *S. Aureus*. Zone of inhibition images of 2% agar plates inoculated with bacteria and incubated with test samples (c) and antibiotic control (a) and 2% LB broth negative control (b) over a period of 20 h.

HA-Dopa hydrogel was included as a control but interestingly demonstrated bacteria inhibitory activity (**Figure 4.9 (i)**). On further testing of the crosslinker sodium meta periodate (PI) used in formulation of HA-Dopa hydrogels we found that PI at 12 % w/v has an inhibitory effect on growth (**Figure 4.9 (iv) & ix**) of both bacterial specie which may explain the antimicrobial observation of HA-Dopa hydrogels. The nanocomposites blended with gentamycin loaded polydopamine nanoparticles showed a relatively higher inhibitory activity in both bacterial species compared to the ones blended with gentamycin loaded polydopamine coated PLGA nanoparticles (**Figure 4.9 (ii), (iii), (vii), (viii) respectively**) (**Figure 4.10**)

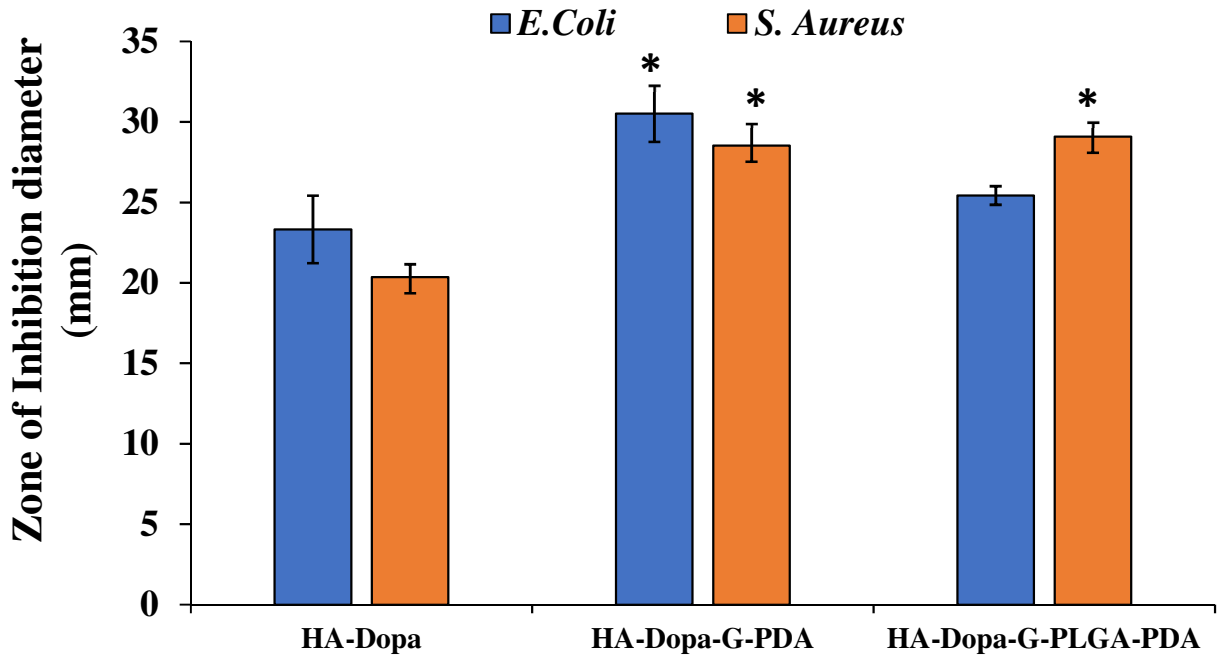

Figure 4. 10: Quantification of the diameters of zones of inhibition produced by antimicrobial nanocomposites.

We further tested the bactericidal effects of these nanocomposites by performing another time kill kinetic analysis of nanocomposite incubations in active bacterial broth culture over a period of 24 hours. The results of this analysis (**Figure 4.11**) revealed the inhibitory effects of the control HA-Dopa hydrogels, it was important to note that HA-Dopa hydrogels were found to be bacteriostatic and not bactericidal since the viable bacterial counts in both *E. Coli* and *S. Aureus* did not reach log reductions more than a single fold over the period of 24 h and also the growth kinetic profile of the inoculums treated with 1X MIC concentrations of gentamycin were similar to the HA-Dopa hydrogel group except at the 24 h time point for both bacteria (**Figure 4.11 A-B**). The antimicrobial nanocomposites, however, showed bactericidal effects on both bacterial species with

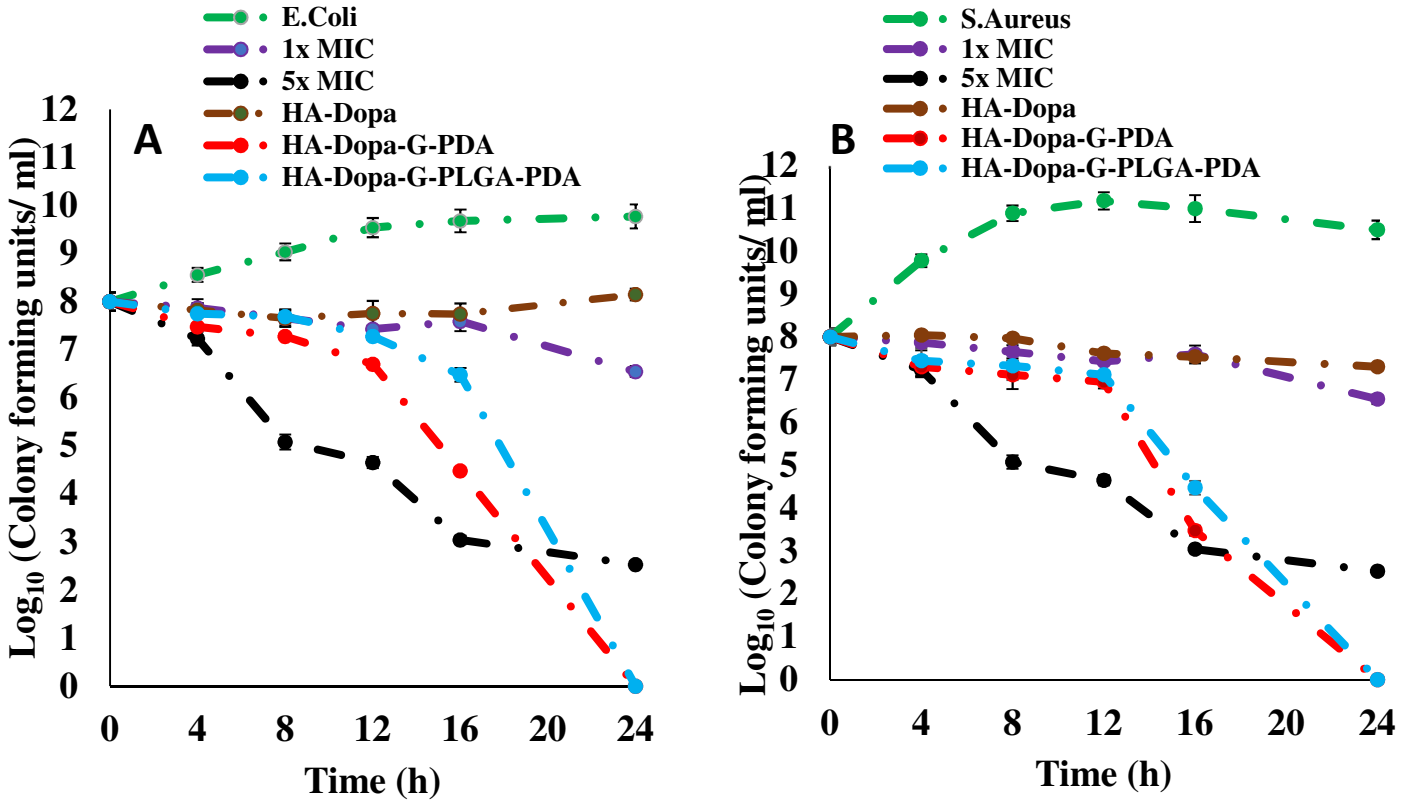

Figure 4.11: I*n vitro* bacterial growth kinetics and time kill analysis of antimicrobial nanocomposites. (A) Growth kinetics of *E. Coli* cultures treated with nanocomposites blended with gentamycin loaded nanoparticles at 12.5% w/v in terms of Log_{10} (Colony forming units/ml) over a time period of 24 h. **(B)** Growth kinetics of *S. Aureus* cultures treated with nanocomposites blended with gentamycin loaded nanoparticles at 12.5 % w/v in terms of Log_{10} (Colony forming units/ml) over a time period of 24 h

polydopamine containing nanocomposites have a relatively greater (3-fold log reduction, for *E. coli* and 3.5-fold log reduction in *S. Aureus*) bactericidal effect compared to those containing polydopamine coated PLGA nanoparticles (1-fold log reduction, for *E. coli* and 2.5-fold log reduction in *S. Aureus*). All nanocomposites reached absolute reduction in bacterial viability by the 24-hour time point.

Chapter 5

Conclusions and Future Outlook

5.1) Summary

In Summary, we have developed mussel inspired tissue adhesives whose adhesion to the tissue can be tailored by the choice and concentration of the polymers used as well as the properties of nanoparticles. These nanocomposite adhesives were degradable and showed enhanced adhesive properties on the inclusion of nanoparticles into the polymers. The *in vivo* testing of the alginate-dopamine nanocomposites revealed these systems to be non-inflammatory in general and degradable within a period of 4 weeks in a rat sub cutaneous model.

The optimization of adhesive strengths by varying the polymer types, their concentrations along with nanoparticle types and concentrations revealed new improved adhesives in the form of hyaluronic acid dopamine polymers combined with polydopamine based nanoparticles. These optimized adhesives were then developed into antimicrobial adhesives which successfully demonstrated bactericidal effects on *E. Coli* and *S. Aureus* species while being bio-degradable.

5.2) Limitations and Future Work

A few limitations of the work performed in this thesis relate to the adhesive strengths of the nanocomposites developed in chapters 2-4. Although they have a moderate adhesion relative to other adhesives developed by different research groups, it is at the cost of using a high polymer concentration (40% w/v) and crosslinker (PI) concentrations (12% w/v) which makes the bare hydrogels slightly toxic as we see in the cytocompatibility studies on human skin cells with the Alg-Dopa and HA-Dopa groups. This aspect needs to be improved in future attempts at this research direction by exploring other suitable grafting techniques of dopamine onto HA polymers and also other polysaccharide and cross-linking agents. In addition, it is also imperative to look at the *in vivo* biocompatibility of the HA-dopamine-polydopamine nanocomposites in a rat

subcutaneous model. It would also be important to look at the tissue penetration profiles of polydopamine blended nanocomposites using tissue sections and image analyses.

On a separate note, in order to fully realize the adhesive potential of the nanocomposite materials developed in here, future investigations into the mechanisms of nanoparticle mediated increase in adhesion are warranted. For example at the present state of research, we postulate that the caused increase in adhesive properties might be due to the high surface area to volume ratio of nanoscale particles and the result of surface interactions such as Vander walls forces, capillary forces, electrostatic forces, and surface roughness between the polymeric matrix and the nanoparticles being intensified at the nanoscale leading to improved mechanical and surface properties of the resulting nanocomposites. This phenomenon needs to be experimentally validated in future studies by looking at polydopamine interactions with a hydrogel substrate as well as a tissue surface.

Finally, the antimicrobial nanocomposites developed in Aim 3 exert their bacteriostatic effect via the use of antibiotics, which is a current point of contention in the current research effort to combat widespread and fast emerging antibiotic resistance in bacterial strains. It is important to develop antimicrobial adhesives, which rely on physical means like binding and damaging bacterial cell walls to cause cell death as these mechanisms of antimicrobial effect are not prone to the development of bacterial resistance.

.

References

1. Bhatia, S.K., *Traumatic Injuries Chapter 10 Traumatic Injuries*, in *Biomaterials for Clinical Applications*. 2010, Springer New York: New York, NY. p. 213-258.
2. Bhagat, V. and M.L. Becker, *Degradable Adhesives for Surgery and Tissue Engineering.* Biomacromolecules, 2017. **18**(10): p. 3009-3039.
3. Duarte, A.P., et al., *Surgical adhesives: Systematic review of the main types and development forecast.* Progress in Polymer Science, 2012. **37**(8): p. 1031-1050.
4. Ferreira, P., H. Gil, and P. Alves, *An overview in surgical adhesives*. 2013.
5. Khanlari, S. and M.A. Dubé, *Bioadhesives: A Review.* Macromolecular Reaction Engineering, 2013. **7**(11): p. 573-587.
6. Reece, T.B., T.S. Maxey, and I.L. Kron, *A prospectus on tissue adhesives.* Am J Surg, 2001. **182**(2 Suppl): p. 40s-44s.
7. Kazemzadeh-Narbat, M., N. Annabi, and A. Khademhosseini, *Surgical sealants and high strength adhesives*. 2015, ELSEVIER SCI LTD THE BOULEVARD, LANGFORD LANE, KIDLINGTON, OXFORD OX5 1GB, OXON, ENGLAND.
8. Li, L. and H. Zeng, *Marine mussel adhesion and bio-inspired wet adhesives.* Biotribology, 2016. **5**(Supplement C): p. 44-51.
9. Marshall, S.J., et al., *A review of adhesion science.* Dental Materials, 2010. **26**(2): p. e11-e16.
10. Ahuja, A., R.K. Khar, and J. Ali, *Mucoadhesive Drug Delivery Systems.* Drug Development and Industrial Pharmacy, 1997. **23**(5): p. 489-515.
11. Modaresifar, K., S. Azizian, and A. Hadjizadeh, *Nano/Biomimetic Tissue Adhesives Development: From Research to Clinical Application.* Polymer Reviews, 2016. **56**(2): p. 329-361.
12. Mahdavi, A., et al., *A biodegradable and biocompatible gecko-inspired tissue adhesive.* Proceedings of the National Academy of Sciences, 2008. **105**(7): p. 2307-2312.
13. Yang, S.Y., et al., *A Bio-Inspired Swellable Microneedle Adhesive for Mechanical Interlocking with Tissue.* Nature communications, 2013. **4**: p. 1702-1702.
14. Kjaergard, H.K. and U.S. Weis-Fogh, *Important factors influencing the strength of autologous fibrin glue; the fibrin concentration and reaction time--comparison of strength with commercial fibrin glue.* Eur Surg Res, 1994. **26**(5): p. 273-6.
15. Spotnitz, W.D., *Fibrin Sealant: The Only Approved Hemostat, Sealant, and Adhesive—a Laboratory and Clinical Perspective.* ISRN Surgery, 2014. **2014**: p. 28.
16. Miura, S., et al., *Efficacy of Slow-releasing Anticancer Drug Delivery Systems on Transplantable Osteosarcomas in Rats.* Japanese Journal of Clinical Oncology, 1995. **25**(3): p. 61-71.
17. Tredwell, S., et al., *Use of fibrin sealants for the localized, controlled release of cefazolin.* Canadian Journal of Surgery, 2006. **49**(5): p. 347-352.
18. Kitazawa, H., et al., *Microdialysis Assessment of Fibrin Glue Containing Sodium Alginate for Local Delivery of Doxorubicin in Tumor-Bearing Rats.* Biological & Pharmaceutical Bulletin, 1997. **20**(3): p. 278-281.
19. Kawamura, M., et al., *Frequency of transmission of human parvovirus B19 infection by fibrin sealant used during thoracic surgery.* The Annals of Thoracic Surgery, 2002. **73**(4): p. 1098-1100.
20. Hino, M., et al., *Transmission of symptomatic parvovirus B19 infection by fibrin sealant used during surgery.* British Journal of Haematology, 2000. **108**(1): p. 194-195.
21. Berruyer, M., et al., *Immunization by bovine thrombin used with fibrin glue during cardiovascular operations. Development of thrombin and factor V inhibitors.* The Journal of thoracic and cardiovascular surgery, 1993. **105**(5): p. 892-897.

22. Rapaport, S.I., et al., *Clinical Significance of Antibodies to Bovine and Human Thrombin and Factor V After Surgical Use of Bovine Thrombin.* American Journal of Clinical Pathology, 1992. **97**(1): p. 84-91.
23. Kober, B.J., et al., *Anaphylactic Reaction After Systemic Application of Aprotinin Triggered by Aprotinin-Containing Fibrin Sealant.* Anesthesia & Analgesia, 2008. **107**(2): p. 406-409.
24. Conrad, K. and A. Yoskovitch, *The use of fibrin glue in the correction of pollybeak deformity: A preliminary report.* Archives of Facial Plastic Surgery, 2003. **5**(6): p. 522-527.
25. Albes, J.M., et al., *Biophysical properties of the gelatin-resorcinformaldehyde/glutaraldehyde adhesive.* The Annals of Thoracic Surgery, 1993. **56**(4): p. 910-915.
26. *A novel collagen-based composite offers effective hemostasis for multiple surgical indications: Results of a randomized controlled trial.* Surgery, 2001. **129**(4): p. 445-450.
27. Nelson, P.A., et al., *Serological analysis of patients treated with a new surgical hemostat containing bovine proteins and autologous plasma.* Journal of Biomedical Materials Research, 2001. **58**(6): p. 710-719.
28. Bochicchio, G., et al., *The combination of platelet-enriched autologous plasma with bovine collagen and thrombin decreases the need for multiple blood transfusions in trauma patients with retroperitoneal bleeding.* J Trauma, 2004. **56**(1): p. 76-9.
29. Farndale, R.W., et al., *The role of collagen in thrombosis and hemostasis.* J Thromb Haemost, 2004. **2**(4): p. 561-73.
30. Oz, M.C., et al., *Controlled clinical trial of a novel hemostatic agent in cardiac surgery. The Fusion Matrix Study Group.* Ann Thorac Surg, 2000. **69**(5): p. 1376-82.
31. Renkens, K.L., Jr., et al., *A multicenter, prospective, randomized trial evaluating a new hemostatic agent for spinal surgery.* Spine (Phila Pa 1976), 2001. **26**(15): p. 1645-50.
32. Spotnitz, W.D. and S. Burks, *Hemostats, sealants, and adhesives: components of the surgical toolbox.* Transfusion, 2008. **48**(7): p. 1502-16.
33. Scognamiglio, F., et al., *Adhesive and sealant interfaces for general surgery applications.* J Biomed Mater Res B Appl Biomater, 2016. **104**(3): p. 626-39.
34. Kong, M., et al., *Antimicrobial properties of chitosan and mode of action: A state of the art review.* International Journal of Food Microbiology, 2010. **144**(1): p. 51-63.
35. Rickett, T.A., et al., *Rapidly photo-cross-linkable chitosan hydrogel for peripheral neurosurgeries.* Biomacromolecules, 2011. **12**(1): p. 57-65.
36. Lauto, A., et al., *Chitosan adhesive for laser tissue repair: in vitro characterization.* Lasers Surg Med, 2005. **36**(3): p. 193-201.
37. Foster, L.J. and E. Karsten, *A chitosan based, laser activated thin film surgical adhesive, 'SurgiLux': preparation and demonstration.* J Vis Exp, 2012(68).
38. Mehdizadeh, M. and J. Yang, *Design strategies and applications of tissue bioadhesives.* Macromol Biosci, 2013. **13**(3): p. 271-88.
39. Moulay, S., *Dopa/Catechol-Tethered Polymers: Bioadhesives and Biomimetic Adhesive Materials.* Polymer Reviews, 2014. **54**(3): p. 436-513.
40. Waite, J.H., *Adhesion a la moule.* Integr Comp Biol, 2002. **42**(6): p. 1172-80.
41. Lin, Q., et al., *Adhesion mechanisms of the mussel foot proteins mfp-1 and mfp-3.* Proceedings of the National Academy of Sciences, 2007. **104**(10): p. 3782-3786.
42. Lee, B.P., et al., *Mussel-Inspired Adhesives and Coatings.* Annual Review of Materials Research, 2011. **41**(1): p. 99-132.
43. Yang, B., et al., *In Vivo Residue-Specific Dopa-Incorporated Engineered Mussel Bioglue with Enhanced Adhesion and Water Resistance.* Angewandte Chemie, 2014. **126**(49): p. 13578-13582.

44. Kord Forooshani, P. and B.P. Lee, *Recent approaches in designing bioadhesive materials inspired by mussel adhesive protein.* Journal of Polymer Science Part A: Polymer Chemistry, 2017. **55**(1): p. 9-33.
45. Gallivan, J.P. and D.A. Dougherty, *A Computational Study of Cation−π Interactions vs Salt Bridges in Aqueous Media: Implications for Protein Engineering.* Journal of the American Chemical Society, 2000. **122**(5): p. 870-874.
46. Lu, Q., et al., *Nanomechanics of Cation–π Interactions in Aqueous Solution.* Angewandte Chemie International Edition, 2013. **52**(14): p. 3944-3948.
47. Lee, B.P., et al., *Rapid Gel Formation and Adhesion in Photocurable and Biodegradable Block Copolymers with High DOPA Content.* Macromolecules, 2006. **39**(5): p. 1740-1748.
48. McDowell, L.M., et al., *Rotational echo double resonance detection of cross-links formed in mussel byssus under high-flow stress.* J Biol Chem, 1999. **274**(29): p. 20293-5.
49. Yu, M., J. Hwang, and T.J. Deming, *Role of l-3,4-Dihydroxyphenylalanine in Mussel Adhesive Proteins.* Journal of the American Chemical Society, 1999. **121**(24): p. 5825-5826.
50. Lee, H., N.F. Scherer, and P.B. Messersmith, *Single-molecule mechanics of mussel adhesion.* Proc Natl Acad Sci U S A, 2006. **103**(35): p. 12999-3003.
51. Yu, J., et al., *Adhesion of mussel foot protein-3 to TiO2 surfaces: the effect of pH.* Biomacromolecules, 2013. **14**(4): p. 1072-7.
52. Akdogan, Y., et al., *Intrinsic Surface-Drying Properties of Bioadhesive Proteins.* Angewandte Chemie, 2014. **126**(42): p. 11435-11438.
53. Wei, W., et al., *An Underwater Surface-Drying Peptide Inspired by a Mussel Adhesive Protein.* Advanced Functional Materials, 2016. **26**(20): p. 3496-3507.
54. Cencer, M., et al., *Effect of nitro-functionalization on the cross-linking and bioadhesion of biomimetic adhesive moiety.* Biomacromolecules, 2015. **16**(1): p. 404-10.
55. Amstad, E., et al., *Influence of Electronegative Substituents on the Binding Affinity of Catechol-Derived Anchors to Fe3O4 Nanoparticles.* The Journal of Physical Chemistry C, 2011. **115**(3): p. 683-691.
56. Ding, X., et al., *Nitro-Group Functionalization of Dopamine and its Contribution to the Viscoelastic Properties of Catechol-Containing Nanocomposite Hydrogels.* Macromolecular Chemistry and Physics, 2015. **216**(10): p. 1109-1119.
57. Amstad, E., et al., *Ultrastable Iron Oxide Nanoparticle Colloidal Suspensions Using Dispersants with Catechol-Derived Anchor Groups.* Nano Letters, 2009. **9**(12): p. 4042-4048.
58. Cencer, M., et al., *Effect of Nitro-Functionalization on the Cross-Linking and Bioadhesion of Biomimetic Adhesive Moiety.* Biomacromolecules, 2015. **16**(1): p. 404-410.
59. Shafiq, Z., et al., *Bioinspired Underwater Bonding and Debonding on Demand.* Angewandte Chemie International Edition, 2012. **51**(18): p. 4332-4335.
60. Lee, B.P., J.L. Dalsin, and P.B. Messersmith, *Synthesis and gelation of DOPA-modified poly(ethylene glycol) hydrogels.* Biomacromolecules, 2002. **3**(5): p. 1038-47.
61. Mehdizadeh, M., et al., *Injectable citrate-based mussel-inspired tissue bioadhesives with high wet strength for sutureless wound closure.* Biomaterials, 2012. **33**(32): p. 7972-83.
62. Huang, K., et al., *Synthesis and characterization of self-assembling block copolymers containing bioadhesive end groups.* Biomacromolecules, 2002. **3**(2): p. 397-406.
63. Michael, B., et al., *Biomechanical properties of Achilles tendon repair augmented with a bioadhesive-coated scaffold.* Biomedical Materials, 2011. **6**(1): p. 015014.
64. Barrett, D.G., G.G. Bushnell, and P.B. Messersmith, *Mechanically Robust, Negative-Swelling, Mussel-Inspired Tissue Adhesives.* Advanced Healthcare Materials, 2013. **2**(5): p. 745-755.

65. Kim, K., et al., *Bio-inspired catechol conjugation converts water-insoluble chitosan into a highly water-soluble, adhesive chitosan derivative for hydrogels and LbL assembly.* Biomaterials Science, 2013. **1**(7): p. 783-790.
66. Lee, C., et al., *Bioinspired, calcium-free alginate hydrogels with tunable physical and mechanical properties and improved biocompatibility.* Biomacromolecules, 2013. **14**(6): p. 2004-13.
67. Park, J.Y., et al., *Cell-repellant dextran coatings of porous titania using mussel adhesion chemistry.* Macromol Biosci, 2013. **13**(11): p. 1511-9.
68. Neto, A.I., et al., *Nanostructured Polymeric Coatings Based on Chitosan and Dopamine-Modified Hyaluronic Acid for Biomedical Applications.* Small, 2014. **10**(12): p. 2459-2469.
69. Pechey, A., et al., *Anti-Adhesive Coating and Clearance of Device Associated Uropathogenic Escherichia coli Cystitis.* The Journal of Urology, 2009. **182**(4): p. 1628-1636.
70. Shao, H., K.N. Bachus, and R.J. Stewart, *A Water-Borne Adhesive Modeled after the Sandcastle Glue of P. californica.* Macromolecular Bioscience, 2009. **9**(5): p. 464-471.
71. Lee, H., B.P. Lee, and P.B. Messersmith, *A reversible wet/dry adhesive inspired by mussels and geckos.* Nature, 2007. **448**: p. 338.
72. Westwood, G., T.N. Horton, and J.J. Wilker, *Simplified Polymer Mimics of Cross-Linking Adhesive Proteins.* Macromolecules, 2007. **40**(11): p. 3960-3964.
73. Matos-Pérez, C.R., J.D. White, and J.J. Wilker, *Polymer Composition and Substrate Influences on the Adhesive Bonding of a Biomimetic, Cross-Linking Polymer.* Journal of the American Chemical Society, 2012. **134**(22): p. 9498-9505.
74. Skelton, S., et al., *Biomimetic adhesive containing nanocomposite hydrogel with enhanced materials properties.* Soft Matter, 2013. **9**(14): p. 3825-3833.
75. Liu, J., et al., *pH-Detachable Polymer Brushes Formed Using Titanium–Diol Coordination Chemistry and Living Radical Polymerization (RAFT).* Macromolecules, 2009. **42**(8): p. 2931-2939.
76. Zobrist, C., et al., *Functionalization of Titanium Surfaces with Polymer Brushes Prepared from a Biomimetic RAFT Agent.* Macromolecules, 2011. **44**(15): p. 5883-5892.
77. Fan, X., L. Lin, and P.B. Messersmith, *Cell Fouling Resistance of Polymer Brushes Grafted from Ti Substrates by Surface-Initiated Polymerization: Effect of Ethylene Glycol Side Chain Length.* Biomacromolecules, 2006. **7**(8): p. 2443-2448.
78. Fan, X., et al., *Biomimetic Anchor for Surface-Initiated Polymerization from Metal Substrates.* Journal of the American Chemical Society, 2005. **127**(45): p. 15843-15847.
79. Tatehata, H., et al., *Model polypeptide of mussel adhesive protein. I. Synthesis and adhesive studies of sequential polypeptides (X-Tyr-Lys)n and (Y-Lys)n.* Journal of Applied Polymer Science, 2000. **76**(6): p. 929-937.
80. Schnurrer, J. and C.-M. Lehr, *Mucoadhesive properties of the mussel adhesive protein.* International Journal of Pharmaceutics, 1996. **141**(1): p. 251-256.
81. Ninan, L., et al., *Adhesive strength of marine mussel extracts on porcine skin.* Biomaterials, 2003. **24**(22): p. 4091-4099.
82. Sean, A.B., et al., *Thermal gelation and tissue adhesion of biomimetic hydrogels.* Biomedical Materials, 2007. **2**(4): p. 203.
83. Lee, Y., et al., *Thermo-sensitive, injectable, and tissue adhesive sol-gel transition hyaluronic acid/pluronic composite hydrogels prepared from bio-inspired catechol-thiol reaction.* Soft Matter, 2010. **6**(5): p. 977-983.
84. Brubaker, C.E. and P.B. Messersmith, *Enzymatically Degradable Mussel-Inspired Adhesive Hydrogel.* Biomacromolecules, 2011. **12**(12): p. 4326-4334.
85. Wang, J., et al., *Co-polypeptides of 3,4-dihydroxyphenylalanine and l-lysine to mimic marine adhesive protein.* Biomaterials, 2007. **28**(23): p. 3456-3468.

86. Hoffmann, B., et al., *Characterisation of a new bioadhesive system based on polysaccharides with the potential to be used as bone glue.* Journal of Materials Science: Materials in Medicine, 2009. **20**(10): p. 2001-2009.
87. Murphy, J.L., et al., *Adhesive Performance of Biomimetic Adhesive-Coated Biologic Scaffolds.* Biomacromolecules, 2010. **11**(11): p. 2976-2984.
88. Chung, H. and R.H. Grubbs, *Rapidly Cross-Linkable DOPA Containing Terpolymer Adhesives and PEG-Based Cross-Linkers for Biomedical Applications.* Macromolecules, 2012. **45**(24): p. 9666-9673.
89. Guo, J., et al., *Synthesis and characterization of anti-bacterial and anti-fungal citrate-based mussel-inspired bioadhesives.* Biomaterials, 2016. **85**(Supplement C): p. 204-217.
90. Guo, J., et al., *Click chemistry improved wet adhesion strength of mussel-inspired citrate-based antimicrobial bioadhesives.* Biomaterials, 2017. **112**(Supplement C): p. 275-286.
91. Xue, J., et al., *Preparation and characterization of a photocrosslinkable bioadhesive inspired by marine mussel.* Journal of Photochemistry and Photobiology B: Biology, 2013. **119**(Supplement C): p. 31-36.
92. Chen, W., et al., *A mussel-Inspired poly(γ-glutamic acid) tissue adhesive with high wet strength for wound closure.* J. Mater. Chem. B, 2017.
93. Kim, B.J., et al., *Mussel-Mimetic Protein-Based Adhesive Hydrogel.* Biomacromolecules, 2014. **15**(5): p. 1579-1585.
94. Jeon, E.Y., et al., *Rapidly light-activated surgical protein glue inspired by mussel adhesion and insect structural crosslinking.* Biomaterials, 2015. **67**: p. 11-19.
95. Zhou, J., et al., *Adhesion Properties of Catechol-Based Biodegradable Amino Acid-Based Poly(ester urea) Copolymers Inspired from Mussel Proteins.* Biomacromolecules, 2015. **16**(1): p. 266-274.
96. Zhou, J., V. Bhagat, and M.L. Becker, *Poly(ester urea)-Based Adhesives: Improved Deployment and Adhesion by Incorporation of Poly(propylene glycol) Segments.* ACS Applied Materials & Interfaces, 2016. **8**(49): p. 33423-33429.
97. Ji, Y., et al., *Mussel-inspired soft-tissue adhesive based on poly(diol citrate) with catechol functionality.* Journal of Materials Science: Materials in Medicine, 2015. **27**(2): p. 30.
98. Fan, C., et al., *A mussel-inspired double-crosslinked tissue adhesive intended for internal medical use.* Acta Biomater, 2016. **33**: p. 51-63.
99. Shi, Y., et al., *Enzymatically Degradable Polyester-Based Adhesives.* ACS Biomaterials Science & Engineering, 2015. **1**(10): p. 971-977.
100. Shan, M., et al., *A pH, glucose, and dopamine triple-responsive, self-healable adhesive hydrogel formed by phenylborate-catechol complexation.* Polymer Chemistry, 2017. **8**(19): p. 2997-3005.
101. Lu, D., et al., *Mussel-Inspired Thermoresponsive Polypeptide–Pluronic Copolymers for Versatile Surgical Adhesives and Hemostasis.* ACS Applied Materials & Interfaces, 2017. **9**(20): p. 16756-16766.
102. Annabi, N., et al., *Surgical Materials: Current Challenges and Nano-enabled Solutions.* Nano today, 2014. **9**(5): p. 574-589.
103. Mehdizadeh, M. and J. Yang, *Design Strategies and Applications of Tissue Bioadhesives.* Macromolecular Bioscience, 2013. **13**(3): p. 271-288.
104. Leggat, P.A., D.R. Smith, and U. Kedjarune, *SURGICAL APPLICATIONS OF CYANOACRYLATE ADHESIVES: A REVIEW OF TOXICITY.* ANZ Journal of Surgery, 2007. **77**(4): p. 209-213.
105. Sierra, D.H., *Fibrin sealant adhesive systems: a review of their chemistry, material properties and clinical applications.* J Biomater Appl, 1993. **7**(4): p. 309-52.
106. Hyon, S.-H., et al., *Low cytotoxic tissue adhesive based on oxidized dextran and epsilon-poly-l-lysine.* Journal of Biomedical Materials Research Part A, 2014. **102**(8): p. 2511-2520.

107. Mahdavi, A., et al., *A biodegradable and biocompatible gecko-inspired tissue adhesive.* Proc Natl Acad Sci U S A, 2008. **105**(7): p. 2307-12.
108. Kluge, J.A., et al., *Spider silks and their applications.* Trends Biotechnol, 2008. **26**(5): p. 244-51.
109. Haller, C.M., et al., *Mussel-mimetic tissue adhesive for fetal membrane repair: An ex vivo evaluation.* Acta Biomaterialia, 2012. **8**(12): p. 4365-4370.
110. Waite, J.H., *Nature's underwater adhesive specialist.* International Journal of Adhesion and Adhesives, 1987. **7**(1): p. 9-14.
111. Zhu, W., et al., *A mussel-inspired double-crosslink tissue adhesive on rat mastectomy model: seroma prevention and in vivo biocompatibility.* Journal of Surgical Research, 2017.
112. Zhang, H., et al., *Mussel-inspired hyperbranched poly(amino ester) polymer as strong wet tissue adhesive.* Biomaterials, 2014. **35**(2): p. 711-9.
113. Kord Forooshani, P. and B.P. Lee, *Recent approaches in designing bioadhesive materials inspired by mussel adhesive protein.* J Polym Sci A Polym Chem, 2017. **55**(1): p. 9-33.
114. Guo, J., et al., *Click chemistry improved wet adhesion strength of mussel-inspired citrate-based antimicrobial bioadhesives.* Biomaterials, 2017. **112**: p. 275-286.
115. Cohen, B., et al., *Gelatin–alginate novel tissue adhesives and their formulation–strength effects.* Acta Biomaterialia, 2013. **9**(11): p. 9004-9011.
116. Foster, L.J. and E. Karsten, *A chitosan based, laser activated thin film surgical adhesive, 'SurgiLux': preparation and demonstration.* J Vis Exp, 2012(68): p. 3527.
117. Shin, J., et al., *Tissue Adhesive Catechol-Modified Hyaluronic Acid Hydrogel for Effective, Minimally Invasive Cell Therapy.* Advanced Functional Materials, 2015. **25**(25): p. 3814-3824.
118. Han, L., et al., *Mussel-Inspired Adhesive and Tough Hydrogel Based on Nanoclay Confined Dopamine Polymerization.* ACS Nano, 2017. **11**(3): p. 2561-2574.
119. Fan, C., et al., *A mussel-inspired double-crosslinked tissue adhesive intended for internal medical use.* Acta Biomaterialia, 2016. **33**: p. 51-63.
120. Han, L., et al., *Tough, self-healable and tissue-adhesive hydrogel with tunable multifunctionality.* NPG Asia Mater, 2017. **9**: p. e372.
121. Ji, Y., et al., *Mussel-inspired soft-tissue adhesive based on poly(diol citrate) with catechol functionality.* J Mater Sci Mater Med, 2016. **27**(2): p. 30.
122. Rose, S., et al., *Nanoparticle solutions as adhesives for gels and biological tissues.* Nature, 2014. **505**(7483): p. 382-385.
123. Jeon, O., et al., *The effect of oxidation on the degradation of photocrosslinkable alginate hydrogels.* Biomaterials, 2012. **33**(13): p. 3503-3514.
124. Kristiansen, K.A., A. Potthast, and B.E. Christensen, *Periodate oxidation of polysaccharides for modification of chemical and physical properties.* Carbohydr Res, 2010. **345**(10): p. 1264-71.
125. Papageorgiou, S.K., et al., *Metal–carboxylate interactions in metal–alginate complexes studied with FTIR spectroscopy.* Carbohydrate Research, 2010. **345**(4): p. 469-473.
126. Wang, X., et al., *Dopamine-Modified Alginate Beads Reinforced by Cross-Linking via Titanium Coordination or Self-Polymerization and Its Application in Enzyme Immobilization.* Industrial & Engineering Chemistry Research, 2013. **52**(42): p. 14828-14836.
127. Hwang, D.S., et al., *Adhesion mechanism in a DOPA-deficient foot protein from green mussels.* Soft Matter, 2012. **8**(20): p. 5640-5648.
128. Hou, J., et al., *Enzymatically crosslinked alginate hydrogels with improved adhesion properties.* Polymer Chemistry, 2015. **6**(12): p. 2204-2213.
129. Alegre-Requena, J.V., et al., *Regulatory parameters of self-healing alginate hydrogel networks prepared via mussel-inspired dynamic chemistry.* New Journal of Chemistry, 2016. **40**(10): p. 8493-8501.

130. Kim, S., et al., *Mussel-Inspired Approach to Constructing Robust Multilayered Alginate Films for Antibacterial Applications.* Advanced Functional Materials, 2016. **26**(23): p. 4099-4105.
131. Jalali, N., et al., *Surface modification of poly(lactide-co-glycolide) nanoparticles by d-α-tocopheryl polyethylene glycol 1000 succinate as potential carrier for the delivery of drugs to the brain.* Colloids and Surfaces A: Physicochemical and Engineering Aspects, 2011. **392**(1): p. 335-342.
132. Silva, A.T.C.R., et al., *Synthesis, Characterization, and Study of PLGA Copolymer <i>in Vitro</i> Degradation.* Journal of Biomaterials and Nanobiotechnology, 2015. **06**(01): p. 8-19.
133. Bouhadir, K.H., et al., *Degradation of partially oxidized alginate and its potential application for tissue engineering.* Biotechnol Prog, 2001. **17**(5): p. 945-50.
134. Boontheekul, T., H.J. Kong, and D.J. Mooney, *Controlling alginate gel degradation utilizing partial oxidation and bimodal molecular weight distribution.* Biomaterials, 2005. **26**(15): p. 2455-65.
135. Makadia, H.K. and S.J. Siegel, *Poly Lactic-co-Glycolic Acid (PLGA) as Biodegradable Controlled Drug Delivery Carrier.* Polymers, 2011. **3**(3): p. 1377-1397.
136. Zolnik, B.S. and D.J. Burgess, *Effect of acidic pH on PLGA microsphere degradation and release.* Journal of Controlled Release, 2007. **122**(3): p. 338-344.
137. Kim, H.J., et al., *Mussel adhesion-employed water-immiscible fluid bioadhesive for urinary fistula sealing.* Biomaterials, 2015. **72**: p. 104-111.
138. Lee, B.P., et al., *Mussel-Inspired Adhesives and Coatings.* Annual review of materials research, 2011. **41**: p. 99-132.
139. Peak, C.W., J.J. Wilker, and G. Schmidt, *A review on tough and sticky hydrogels.* Colloid and Polymer Science, 2013. **291**(9): p. 2031-2047.
140. Shen, M., et al., *Rheology and Adhesion of Poly(acrylic acid)/Laponite Nanocomposite Hydrogels as Biocompatible Adhesives.* Langmuir, 2014. **30**(6): p. 1636-1642.
141. Menon, J.U., et al., *Effects of surfactants on the properties of PLGA nanoparticles.* Journal of Biomedical Materials Research Part A, 2012. **100A**(8): p. 1998-2005.
142. Kona, S., et al., *BIODEGRADABLE NANOPARTICLES MIMICKING PLATELET BINDING AS A TARGETED AND CONTROLLED DRUG DELIVERY SYSTEM.* International Journal of Pharmaceutics, 2012. **423**(2): p. 516-524.
143. Li, Y., et al., *Size-dependent cytotoxicity of amorphous silica nanoparticles in human hepatoma HepG2 cells.* Toxicology in Vitro, 2011. **25**(7): p. 1343-1352.
144. Sun, L., et al., *Cytotoxicity and mitochondrial damage caused by silica nanoparticles.* Toxicology in Vitro, 2011. **25**(8): p. 1619-1629.
145. Napierska, D., et al., *Size-Dependent Cytotoxicity of Monodisperse Silica Nanoparticles in Human Endothelial Cells.* Small, 2009. **5**(7): p. 846-853.
146. Park, Y.-H., et al., *Effect of the size and surface charge of silica nanoparticles on cutaneous toxicity.* Molecular & Cellular Toxicology, 2013. **9**(1): p. 67-74.
147. Zimmermann, U., et al., *Production of mitogen-contamination free alginates with variable ratios of mannuronic acid to guluronic acid by free flow electrophoresis.* ELECTROPHORESIS, 1992. **13**(1): p. 269-274.
148. Yang, D. and K.S. Jones, *Effect of alginate on innate immune activation of macrophages.* Journal of biomedical materials research. Part A, 2009. **90**(2): p. 411-8.
149. Tam, S.K., et al., *Factors influencing alginate gel biocompatibility.* Journal of Biomedical Materials Research Part A, 2011. **98A**(1): p. 40-52.
150. Lee, K.Y. and D.J. Mooney, *Alginate: Properties and biomedical applications.* Progress in Polymer Science, 2012. **37**(1): p. 106-126.

151. Thambi, T., V.H.G. Phan, and D.S. Lee, *Stimuli-Sensitive Injectable Hydrogels Based on Polysaccharides and Their Biomedical Applications.* Macromolecular Rapid Communications, 2016. **37**(23): p. 1881-1896.
152. Jiang, W.W., et al., *Phagocyte responses to degradable polymers.* Journal of biomedical materials research. Part A, 2007. **82**(2): p. 492-7.
153. Thoniyot, P., et al., *Nanoparticle–Hydrogel Composites: Concept, Design, and Applications of These Promising, Multi-Functional Materials.* Advanced Science, 2015. **2**(1-2): p. 1400010-n/a.
154. Lang, N., et al., *A blood-resistant surgical glue for minimally invasive repair of vessels and heart defects.* Sci Transl Med, 2014. **6**(218): p. 218ra6.
155. Fan, C., et al., *A mussel-inspired double-crosslinked tissue adhesive intended for internal medical use.* Acta Biomaterialia, 2016. **33**(Supplement C): p. 51-63.
156. Jeon, E.Y., et al., *Rapidly light-activated surgical protein glue inspired by mussel adhesion and insect structural crosslinking.* Biomaterials, 2015. **67**(Supplement C): p. 11-19.
157. Xie, D., et al., *Development of Injectable Citrate-Based Bioadhesive Bone Implants.* Journal of materials chemistry. B, Materials for biology and medicine, 2015. **3**: p. 387-398.
158. Meddahi-Pellé , A., et al., *Organ Repair, Hemostasis, and In Vivo Bonding of Medical Devices by Aqueous Solutions of Nanoparticles.* Angewandte Chemie International Edition, 2014. **53**(25): p. 6369-6373.
159. Ho, C.C. and S.J. Ding, *Structure, properties and applications of mussel-inspired polydopamine.* J Biomed Nanotechnol, 2014. **10**(10): p. 3063-84.
160. Jiang, X., Y. Wang, and M. Li, *Selecting water-alcohol mixed solvent for synthesis of polydopamine nano-spheres using solubility parameter.* Scientific Reports, 2014. **4**: p. 6070.
161. Kelong, A., et al., *Sp2 C-Dominant N-Doped Carbon Sub-micrometer Spheres with a Tunable Size: A Versatile Platform for Highly Efficient Oxygen-Reduction Catalysts.* Advanced Materials, 2013. **25**(7): p. 998-1003.
162. Jian, Y., et al., *Polydopamine Spheres as Active Templates for Convenient Synthesis of Various Nanostructures.* Small, 2013. **9**(4): p. 596-603.
163. Huang, Y., et al., *Mimicking Melanosomes: Polydopamine Nanoparticles as Artificial Microparasols.* ACS Central Science, 2017. **3**(6): p. 564-569.
164. Cao, Z., M.J. Stevens, and A.V. Dobrynin, *Adhesion and Wetting of Nanoparticles on Soft Surfaces.* Macromolecules, 2014. **47**(9): p. 3203-3209.
165. Carrillo, J.-M.Y., E. Raphael, and A.V. Dobrynin, *Adhesion of Nanoparticles.* Langmuir, 2010. **26**(15): p. 12973-12979.
166. Cao, Z., et al., *Adhesion and Wetting of Soft Nanoparticles on Textured Surfaces: Transition between Wenzel and Cassie–Baxter States.* Langmuir, 2015. **31**(5): p. 1693-1703.
167. Carrillo, J.-M.Y. and A.V. Dobrynin, *Dynamics of nanoparticle adhesion.* The Journal of Chemical Physics, 2012. **137**(21): p. 214902.
168. Yuan, H., et al., *Variable Nanoparticle-Cell Adhesion Strength Regulates Cellular Uptake.* Physical Review Letters, 2010. **105**(13): p. 138101.
169. Barbul, A., et al., *Nanoparticle-decorated erythrocytes reveal that particle size controls the extent of adsorption, cell shape, and cell deformability.* ACS Applied Nano Materials, 2018.
170. *Surface energy and the contact of elastic solids.* Proceedings of the Royal Society of London. A. Mathematical and Physical Sciences, 1971. **324**(1558): p. 301-313.
171. Derjaguin, B.V., V.M. Muller, and Y.P. Toporov, *Effect of contact deformations on the adhesion of particles.* Journal of Colloid and Interface Science, 1975. **53**(2): p. 314-326.
172. Felicetti, M.A., et al., *Influence of Particle Size, Applied Compression, and Substratum Material on Particle−Surface Adhesion Force Using the Centrifuge Technique.* Industrial & Engineering Chemistry Research, 2009. **48**(2): p. 877-887.

173. Rimai, D.S., M.C. Ezenyilimba, and D.J. Quesnel, *Effects of Electrostatic and van der Waals Interactions on the Adhesion of Spherical 7 µm Particles.* The Journal of Adhesion, 2005. **81**(3-4): p. 245-269.
174. Segeren, L.H.G.J., et al., *Microparticle adhesion studies by atomic force microscopy.* Journal of Adhesion Science and Technology, 2002. **16**(7): p. 793-828.
175. Cox, L.M., et al., *Influences of Substrate Adhesion and Particle Size on the Shape Memory Effect of Polystyrene Particles.* Langmuir, 2016. **32**(15): p. 3691-3698.
176. Shin, K., et al., *Multifunctional nanoparticles as a tissue adhesive and an injectable marker for image-guided procedures.* Nature Communications, 2017. **8**: p. 15807.
177. Ramakrishna, S.N., et al., *Controlling Adhesion Force by Means of Nanoscale Surface Roughness.* Langmuir, 2011. **27**(16): p. 9972-9978.
178. Su, G.M., et al., *Tailored Nanoparticles for Enhancing Polymer Adhesion.* Macromolecules, 2011. **44**(13): p. 5256-5261.
179. I., N.A., et al., *Nanostructured Polymeric Coatings Based on Chitosan and Dopamine-Modified Hyaluronic Acid for Biomedical Applications.* Small, 2014. **10**(12): p. 2459-2469.
180. Wu, F., et al., *Multifunctional Coating Based on Hyaluronic Acid and Dopamine Conjugate for Potential Application on Surface Modification of Cardiovascular Implanted Devices.* ACS Applied Materials & Interfaces, 2016. **8**(1): p. 109-121.
181. Yuhan, L., et al., *Bioinspired Surface Immobilization of Hyaluronic Acid on Monodisperse Magnetite Nanocrystals for Targeted Cancer Imaging.* Advanced Materials, 2008. **20**(21): p. 4154-4157.
182. Seonki, H., et al., *Hyaluronic Acid Catechol: A Biopolymer Exhibiting a pH-Dependent Adhesive or Cohesive Property for Human Neural Stem Cell Engineering.* Advanced Functional Materials, 2013. **23**(14): p. 1774-1780.
183. Jisoo, S., et al., *Tissue Adhesive Catechol-Modified Hyaluronic Acid Hydrogel for Effective, Minimally Invasive Cell Therapy.* Advanced Functional Materials, 2015. **25**(25): p. 3814-3824.
184. Haeshin, L., R. Junsung, and M.P. B., *Facile Conjugation of Biomolecules onto Surfaces via Mussel Adhesive Protein Inspired Coatings.* Advanced Materials, 2009. **21**(4): p. 431-434.
185. Kastrup, C.J., et al., *Painting blood vessels and atherosclerotic plaques with an adhesive drug depot.* Proceedings of the National Academy of Sciences of the United States of America, 2012. **109**(52): p. 21444-21449.
186. Nikhil, P., et al., *Biodegradable Nanoparticles Enhanced Adhesiveness of Mussel-Like Hydrogels at Tissue Interface.* Advanced Healthcare Materials, 2018. **7**(7): p. 1701069.
187. Gardner, D.J., et al., *Polymer nanocomposites from the surface energy perspective.* Reviews of Adhesion and Adhesives, 2013. **1**(2): p. 175-215.
188. Gersappe, D., *Molecular mechanisms of failure in polymer nanocomposites.* Phys Rev Lett, 2002. **89**(5): p. 058301.
189. Fantner, G.E., et al., *Sacrificial Bonds and Hidden Length: Unraveling Molecular Mesostructures in Tough Materials.* Biophysical Journal, 2006. **90**(4): p. 1411-1418.
190. M., D., A. P., and R.-H. E., *Bionanocomposites: A New Concept of Ecological, Bioinspired, and Functional Hybrid Materials.* Advanced Materials, 2007. **19**(10): p. 1309-1319.
191. Ku, S.H. and C.B. Park, *Human endothelial cell growth on mussel-inspired nanofiber scaffold for vascular tissue engineering.* Biomaterials, 2010. **31**(36): p. 9431-7.
192. Robson, M.C., *WOUND INFECTION: A Failure of Wound Healing Caused by an Imbalance of Bacteria.* Surgical Clinics of North America, 1997. **77**(3): p. 637-650.
193. Edwards, R. and K.G. Harding, *Bacteria and wound healing.* Current Opinion in Infectious Diseases, 2004. **17**(2): p. 91-96.

194. Robson, M.C., B.D. Stenberg, and J.P. Heggers, *Wound healing alterations caused by infection.* Clinics in plastic surgery, 1990. **17**(3): p. 485-492.
195. Guo, S. and L.A. DiPietro, *Factors Affecting Wound Healing.* Journal of Dental Research, 2010. **89**(3): p. 219-229.
196. Kavitha, K.V., et al., *Choice of wound care in diabetic foot ulcer: A practical approach.* World Journal of Diabetes, 2014. **5**(4): p. 546-556.
197. Abed, N., et al., *An efficient system for intracellular delivery of beta-lactam antibiotics to overcome bacterial resistance.* Scientific Reports, 2015. **5**: p. 13500.
198. Ho, J., et al., *Current Advancements and Strategies in Tissue Engineering for Wound Healing: A Comprehensive Review.* Advances in Wound Care, 2017. **6**(6): p. 191-209.
199. Hansbrough, J.F., et al., *Development of a temporary living skin replacement composed of human neonatal fibroblasts cultured in Biobrane, a synthetic dressing material.* Surgery, 1994. **115**(5): p. 633-644.
200. Phillips, T.J. and B.A. Gilchrest, *Cultured epidermal allografts as biological wound dressings.* Prog Clin Biol Res, 1991. **365**: p. 77-94.
201. Hart, C.E., A. Loewen-Rodriguez, and J. Lessem, *Dermagraft: Use in the Treatment of Chronic Wounds.* Advances in Wound Care, 2012. **1**(3): p. 138-141.
202. Griffiths, M., et al., *Survival of Apligraf in acute human wounds.* Tissue engineering, 2004. **10**(7-8): p. 1180-1195.
203. Hu, S., et al., *Evaluation of Apligraf persistence and basement membrane restoration in donor site wounds: a pilot study.* Wound Repair Regen, 2006. **14**(4): p. 427-33.
204. Swaim, S.F., *Skin Grafts.* Veterinary Clinics of North America: Small Animal Practice, 1990. **20**(1): p. 147-175.
205. Serena, T.E., *Use of epidermal grafts in wounds: a review of an automated epidermal harvesting system.* Journal of Wound Care, 2015. **24**(Sup4b): p. 30-34.
206. Veiga, A.S. and J.P. Schneider, *Antimicrobial hydrogels for the treatment of infection.* Biopolymers, 2013. **100**(6): p. 637-644.
207. Kamoun, E.A., E.-R.S. Kenawy, and X. Chen, *A review on polymeric hydrogel membranes for wound dressing applications: PVA-based hydrogel dressings.* Journal of Advanced Research, 2017. **8**(3): p. 217-233.
208. Sampath, S.S. and D.H. Robinson, *Comparison of New and Existing Spectrophotometric Methods for the Analysis of Tobramycin and Other Aminoglycosides.* Journal of Pharmaceutical Sciences, 1990. **79**(5): p. 428-431.
209. Wiegand, I., K. Hilpert, and R.E. Hancock, *Agar and broth dilution methods to determine the minimal inhibitory concentration (MIC) of antimicrobial substances.* Nat Protoc, 2008. **3**(2): p. 163-75.
210. Jurcisek, J.A., et al., *In vitro Biofilm Formation in an 8-well Chamber Slide.* Journal of Visualized Experiments : JoVE, 2011(47): p. 2481.
211. Lawrence, J.V. and S. Maier, *Correction for the inherent error in optical density readings.* Applied and Environmental Microbiology, 1977. **33**(2): p. 482-484.
212. Koch, A.L., *Turbidity measurements of bacterial cultures in some available commercial instruments.* Analytical Biochemistry, 1970. **38**(1): p. 252-259.
213. Koch, A.L., *Theory of the angular dependence of light scattered by bacteria and similar-sized biological objects.* Journal of Theoretical Biology, 1968. **18**(1): p. 133-156.
214. Vogel, S.J., M. Tank, and N. Goodyear, *Variation in detection limits between bacterial growth phases and precision of an ATP bioluminescence system.* Lett Appl Microbiol, 2014. **58**(4): p. 370-5.

Biographical Information

Nikhil Pandey was born in Hyderabad, India to a physicist father and a teacher mother who inculcated in him an aptitude, desire and importance of education. He pursued his bachelor's in engineering in biotechnology from the prestigious Panjab University in the north of India and later worked in a small startup diagnostic company RAS life science, Hyderabad attempting to purify the polymerase chain reaction enzyme Taq Polymerase from recombinant *E. Coli* bacteria.

Following a year working at RAS, he came to the United States of America to pursue a master's degree in biomedical engineering at the University of Texas at Arlington in the year 2010 during which he secured a fruitful volunteer position in Dr. Kytai. T. Nguyen's research group working with Dr. Aniket Wadajkar, a doctoral student of Dr. Nguyen at that time. He worked extensively on polymeric magnetic nanoparticles for prostate cancer and thyroid cancer therapy gaining extensively useful skills in nanoparticle characterization and research.

After his graduation from UT Arlington and from Dr. Nguyen's group in 2012, he secured a research associate position at the University of California San Francisco working with an ophthalmologist Dr. Jacque Duncan and on her collaboration with Dr. Austin Roorda's group in UC Berkeley. He worked on imaging and analyzing data obtained by an adaptive optics scanning laser ophthalmoscope on patients with inherent retinal degenerations for a year.

Spurred by the research experience in image processing and wanting to further advance his education and knowledge of bioengineering, he decided to come back to his alma mater and his mentor Dr. Kytai T. Nguyen to pursue a doctorate in biomedical engineering with an emphasis on tissue engineering in the year 2014. Since then he has been working with Dr. Kytai T. Nguyen and

Dr. Yi Hong and on their collaboration project with Dr. Phillipe Zimmern at the University of Texas Southwestern (UTSW) medical center, Dallas, trying to develop a degradable tissue adhering nanocomposite material for prolapse prevention.

The efforts on this dissertation research have yielded several conference publications in national meetings of BMES (2014-2017), Society for Biomaterials (2016) and Society for urodynamics and female pelvic organ prolapse (2018) to name a few, a peer reviewed research paper publish in advanced health care materials (2017) and a NIH RO1 research grant. He currently finalizes two other experimental manuscripts for publication in peer reviewed journals.

In addition to being Dr. Nguyen's doctoral student, Nikhil also currently serves as her lab manager since 2014. Apart from a full-time research work load, Nikhil enjoys swimming, running, ping pong, bowling and reading science fiction and poetry. He aspires to author a science fiction read in the future.